

**GROWTH AND CHARACTERIZATION OF DIAMMONIUM
HYDROGEN CITRATE AND CITRIC ACID
MONOHYDRATE SINGLE CRYSTALS**

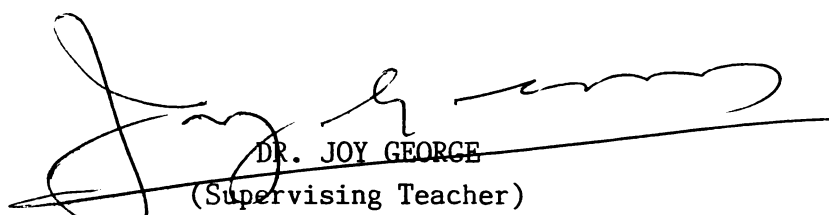
**THESIS SUBMITTED BY
GEORGE PETER
IN PARTIAL FULFILMENT OF THE REQUIREMENTS
FOR THE DEGREE OF
DOCTOR OF PHILOSOPHY**

**SOLID STATE PHYSICS LABORATORY
DEPARTMENT OF PHYSICS
COCHIN UNIVERSITY OF SCIENCE & TECHNOLOGY**

1 9 8 6

CERTIFICATE

Certified that this thesis is based on the work done by Sri George Peter under my guidance in the Department of Physics, Cochin University of Science and Technology, and no part of this thesis has been presented by him for any other degree.

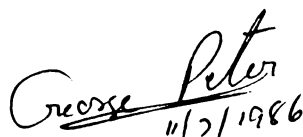

DR. JOY GEORGE
(Supervising Teacher)
PROFESSOR OF INDUSTRIAL PHYSICS
DEPARTMENT OF PHYSICS
COCHIN UNIVERSITY OF SCIENCE AND TECHNOLOGY

COCHIN - 22
11th JULY 1986.

DECLARATION

Certified that the work presented in this thesis is based on the original work done by me under the guidance of Professor Joy George in the Department of Physics, Cochin University of Science and Technology, and has not been included in any other thesis submitted previously for the award of any degree.

Cochin - 22
11th of July 1986.


11/7/1986
GEORGE PETER

SYNOPSIS

GROWTH AND CHARACTERIZATION OF
DIAMMONIUM HYDROGEN CITRATE AND
CITRIC ACID MONOHYDRATE
SINGLE CRYSTALS

Over the past years there has been considerable interest in the growth of single crystals both from the point of view of basic research and technological application. With the revolutionary emergence of solid state electronics which is based on single crystal technology, basic and applied studies on crystal growth and characterization have gained a more significant role in material science. These studies are being carried out for single crystals not only of semiconductor and other electronic materials but also of metals and insulators.

A number of organic crystals exhibit high quantum efficiency of photoconductivity, interesting photoelectric and photomagnetic properties, pronounced anisotropy of optical and electrical parameters, high electronic polarizability and other interesting characteristics.

Many organic crystals belonging to the orthorhombic class exhibit ferroelectric, electrooptic, triboluminescent and piezoelectric properties. Diammonium Hydrogen Citrate (DAHC) crystals are reported to be piezoelectric and triboluminescent /1/. Koptsik et al. /2/ have

reported the piezoelectric nature of Citric Acid Monohydrate (CA) crystals. And since not much work has been done on these crystals, it has been thought useful to grow and characterize these crystals.

This thesis presents a study of the growth of these crystals from solution and their defect structures. The results of the micro-indentation and thermal analysis are presented. Dielectric, fractographic, infrared (IR) and ultraviolet (UV) studies of DAHC crystals are also reported.

Although, the general principles of crystal growth can be applied for all materials, the precise method of crystal growth varies from one material to another. Therefore, from among the three categories of crystal growth methods, namely, growth from melt, from solution, and from vapour, growth from solution was found to be the best suited for the growth of DAHC and CA crystals.

DAHC ($C_6H_{14}N_2O_7$) single crystals belong to the noncentrosymmetric orthorhombic system with point group $mm2$ /3/. Large and perfect crystals of size upto $(60 \times 27 \times 5) \text{mm}^3$ were grown by slow evaporation in a constant temperature bath.

Roelofsen /4/ has assigned CA ($C_6H_8O_7 \cdot H_2O$) crystals to the point group 222 in the orthorhombic system. Crystals of size $(30 \times 30 \times 10) \text{mm}^3$ have been grown by slow evaporation below 36.6°C .

Crystals with different external morphology were obtained during crystallization of DAHC and CA. This is explained on the basis of external factors such as degree of supersaturation, supply of crystallizing particles and the presence of foreign materials. The faces were identified by angular measurements using goniometer.

Microscopic observations of the as grown surfaces of DAHC and CA crystals give evidence to layer growth mechanism being active in the growth of these crystals.

Dislocation etch studies have been carried out to assess the perfection of DAHC and CA crystals. Dislocations in DAHC crystals were delineated by propionic acid which was found to be a reliable dislocation etchant for the (001) face. Dislocation loops, helices, clusters, impurity centers and slip lines are observed with this etchant. The etch pit density is found to be of the order of $1.2 \times 10^2/\text{cm}^2$. Deep and shallow pits are observed at the intersection of dislocations on the (001) face. The shallow pits are attributed to dislocation loops. Propionic acid is also capable of etching dislocation sites on the (110) cleavage face. Other etchants have been tried and formic acid, acetic acid and methyl alcohol were also found to be capable of bringing out dislocations on the (001) face. The shape of the pit is found to depend on the type of the etchant used. The etch pit formation in DAHC crystals is explained on the basis of the thermodynamic theories of etching. For CA crystals also, propionic acid is found

to be a good dislocation etchant.

Microindentation analysis of DAHC and CA crystals was done using Vickers pyramidal indenter to study the hardness, toughness, brittleness and the nature of cracks. The loading time was chosen as 15 secs as the area of impression did not bear any observable dependence on loading. The hardness of DAHC was found to be 0.68 GPa. The variation of hardness with load was analysed upto a load of 12.5 gms. The special feature of the variation is the sharp increase in hardness with increase in load. The major contribution to the increase in hardness with load in DAHC is attributed to the high stress required for homogeneous nucleation of dislocations in the small dislocation free regions indented. The fracture toughness of DAHC is $0.17 \text{ MPa m}^{1/2}$. Loads upto 25 gms were used for the toughness evaluation. Beyond this load, chipping of material occurs. The toughness value is found to increase with increase in load in a regular manner. Brittleness of DAHC is found to be $4.04 \mu \text{ m}^{-1/2}$. To study the nature of the threshold crack on (001) and (110) faces of DAHC, the indented specimens were viewed under an optical microscope for different loads from 0.5 gm to the point when well developed cracks are formed. The indented surface was also studied after etching with propionic acid. Surface removal technique has shown that the threshold crack is radial and originate from the surface.

From the indentation studies, hardness of CA was found to be

0.588 GPa. The variation of hardness with load is found to have a minimum around 7.5 gms. Beyond 12.5 gms well developed cracks appear. The toughness of CA as evaluated from the crack length observed around the indentation at load greater than 12.5 gms is $0.132 \text{ MPa m}^{1/2}$. The variation of toughness with load shows a minimum at around 20 gms. Brittleness of CA is $4.48 \mu\text{m}^{-1/2}$.

The cleavage facets of nonmetallic crystals provide valuable information regarding the imperfection structures of the crystal, the crystallographic mechanisms involved in deformation and fracture, the path of the cleavage traverse as influenced by crystallography, local stress resolutions and other phenomena relating to both intergranular and intragranular characteristics of the crystal. The (110) cleavage surface of DAHC exhibit typical examples of hackle structure. Such hackle structures are often found in the case of materials having pronounced directional weakness. Radial features known as Wallner lines are also observed, which indicate the specific stress patterns produced by the rupturing force as it traverse the crystal. They are said to be observed along with hackle markings on cleavages. Many other interesting crystallographic markings are also presented and discussed.

Dielectric studies were made on DAHC crystal along the three mutually perpendicular crystal axes in the region of temperature 133°K to 373°K and frequency 200 Hz to 20,000 Hz. The dielectric permitti-

vity (ϵ) and the loss tangent ($\tan\delta$) measurements were made in a low temperature dielectric cell with heating arrangement, using a 0.1% universal bridge TF 1313A of Marconi Instruments Ltd., U.K. To vary the frequency, an external oscillator was used.

The variation of dielectric permittivity with temperature for different frequencies shows similarity in all the three directions. ϵ increases slightly with temperature upto a certain point and thereafter shoots up to high values.

The variation of dielectric loss tangent with temperature also shows characteristics similar to the dielectric permittivity variation for all the three axes. Loss tangent is frequency dependent above a certain temperature. The loss is found to be negligible at low temperatures.

The IR spectrum of DAHC was recorded in the region 4000 - 200 cm^{-1} using nujol mull and KBr pellets on a Perkin-Elmer IR spectrophotometer. Absorption of DAHC are observed at frequencies 3400, 3200, 3060, 2860, 1690, 1600, 1330, 1270, 1230 and 1090 cm^{-1} . These bands are tentatively assigned to the functional groups in DAHC.

UV spectrum of DAHC was recorded in water using a double beam spectrophotometer, Shimadzu UV-190. The spectrum was obtained in a wavelength range 195 to 500 nm. The only absorption band observed

at 210 nm is discussed.

Differential scanning calorimeter (DSC) was used for the thermal analysis of DAHC and CA crystals. The samples were sealed in Al sample pans and heated at the rate of 20^oK/min in dry nitrogen atmosphere. The measurements were made from room temperature upto the melting point of these crystals. The calorimeter traces obtained for DAHC and CA are presented and discussed.

REFERENCES

1. B.P.CHANDRA and M.ELYAS, J. Phys. C.
Solid State Phys. 12(1979)L695.
2. V.A.KOPTSIK et al., Vestnik Moskov. Univ. Ser. Mat. Meth. Astron.
Fiz. Khim., 13(1958)91.
3. W.E.LOVE and A.L.PATTERSON, Acta Crystallogr. 13(1960)426.
4. G.ROELOFSEN, Struct. Commun. 1(1972)23.

CONTENTS

	Page
	INTRODUCTION 1
CHAPTER ONE	References 7
CHAPTER ONE	CRYSTAL GROWTH - THEORY AND TECHNIQUES 8
1.1	Theories of crystal growth 8
1.2	Techniques of crystal growth 22
	References 32
CHAPTER TWO	DISLOCATIONS AND ETCHING 33
2.1	Dislocations in crystals 33
2.2	Etching of crystals 40
	References 48
CHAPTER THREE	DEFORMATION AND FRACTURE 52
3.1	Indentation stress fields 52
3.2	Hardness 54
3.3	Toughness 57
3.4	Brittleness 63
	References 65
CHAPTER FOUR	EXPERIMENTAL TECHNIQUES 67
4.1	Growth techniques 67
4.2	Identification of faces 68
4.3	Specimen preparation 68
4.4	Dislocation etching studies 72

4.5	Microindentation analysis	73
4.6	Fractographic studies	75
4.7	Dielectric measurement	77
4.8	Spectral and thermal studies	80
	References	81
CHAPTER FIVE	GROWTH AND MORPHOLOGY OF DAHC AND CA	
	SINGLE CRYSTALS	82
5.1	Introduction	82
5.2	Experimental	83
5.3	Results and discussion	84
5.4	Conclusions	96
	References	97
CHAPTER SIX	DISLOCATION ETCHING STUDIES OF DAHC AND CA	
	SINGLE CRYSTALS	98
6.1	Introduction	98
6.2	Experimental	98
6.3	Results and discussion	99
6.4	Conclusions	131
	References	135
CHAPTER SEVEN	MICROINDENTATION ANALYSIS OF DAHC AND CA	
	SINGLE CRYSTALS	137
7.1	Introduction	137
7.2	Experimental	137
7.3	Results and discussion	138

7.4	Conclusions	158
	References	158
CHAPTER EIGHT	FRAC TOGRAPHIC STUDIES OF DAHC CRYSTALS	161
8.1	Introduction	161
8.2	Gleavage of crystals	162
8.3	Stress necessary for cleavage	165
8.4	Experimental	166
8.5	Results and discussion	166
8.6	Conclusions	181
	References	181
CHAPTER NINE	DIELECTRIC PROPERTIES OF DAHC CRYSTALS	183
9.1	Introduction	183
9.2	Polarization of dielectrics	183
9.3	Dependence of permittivity on frequency and temperature	188
9.4	Dielectric losses	189
9.5	Dependence of loss tangent on frequency and temperature	193
9.6	Experimental	197
9.7	Results and discussion	199
9.8	Conclusions	204
	References	205
CHAPTER TEN	SPECTRAL AND THERMAL STUDIES	206
10.1	Introduction	206

10.2	Experimental	209
10.3	Results and discussion	209
10.4	Conclusions	218
	References	221

INTRODUCTION

A number of organic crystals open up new promising avenues for practical applications due to their high quantum efficiency of photoconductivity, interesting photoelectric, photomagnetic, piezoelectric and triboluminescent properties, pronounced anisotropy of optical and electrical parameters, high electronic polarizability and other properties. Due to the weakness of Van der Waals interaction in molecular crystals, the main electronic characteristics of molecules undergo only slight changes in the process of solid phase formation. The greater influence of molecular properties over the crystalline properties brings about a marked tendency of localization of charge carriers and excitons on individual molecules of the crystal resulting in a number of qualitatively new properties such as electronic polarization of the lattice by a localized charge carrier, vibronic relaxation of molecules in the process of the formation of genuine ionic states, formation of local states of polarization origin in the regions of structural defects of the crystal etc., in these crystals. Also, the possibility of synthesizing crystals of a large variety of new materials with interesting properties exist, once the link between structure and properties of organic crystals are known.

The growth of single crystals of organic compounds is rather difficult compared to the growth of inorganic crystals. Unavailability

of suitable solvents, tendency to yield only small crystals and crystal aggregates, supercooling tendency, low thermal conductivity and thermal decomposition of organic materials often pose difficulties in crystal growth. Since organic materials often contain impurities, extensive purification procedures are to be applied before growth.

Defects, especially, dislocations influence a number of useful properties of crystals. The presence of dislocations are known to alter their plastic, electronic, magnetic, superconductive, piezoelectric, dielectric and various other properties. Therefore, a thorough knowledge of the defects and imperfections is an unavoidable first step in the characterization of crystals. Etching is widely accepted as one of the best methods for the study of defects, in particular, dislocations.

Analysis of deformation and fracture characteristics is vital in characterizing a crystal for device applications. Hardness and toughness are the key parameters quantifying resistance of a crystal to deformation and fracture, and brittleness is a measure of the relative susceptibility of the material to these competing mechanical processes. Among a large number of experimental methods used for the measurement of these parameters, microindentation is the best suited for organic crystals and Vickers pyramid indenter the most widely accepted indenter for microindentation.

The crystallographic mechanism involved in deformation, fracture and other intergranular and intragranular characteristics of nonmetallic crystals can be studied by the fractographic technique. It also provides valuable information regarding imperfection structures in crystals.

Dielectric studies have provided very valuable information regarding phase transitions, molecular motion, relaxation processes etc. in organic solids. The most important property of an organic dielectric crystal is that it can be polarized under the action of an external electric field. Dielectric permittivity is the basic parameter describing the dielectric crystal from the view point of its polarization. The dissipation of electric energy during the process of polarization by an electric field is measured by the dielectric loss tangent. An accurate and convenient method for the measurement of these quantities is based on the measurement of capacitance using bridges working on the principle of Wheatstone's bridge. The variation of these dielectric parameters with temperature can also be studied using proper dielectric cells.

Comparison of infrared (IR) and ultraviolet (UV) spectra of a crystalline and a noncrystalline sample of an organic solid can reveal the specific features related to the orderly arrangement of molecules and atoms in space of the solid. Fundamental data on mechanics of molecules can also be obtained from spectral studies. Depending on

the range of interest standard spectrometers are used for recording the spectral data. Thermal analysis using differential scanning calorimeter (DSC) is now widely employed to study a number of thermodynamic properties. DSC traces give information regarding phase transitions in crystalline samples.

Many organic crystals belonging to the orthorhombic class exhibit ferroelectric, piezoelectric and triboluminescent etc. properties. Diammonium hydrogen citrate (DAHC) single crystal having molecular formula, $C_6H_{14}N_2O_7$, belongs to the orthorhombic system with space group Pn2b, lattice parameters $a = 10.767$, $b = 14.736$ and $c = 6.165$ \AA and has four molecules per unit cell /1/. The crystal is reported to be piezoelectric and triboluminescent /2/.

Citric acid monohydrate (CA) single crystal with molecular formula, $C_6H_8O_7 \cdot H_2O$, is assigned to the point group mmm of the orthorhombic system by Groth /3/. But, Burns and Iball /4/ and later Roelofsen /5/ have assigned CA crystal to the point group 222, with $a = 6.290$, $b = 9.318$ and $c = 15.39$ \AA having four molecules per unit cell. Koptsik et al. /6/ have reported the piezoelectric nature of this crystal. The elastic constants of citric acid monohydrate have been computed from compressional and shear wave velocity measurements along different directions by Khan et al. /7/.

Since not much work has been reported on the growth and characte-

rization of these crystals, it has been thought useful to study these crystals and the results of these investigations are presented in this thesis.

The thesis contains ten chapters. The first chapter describes briefly the theory and techniques of crystal growth. In the second chapter, dislocations and etching as applied to non-metallic crystals are briefly discussed. In chapter three, the basic theory and techniques for the evaluation of hardness, toughness and brittleness are presented. The details of the experimental techniques that are used in the present study are given in chapter four. In chapters five to ten, the details of investigations on the growth and characterization of DAHC and CA single crystals and the results obtained are discussed.

Part of these investigations have been published in the following papers.

1. "Microindentation analysis of diammonium hydrogen citrate single crystals", J. Mater. Sci. 20(1985)3150.
2. "Dislocation etch studies on diammonium hydrogen citrate single crystals", Cryst. Res. Technol. (accepted for publication).
3. "Growth and characterization of diammonium hydrogen citrate", Proceedings of the National Seminar on Crystal Growth, Anna University, Madras, (4-6 October, 1982) p.16.

4. "Dielectric properties of diammonium hydrogen citrate single crystals", Proceedings of the Third National Seminar on Ferroelectrics and Dielectrics, I.I.Sc., Bangalore, (17-19 October, 1984) p.27.
5. "Deformation characteristics of diammonium hydrogen citrate single crystals", Proceedings of the Solid State Symposium, BARC, Bombay, (23-25 December, 1984) p.237.
6. "Defect characterization in single crystals of diammonium hydrogen citrate by chemical etching", Proceedings of the XVI National Seminar on Crystallography, University of Delhi, Delhi, (2-4 January, 1985) p.200.
7. "Defect characterization in citric acid monohydrate single crystals", Proceedings of the XVII National Seminar on Crystallography I.I.T, Madras, (20-22 December, 1985) p.38.
8. "Dislocation etch pit studies on diammonium hydrogen citrate single crystals", Proceedings of the Solid State Symposium, Nagpur University, Nagpur, (27-30 December, 1985) p.47.
9. " A study of dislocation etch pits on diammonium hydrogen citrate single crystals" (Communicated)
10. "Microindentation analysis of citric acid monohydrate single crystals" (Communicated).
11. "Dielectric studies of diammonium hydrogen citrate single crystals" (Communicated).

REFERENCES

1. W.E.LOVE and A.L.PATTERSON, Acta Crystallogr. 13(1960)426.
2. B.P.CHANDRA and M.ELYAS, J. Phys. C., Solid state
Phys. 12(1979)L695.
3. P.GROTH, Chem. Kryst. Vol.3, Engelmann, Leipzig (1910).
4. D.M.BURNS and J.IBALL, Acta Cryst. 7(1954)137.
6. V.A.KOPTSIK et al., Vestnik. Moskov. Univ.
Ser. Mat. Met. Astron. Fiz. Kim. 13(1958)91.
7. M.S. KHAN and T.S.NARASIMHAMURTHY, Solid State Commun. 48(1983)169.

CHAPTER ONE

CRYSTAL GROWTH - THEORY AND TECHNIQUES

The production of perfect single crystals for modern industry demands a thorough knowledge of the science and art of crystal growing. The growth of perfect single crystals has been developed over the years by the complimentary interaction of crystal growth theory and practice. Basic methods have been modified to produce perfect and useful crystals and to enhance their applicability to specific materials and classes of materials. The overall crystal growth process is rather complex, as it is influenced by numerous interdependent parameters.

In this chapter the fundamentals of the theories and techniques of crystal growth are outlined. The growth of crystals from solution is dealt in detail.

1.1. THEORIES OF CRYSTAL GROWTH

The theories of crystal growth can be divided into two sections, one dealing with growth of ideal crystals and the other dealing with growth of real crystals.

1.1.1. GROWTH OF IDEAL CRYSTALS

Gibbs /1/ made the first attempt to explain crystal growth on

a thermodynamical basis. He considered crystal growth processes as phase transformations which are driven by chemical potential between the crystallizing and nutrient phases. In the case of such a transformation from vapour to solid forming crystals the minimum free energy condition is given by

$$\sum \sigma F_i \text{ is a minimum}$$

where σ represents the surface free energy of the i^{th} face of area F_i . The above relation holds for the case where the crystal surface is in equilibrium with its vapour.

Curie /2/ and Wulff /3/ developed the criterion of minimum free energy. If D_i is the perpendicular distance of the i^{th} face of the crystal from a fixed point inside the crystal, then the volume of the crystal can be written as

$$V = 1/3 \sum D_i F_i \quad (1.1)$$

The total energy of the crystal is given by the summation

$$E = \sum \sigma_i F_i \quad (1.2)$$

For a very small change in volume

$$dV = \sum F_i dD_i \quad (1.3)$$

where one set of faces is assumed to grow at the expense of another.

From equation 1.1

$$dV = 1/3 \sum (F_i dD_i + D_i dF_i) \quad (1.4)$$

If the volume is kept constant, $dV = 0$ and from equations 1.3 and 1.4 we get the relation

$$\sum D_i dF_i = 0 \quad (1.5)$$

In the minimum energy criterion if the total free energy is constant and any variation of σ_i with F_i is neglected

$$\sum \sigma_i dF_i = 0 \quad (1.6)$$

and from equations 1.5 and 1.6 we get the relation, $D_i \propto \sigma_i$, which means that the crystal should form a polyhedron such that the perpendicular distance from a point within the crystal are proportional to the specific free energies of the appropriate faces. The above theory also implies that on a crystal, the velocities of growth of different faces in the directions of the normals are proportional to the appropriate specific surface free energies.

According to Bravais /4/, the velocities of the growth of the different faces of a crystal would depend upon the densities of lattice points in various planes, i.e. the reticular density. He also suggested that the velocity of growth in a direction normal to a face would be the slowest for the plane of maximum density. The Bravais theory was further developed to take into account of the effect of symmetry operations on Miller indices and to explain crystal morphology. After the theories of Gibbs and Curie /1, 2/, Soehncke /5/ introduced the idea of surface energies by postulating that the faces which possess the greatest reticular densities are those with minimum surface energies, and hence have minimum velocities of growth.

For the purpose of illustrating the growth of a perfect crystal a model was suggested by Kossel /6/ in which the molecules are taken

to be cubes stacked face to face. Each cube is attracted equally by all its six neighbours. In the Kossel model, at absolute zero, the low index faces of a crystal has a completely flat surface partially covered by another layer. There are incomplete steps on the surface having exchange sites called kinks. As the temperature is raised, some of the molecules leave the crystal surface acquiring sufficient energy to overcome the binding energy, while some molecules arrive at the surface, leading to an equilibrium state.

A molecule adsorbed on an atomically smooth crystal surface often migrate considerable distances before it becomes a part of the crystal. The distance through which an adsorbed molecule migrate is given by Einstein's formula

$$x_s^2 = D_s \tau_s \quad (1.7)$$

where D_s represents the diffusion coefficient and τ_s the mean life on the surface. In the model suggested by Kossel-Stranski

$$x_s \simeq a \exp(3\phi/2kT) \quad (1.8)$$

where a is the intermolecular distance, ϕ is the strength of the nearest neighbour bond, k is the Boltzmann constant and T is the absolute temperature. In the above expression the second and higher order neighbour bonding is neglected.

The migrating molecules adhere to the kink sites on the steps. BCF theory /7/ has shown that at any temperature there exist a finite number of kinks on the steps. The mean distance x_0 between the kinks

is given by the relation

$$x_0 \approx 1/2 a \exp (\phi/2kT) \quad (1.9)$$

As the supersaturation is increased more and more molecules join kinks and so the step advances. The rate of advance of a straight step is given by the relation

$$v_{\infty} = (\alpha - 1) x_s \nu e^{-W/kT} \quad (1.10)$$

where α is the saturation ratio, x_s is the mean distance of diffusion of the adsorbed molecule, ν is a frequency factor which is of the order of atomic frequency of vibration $\sim 10^{13} \text{ sec}^{-1}$ in the case of monatomic substances, W is the total evaporation energy.

Qualitatively the above equation implies that all molecules which hit the surface in the zone of width $2x_s$ will reach the advancing step and since the concentration of kinks in the step is fairly large, they will be adsorbed.

A curved step with a radius of curvature ρ advances with a velocity

$$v_{\rho} = v_{\infty} (1 - \rho_c / \rho) \quad (1.11)$$

where ρ_c is the critical radius of curvature defined by the relation

$$\rho_c = a\phi / (2kT \ln \alpha) \quad (1.12)$$

where α is the supersaturation.

On a perfect crystal surface steps are created by thermodynamic fluctuations. Once the step has covered the whole surface, a new layer

is to be initiated. This involves a nucleation process by which a monomolecular island is formed on the edges of which growth proceeds. The nucleation of monomolecular island requires additional energy. If it is assumed that only a single nucleus of monomolecular height is formed having a circular shape with radius r then the excess free energy f of the system is given by

$$f(r) = -kT \ln \alpha \pi r^2 / a^2 + \xi 2\pi r / a \quad (1.13)$$

where α is the supersaturation and ξ is the surface tension at the interface. Once the nucleus is formed due to thermodynamic fluctuations it will spread and again leave it smooth. For further growth a fresh nucleus is to be formed. The growth rate of crystals is governed by nucleation rate rather than the growth velocity of surface steps.

A rigorous analysis of nucleation /7/ shows that the nucleus is not circular, and the free energy per unit length of the edge varies with crystallographic direction. The rate of formation of nuclei is given by

$$Z(S/s_0) \exp (-F_0/kT) \quad (1.14)$$

where Z gives the rate of arrival of fresh molecules at single surface lattice sites, S is the surface area of the crystal face under consideration and s_0 is the area per molecule in the layer. F_0 is the maximum surface free energy at critical radius of the nucleus. Substitution of typical values for the different terms in equation 1.14 brings one to the conclusion that nucleation rate is a sensitive function of supersaturation and below a supersaturation of 25-50 per cent the

probability of nuclei formation is negligible. This was not in agreement with experimental observations /8/, where the growth rate was found to be proportional to supersaturation down to values much lower than the critical supersaturation as calculated from the surface nucleation theory. This, therefore, led to the conclusion that the growth of crystals at low supersaturations could only be explained by the fact that real crystal differ from ideal crystal.

1.1.2. GROWTH OF REAL CRYSTALS

It was Smekal /9/ who first pointed out that an important difference in the properties of crystals is related to the distinction between ideal and real crystals. Certain properties independent of crystal defects were designated by him as structure-insensitive while those dependent on crystal defects were termed structure-sensitive. The imperfections that explained the structure sensitive properties were lattice flaws, interstitial atoms and dislocations.

A revolutionary breakthrough in the field of crystal growth was presented by Burton et al. /7/. The success of their paper was due to the application of concepts, results and methods of theoretical physics to crystal growth. They gave the existing theories a stronger statistical mechanical foundations and proposed the famous spiral growth theory. The mathematical treatment of the spiral growth theory is summarised as follows. If ω is the rotational velocity, the growth

rate is given by the relation

$$R = (\omega/2) h_s \quad (1.15)$$

where h_s is the step height of the spiral step. Assuming this velocity to be constant with time, the step velocity of the curved step is obtained as

$$V_r = V_s (1 - r_c/r) \quad (1.16)$$

where r_c and r are the radii of the critical and real nuclei respectively and V_r and V_s are the velocities of the curved and straight step.

The radius of curvature r of the steps is derived in Cartesian co-ordinates by considering a portion of a circular step, $y = f(x)$ as

$$r = [1 + (y')^2]^{3/2}/y'' \quad (1.17)$$

The velocity normal to a rotating spiral step is given by the relation

$$V_r = r_o \omega / [1 + r_o^2 (d\theta/dr_o)^2]^{1/2} \quad (1.18)$$

where ω is the rotational velocity, r_o is the radius vector and $d\theta$ is an infinitesimal rotation during which the radius changes by dr_o

The velocity of the growing step along the radius of curvature V_r is related to the velocity of a straight step on the surface by (1.16) and therefore

$$V_s (1 - r_c/r) = r_o \omega / [1 + r_o^2 (d\theta/dr_o)^2]^{1/2} \quad (1.19)$$

which for large values of r_o reduces to give

$$\theta = (\omega/V_s) r_o + \text{constant} \quad (1.20)$$

and for small values of r

$$\theta = (1/2r_c)r_o + \text{constant} \quad (1.21)$$

Equations 1.20 and 1.21 represent spiral with constant step spacing, $S_c = 19 r_c$. The spiral growth mechanism was shown to be favourable for the rate versus supersaturation data for growth from vapour measured by Volmer and Schultz /8/. Growth spirals is said to have been observed /10/ on paraffin crystals by Heck, although these were not recognized as growth spirals because this concept was not then developed. Griffin /11/ and later a number of others observed growth spirals through optical and electron microscopic observation techniques /12, 13/. Growth spiral concept is now generally known in crystal growth community and among scientists working in areas where crystallization plays an essential role.

The recent developments in the theory of crystal growth using as a frame of reference the BCF paper /7/, have been mentioned in a recent review by Bennema /14/. It is shown here how and where the BCF theory contributed to a narrowing of the gap between theory and experiment.

1.1.3. GROWTH OF CRYSTALS FROM SOLUTIONS

Growth from pure solutions

During the growth from pure solutions a solute molecule must

break the bonds it has with the solvent and make new bonds in the crystal. It is believed that new molecules are added only at kinks in steps present on the close packed faces of a growing crystal after a crystal has been growing steadily for some time. The kinks on the monomolecular steps are so numerous /7/ that the steps behave as continuous line sinks with a velocity independent of crystallographic orientation and a more or less circular shape indicating the location of the source from which they originated.

The path taken by the solute molecules from the solution to a kink site is not certain. Deposition may either occur directly at the step via volume diffusion or solute molecules may become absorbed on the surface and migrate to the steps by surface diffusion. Both processes are considered to be active in most cases. Their relative importance should depend on the ratio, $D_v C_{ve} a / D_s C_{se}$, where D_v and D_s are the volume and surface diffusion coefficients, C_{ve} and C_{se} are the equilibrium concentrations of solute in the solution and absorbed on the surface, and a is the height of a step. The kinetics of crystal growth can be considered in terms of a) the creation of steps at certain sources and b) their motion away from the sources. Since the flow of steps away from a source has an influence on the rate of step creation, the latter part is considered first.

Flow of steps

It is clear that the velocity of a step will depend on the proxi-

mity of other steps on the surface, for, nearby steps absorb some of the solute. Consider, for example, a series of uniformly spaced straight steps of height, a , separated by distances n^{-1} , where, n is the density of steps normal to their direction of motion. When the steps are very far apart, the velocity of each will be maximum. As the spacing between steps decreases their velocity decreases, becoming a minimum for $na = 1$. In order to understand whisker growth and morphology changes it is also necessary to consider steps which have a step height equal to a multiple of the lattice spacing.

An expression for the flow rate ν giving the number of lattice planes passing a given point on the surface per unit time, can be obtained as a function of 'n'. The relationship between ν and n has been shown by Cabrera /15/ to have the form shown in Fig. 1.1. ν is the value of the rate of lattice planes past a point, ν_{∞} is the maximum value of ν .

Sources of steps

Two main types of sources of steps can be distinguished: 1) points of the crystal surface where dislocations with Burgers vector having non-zero component normal to the surface terminate and 2) surface nucleation at any point on a perfect crystal surface.

According to Cabrera and Levine /16/, dislocations should be

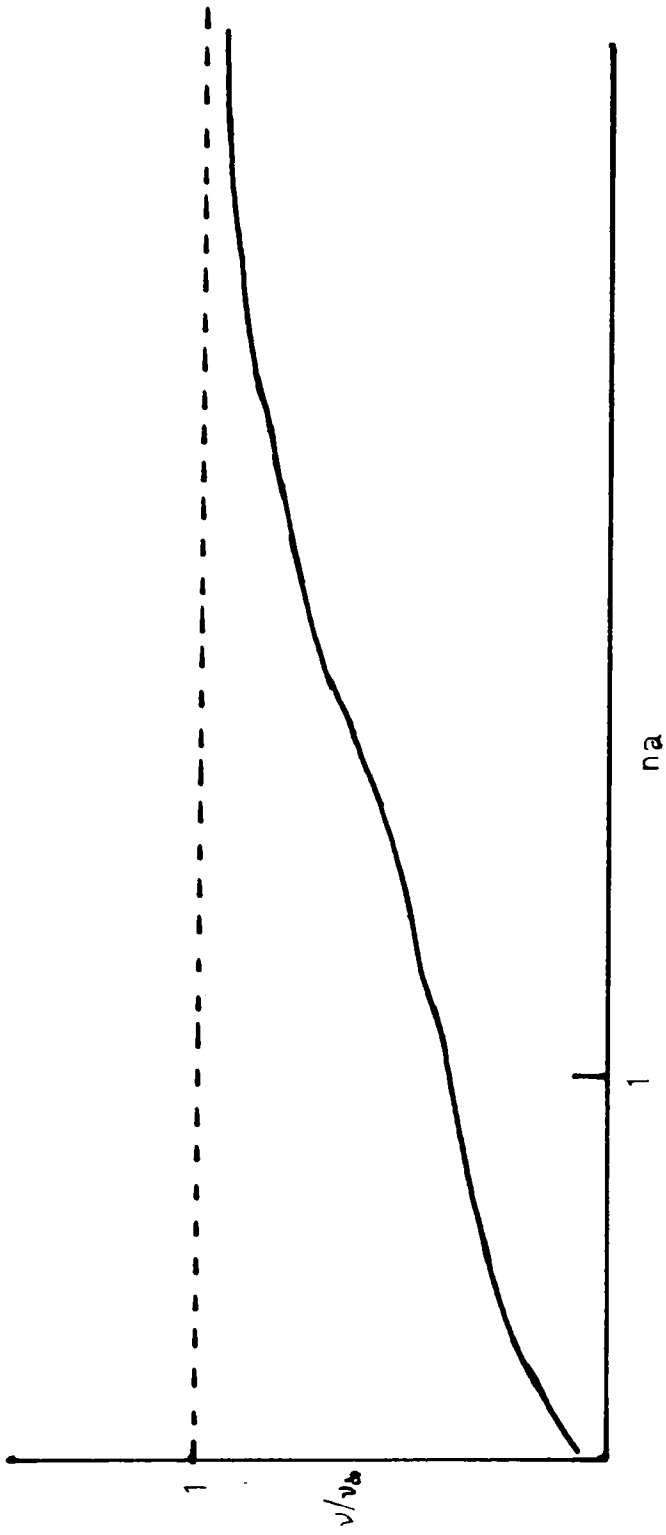


Fig.1.1 Theoretical curve showing the variation of ν/ν_b with na .

the only possible sources at very low supersaturations when there is no diffusion field near the source. Under these conditions, the rate of formation of new steps at the source

$$\nu_0 = \nu_0 / 19 \rho_c \quad (1.22)$$

where ρ_c is the medium radius of curvature of the step corresponding to the supersaturation σ and is given by

$$\rho_c = \gamma \nu / kT \ln(1 + \sigma) \approx \gamma \nu / kT \sigma \quad (1.23)$$

where γ is the surface energy of the edge of the step and ν is the volume of crystal per molecule. Under steady state conditions the step winds itself into a spiral so that the density of steps away from the source satisfies $\nu_0 = \nu$ and hence

$$n = 1/19 \rho_c \quad (1.24)$$

since ν_0 and ρ_c^{-1} are both proportional to σ , ν_0 is proportional to the square of the supersaturation.

For surface nucleation at any point on a perfect crystal surface, new steps must arise by repeated nucleation on the perfect surface of the crystal. Such a process generally requires a very large supersaturation and is observed only rarely.

Two important conclusions of the theory regarding growth in pure solutions are that a single dislocation should be sufficient to grow a large crystal and no mechanism is available for the introduction of further dislocations. But, the presence of a small concentration of impurities, provide a simple mechanism for the introduction of dislocations during growth.

Growth from impure solutions

The growth of crystals from solutions containing other solutes, colloidal particles or suspended material is much more complicated than growth from pure solutions. However, the growth of real crystals generally occurs in such solutions, and to grow useful crystals it is very often necessary to make minor additions to the growth solution in order to influence the growth in some desirable way. An understanding of impurity effects is thus of great interest. The effects of impurities on growth kinetics is briefly discussed below.

The rate of growth is often altered by the presence of impurities, usually by way of reducing the growth velocity at a given supersaturation. The effectiveness of an impurity in reducing the growth rate decreases with temperature /17/. In certain cases addition of impurities results in the increase of growth rate at a given supersaturation. For example, halide ions are known to facilitate reactions at mercury electrodes /18/ and an increase in the rate of growth in thickness of thin plates of lithium fluoride is brought about by additions of 2×10^{-6} mole fraction of ferric fluoride /19/.

If the impurity molecules are immobile on the surface so that they will remain at the points where they reached the surface, the average velocity of advancing step is reduced by the impurities. It is shown that there is a critical supersaturation below which growth is extremely slow. Behind regions of very high impurity content bunch-

ing of steps occurs producing dislocations. In the case of mobile adsorbed impurities, the decrease in velocity due to the impurities will be small. Thus immobile impurities are more effective than mobile ones in retarding and in ultimately stopping the flow of steps and consequently the growth of large crystals.

1.2. TECHNIQUES OF CRYSTAL GROWTH

The discovery of new properties and applications may be said to be directly related to the availability of a large range of single crystals. This section deals with the techniques of crystal growth currently employed.

1.2.1. GROWTH FROM MELT

Growth from melt is by far the fastest of the growth methods, as its rate does not depend on mass transport process. In principle, the crystals of all materials can be obtained from melt, provided they melt congruently, they do not decompose before melting and they do not undergo a phase transformation between the melting point and room temperature.

Czochralski method

In this method the melt is contained in a crucible. A seed fixed

to a holder is brought into contact with the melt and after equilibrium is reached, the seed is pulled along with rotation during growth. Rotation of seed and crucible are employed to optimise compositional and thermal homogenization of the melt and to control the geometric configuration of the crystal. Growth is generally carried out in controlled atmosphere or in vacuum. This method is widely used in silicon industry. Numerous other materials including oxides such as sapphire and ruby can be grown by this method.

The major advantages of this method are that; growth from a free surface accomodates the volume expansion associated with solidification of many materials such as semiconductors; complications that may arise due to wetting of the container by the melt is eliminated; large single crystals can be obtained at high speeds; high crystalline perfection can also be achieved; the method is convenient for doping; during growth the desired ambient atmosphere can be used, controlled and changed. However, the method does not lend itself readily to the growth of materials whose vapour pressure or that of one of their constituents is high at the melting point. The requirement for a crucible in Czochralski growth introduce the possibility of contamination of melt.

Normal freezing and zone melting

In the normal freezing method, the charge is contained in a clo-

sed container which can be mounted horizontally or vertically. A boat can also be used as a container. If a seed is not used, the entire charge is melted; solidification is initiated and the solid-melt interface is advanced horizontally by moving the container through a furnace with appropriate thermal gradients or by moving the furnace past the container. The interface can also be advanced by controlled power reduction. For obtaining specific orientation, a seed is commonly used at one end of the container. Single crystals with a preferred orientation are usually grown using a container with a tapered end. Vertical normal freezing, by advancing the growth interface upwards yields better crystals in some cases. Normal freezing methods are extensively used for growing single crystal of materials with volatile constituents.

In zone melting a molten zone is established at one end of the charge and is advanced by moving either the container or the furnace. By this method a homogeneous distribution of impurities can be achieved. Zone melting is best known as a purification method.

Directional solidification methods are simple and versatile. The vapour pressure of volatile constituents can be easily controlled in directional solidification methods. Growth can be carried out in evacuated and sealed containers. Shape and size of the crystal can also be controlled. Furthermore, growth can be carried out under stabilized thermal gradients which minimize convective interference in

growth and segregation.

The confining configurations in these methods present some limitations. When volume expansion is associated with solidification, pressure can be exerted to the growing crystal leading to high densities of lattice defects.

Float-zoning

Float-zoning is essentially zone melting in a vertical configuration without a container. The zone is sustained by surface tension forces. Thus this method is suitable for materials with high surface tension and low density. The earliest of the crucibleless technique is the Verneuil technique; a molten zone is formed on the top of the seed crystal with an oxygen hydrogen flame or r.f. heating; to the zone powder of the material is fed and growth proceeds by lowering the seed.

The unique advantage of float-zoning is the elimination of the melt container which reduces contamination. The instrumentation for float zoning is relatively simple for small diameter crystals. This method cannot be used for the growth of materials with high vapour pressure or of materials with volatile constituents.

1.2.2. GROWTH FROM SOLUTION

In this process, a saturated solution of the material in an appropriate solvent is used, from which crystals grow after the solution is supersaturated by evaporation of the solvent or by lowering the solution temperature. Solution growth is generally simple and inexpensive. Materials which melt incongruently, decompose before melting or undergo a phase transformation between the melting point and room temperature are grown from solutions. The methods of solution growth are usually classified according to the type of the solvent used. They are mainly aqueous-solution, molten-salt (flux), metallic solution and hydrothermal growth.

Aqueous solution growth

The method rests on obtaining supersaturation without inducing spontaneous nucleation so that growth can proceed on the seed. Supersaturation can be achieved either by evaporation of the solvent or by decrease of the solution temperature.

The method is often simple and inexpensive. It can lead to good quality crystals and lends itself to continuous operation. The growth can be visually inspected. The method is slow and has thus limitations for industrial production.

Flux growth

In this method molten salts are used as solvents. For oxides and solid solutions of oxides which have very high melting points and/or decompose prior to melting these are the only satisfactory solvents. Molten salts of such composition should be contained in platinum or irridium crucibles. Growth from molten salts is obtained by decreasing the temperature of a saturated solution to acquire supersaturation. Seeds are commonly used and these can be withdrawn before the solution is solidified.

Flux growth is carried out at much lower temperatures than corresponding growth from melt. A distinct advantage of the method is that this is the only method for obtaining certain oxide solid solutions. However flux growth is very slow and require precise temperature control. The purity of the crystals grown by this method is often marginal. Flux growth is an expensive technique.

Metallic-solution growth

Single crystals of metallic phases and inorganic compounds are readily obtained by solidification of saturated metallic solutions. Diamonds are being commercially prepared from transition-metal solutions under high pressure. Growth from metallic solution is now widely used for preparation of high quality epitaxial layers and solid solut-

ions of III-V compounds.

In the case of semiconductors the crystalline perfection attained by LPE is better than that by melt growth. The thickness of LPE layers can be controlled to within several hundred angstrom units. The limitations of this method is that the growth is slow and is limited to small crystals or relatively thin layers. The purity of the crystal is limited by the purity of the solvent.

Hydrothermal growth

The technique is basically the same as the aqueous solution growth at elevated temperatures and pressures. The method is primarily used for the growth of large high quality α -quartz crystal used for piezoelectric applications.

In the growth of quartz, α -quartz nutrient is used in an autoclave containing aqueous solution of a base (NaOH). Growth is carried out at about 400°C and pressure of about 2000 bars. High quality large size quartz crystals are obtained by this method. In the hydrothermal method, the major disadvantage stems from the requirements of autoclaves at elevated temperatures and pressures. Besides, considerable period of time is required for growing large crystals.

1.2.3. GROWTH FROM VAPOUR

Bulk crystals as well as thin layers are prepared from vapour phase. Since gases can in general be obtained at very high purity and high purity conditions can be maintained during gaseous processes, vapour phase growth can lead to high purity crystals. The method is extensively used for the growth of high quality thin layers of materials such as Si, II-VI and III-V compound semiconductors; layers of metals and other inorganic compounds can be prepared from the vapour phase. Growth from the vapour phase can be obtained without involving chemical reactions. When chemical reactions are involved they can be irreversible or reversible. Successful growth from vapour phase requires knowledge of the thermodynamic equilibrium among the reacting vapour constituents which may involve species other than the initial species. The kinetics of vapour growth are critically dependent on the concentration or the diffusion of the desired reacting species. The transport and/or equilibria of the species are often controlled by the use of carrier gases.

In the irreversible reaction, the reactants are brought into contact with the seed material at the appropriate temperature and pressure of the reaction. Where the products are not recycled an open tube arrangement is usually employed. This method is widely used in the preparation of Si layers. The thickness and doping level of the layers is readily controlled and very high purity materials are obtai-

ned by this process. But the process is slow.

In the reversible reaction, the solid material can be brought into the vapour phase and then reformed under controlled conditions by reversing the direction of the reaction. Epitaxial layers of III-V compounds and solid solutions of these compounds are prepared by employing appropriate reversible reactions.

This is a method with which single crystals and epitaxial layers of high chemical purity and crystalline perfection can be obtained. The thickness and the doping of the layers can be closely controlled and the process can be recycled. But since the growth is slow, the method is not practical for bulk single crystals.

1.2.4. GEL GROWTH

Growing crystals from gel is successful in the case of materials which cannot be grown from melt, vapour and solution. A number of materials can also be grown by this method to avoid thermal strain often introduced during growth from melt and vapour. In the gel method the growth takes place at low temperatures.

One method for preparing a gel is from a solution of sodium silicate of suitable specific gravity mixed with a component of the final compound to be grown. To grow crystals, on the top of this gel the

other reactant is placed in the form of a solution. This, besides supplying the other component of the material to be crystallized, keeps the gel from drying out. The components slowly diffuse and react to form the compound. Crystals nucleate at the microflaws or dust particles in the gel. A variation of the method of growth is in using a U-tube. The gel is kept at the centre of the vertically kept U-tube. The reactants in the form of solutions, are kept above the gel in the two limbs of the U-tube.

The major factors that control the nucleation and growth of crystals are the concentration of the feed solution, the pH of the gel, aging of the gel and the gel density. The optimum values of the various parameters for a particular material is found out by trial and error.

Since the crystals in gel medium are usually grown at room temperature it will have lower concentration of non-equilibrium defects than those grown at elevated temperatures. The crystals can be observed at all stages of growth. The solute concentration at the growth boundary is self regulating in accordance with the needs of the growth process since the crystals are grown by diffusion. The gel medium provides unconstrained support for the growing crystal. The disadvantages of this method are the slow growth rate, which is essentially diffusion limited, the inability to control the nucleation, and the relatively small sizes of the crystals obtained.

REFERENCES

1. J.G.GIBBS, "Collected works", (Longman's Green and Co.,1928)
2. P.CURIE, Bull. Soc. franc. Miner. 8(1885)145.
3. W.WULFF, Z. Kristallogr. 34(1901)449.
4. A.BRAVAIS, " A Etudes Cristallographiques ",
(Gauthier Villars, Paris, 1866).
5. L.SOEHNCKE, " Entwicklung einer Theorie de.
Kristallstruktur ", (Leipzig, 1879).
6. W.KOSSEL, Nachr. Ges. Wiss. Göttingen, Math-Physik., Kl.(1927)135.
7. W.K.BURTON et al., Phil. Trans. Roy. Soc. London A 243(1951)299.
8. M.VOLMER and W.SHULTZ, Z. Phys. Chem. A 156(1931)1.
9. A.SMEKAL, Handb. Phys 24(1933)795.
10. F.C.FRANK, " Growth and perfection of crystals "
(Wiley, N.Y., 1958).
11. L.J.GRIFFIN, Phil. Mag. 41(1950)196.
12. A.L.VARMA, " Crystal growth and dislocations ",
(Butterworths, London, 1953)
13. W.DEKEYSER and S.AMELINCKX, " Les-Dislocations et la Croissance
Cristalline ", (Paris, 1955).
14. P.BENNEMA, J. Cryst. Growth 69(1984)182.
15. N.CABRERA and D.A.VERMILYEA, " Growth and perfection
of crystals ", (Wiley, N.Y.,, 1958).
16. N.CABRERA and M.M.LEVINE, Phil. Mag. 1(1956)450.
17. H.C.BUCKLEY, " Crystal growth ", (Wiley, N.Y.,1958).
18. J.E.B.RANDLER and K.W.SOMERTON, Trans. Far. Soc. 52(1948)951.
19. G.W.SEARS, J. Chem. Phys. 24(1956)868.

CHAPTER TWO
DISLOCATIONS AND ETCHING

The concept of dislocations originated at the outset of twentieth century and developed mainly by the middle of the century. The classical treatises of Read /1/, Cottrell /2/ and Friedel /3/ were milestones in the development of the theoretical and experimental study of dislocations. The presence of dislocations are known to alter the plastic, electric, magnetic, super conductive, piezoelectric, dielectric etc. properties of crystals.

Etching is one of the widely used techniques to reveal dislocations in crystals. Excellent reviews on the etching of non-metallic crystals are found in literature /4, 5/. Although etching was first applied to dislocations /6/, its domain has expanded to various other fields in defect studies

The first part of this chapter deals with dislocations in crystals, types of dislocations, simple theory of dislocations and observation of dislocations. In the second part, etching of crystals, methods of etching, theories of etching and information obtainable from etching are presented.

2.1 DISLOCATIONS IN CRYSTALS

A perfect crystal is built up from a unit cell by means of a

set of translations,

$$\vec{b} = n_1 \vec{a}_1 + n_2 \vec{a}_2 + n_3 \vec{a}_3 \quad (2.1)$$

where n_1, n_2, n_3 are integers and $\vec{a}_1, \vec{a}_2, \vec{a}_3$ are three non-coplanar basis vectors of the Bravais lattice of the crystal. But a real crystal differs from this periodicity of its unit cell due to the defects which often strongly alter its properties. Such defects can be grouped into four categories, namely, 1) point defects, 2) line defects, 3) surface defects and 4) volume defects. Dislocations are linear defects found in crystals which are produced due to internal stresses.

The most general way to create a dislocation in a crystal with cubic structure is to cut the crystal along a surface bounded by a line and to open the lips of the cut to an angle 90° in order to be able to introduce a crystalline section which can be perfectly stuck inside the lips

Burgers circuit

Consider a translation dislocation obtained from a perfect crystal by a cut and slip of lips relative to each other. If a large circuit is made around the zone of bad crystal it does not close with one to one correspondence with the points of perfect crystal. The vector which must be added to close the circuit is called Burgers vector and the circuit Burgers circuit.

2.1.1 TYPES OF DISLOCATIONS

The two major types of dislocations according to Friedel /3/ are rotation dislocations and translation dislocations. Rotation dislocations occur rarely because of their large elastic energy and is not thus discussed.

Translation dislocations of special interest are edge and screw dislocations. An edge dislocation whose geometry is shown in Fig. 2.1a has Burgers vector perpendicular to the dislocation line. This type of dislocations was introduced in the study of plasticity by Prandtl /7/. The Burgers vector of a screw dislocation is parallel to the dislocation line (Fig. 2.1b). It is produced by a shear of lips cut parallel to the dislocation line. Screw dislocations were first studied by Orowan /8/. A dislocation may be considered to have, in general an edge and a screw component. Since the dislocation line represents the boundary between the slipped and unslipped portions of a crystal, it must either intersect the surface of the crystal or close upon itself within the crystal. The dislocation may of pure edge character in some places of the crystal, pure screw in others and hybrid of both in yet other places. The Burgers vector of a hybrid dislocation makes an angle with the dislocation line.

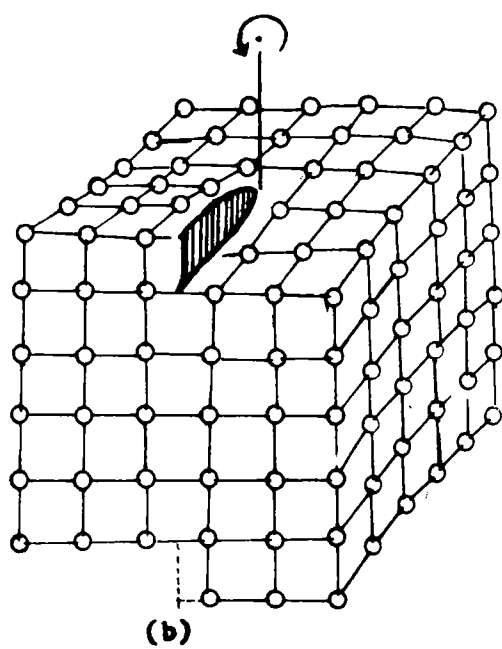
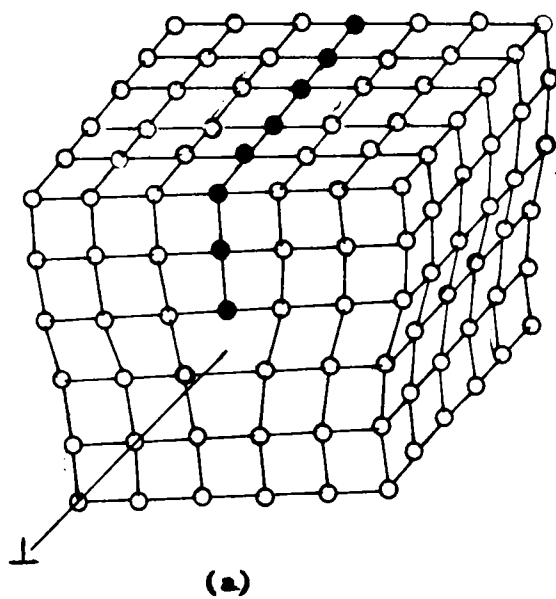


Fig.2.1

Fig.2.1 (a) Geometry of an edge dislocation.

(b) Geometry of a screw dislocation.

2.1.2 SIMPLE THEORY OF DISLOCATIONS

Dislocations cause strains and stresses in a crystal. This increases the elastic strain energy stored. Consideration of the energy of dislocations can be used to explain the following: 1) why moving a dislocation requires low energy compared to moving a whole atomic plane the same way through, 2) the reason for the increase in hardness with increase in strain for crystalline material, 3) the softening of a material by annealing and recrystallization, 4) why low angle grain boundaries form and are stable, 5) why dispersion and precipitation hardening increase the yield stress of crystals, 6) the reason for break of dislocations into partial dislocations and 7) why etch pits indicate the presence of dislocations.

Energy of dislocation

Consider a cylindrical crystal of length 'l' with a screw dislocation of Burgers vector \vec{b} along its axis. The elastic shear strain S in a thin annular section of radius 'r' and thickness dr is,

$$S = b/2\pi r \quad (2.2)$$

where $b = |\vec{b}|$. The energy per unit volume, dE/dV , of the annular region is then,

$$dE/dV = 1/2 GS^2 = G/2 \times (b/2\pi r)^2 \quad (2.3)$$

where G is the elastic shear modulus. By integrating the expression for dE between the limits b and the dimension of the crystal, the

energy of a screw dislocation is obtained as,

$$E \approx 1Gb^2 \quad (2.4)$$

and the energy of an edge dislocation is approximately given by,

$$E \approx 1Gb^2/1-\nu \quad (2.5)$$

where ν is Poisson's ratio. If $\nu = 1/3$, the energy of an edge dislocation is about 3/2 that of a screw dislocation of the same length. Since the energy of edge and screw type dislocations is proportional to b^2 , stable dislocations are those with minimum Burgers vectors.

2.1.3 OBSERVATION OF DISLOCATIONS

A number of methods exist for direct and indirect observation of dislocations. Amelinckx /9/ has reviewed the methods of direct observation of dislocations. The four major categories of these methods are, 1) surface methods, 2) bulk methods, 3) thin film methods and 4) field emission and field ion microscopy.

In the surface methods the first phenomenon to be related to dislocations was crystal growth on close-packed faces and at low supersaturations /10/. Direct evidence for the occurrence of spirals at dislocation sites was obtained by Griffin /11/ on surfaces of beryl crystals. Evaporation, which may be considered as the reverse of growth, under conditions of low under saturation also produces spiral steps related to dislocations. The method was first applied to alkali halides /12/. Etching is considered to be one of the simplest methods

to reveal sites of dislocations. The first direct proof of the applicability of etching to reveal dislocations was given by Gevers et al. /13/ and Horn /14/. Etch pits located at the centers of spirals are attributed to screw dislocations and those located elsewhere are attributed to edge dislocations. The study of cleavage steps provides a limited amount of information on the geometry of dislocations /15/. Slip steps caused by the movement of dislocations have been recorded. Bassett /16/ has revealed slip step traces left by individual dislocations in KBr.

In the bulk methods dislocations are revealed along their length. Decoration technique, which consists in heating a crystal in such a way as to produce visible particles along the dislocation lines, is a simple bulk technique. Different methods are used for specific crystals /9/. A number of X-ray methods are available which reveal images of individual dislocations. X-ray methods are one of the most widely used methods /17, 18/. The birefringence method for observation of dislocations is based on the fact that an isotropic crystal becomes birefringent when stressed. NaCl, for example can be made strongly birefringent by deformation. Kear et al. /19/ have correlated the birefringence bands in LiF with etch pits.

One of the most versatile methods for studying dislocations in thin crystals is transmission electron microscopy developed mainly by Hirsch et al. /20/ and Bollmann /21/. Transmission electron microscopy is used to observe individual partial dislocations in a ribbon,

dislocation reactions in particular structures, dislocation net works in certain structures, dislocations resulting from the agglomeration of point defects, role of dislocations in plastic deformation, the arrangement of dislocations in deformed metals, mechanical twinning, recrystallization, phase transformation, interaction of impurities and dislocations, thin plate effects etc. With high resolution microscopes it is possible to resolve the individual lattice planes in suitably chosen thin crystals and as a consequence to observe the presence of dislocation directly. Moire patterns are used to determine dislocation densities, movement of dislocations etc. The first moire patterns were reported by Mitsuishi et al. /22/. Drechsler /23/ has attributed the spiral features observed in the field ion microscope, while subjecting a tungsten tip to field evaporation, to screw dislocations. Well resolved images of the core structure of edge dislocations in molybdenum are obtained by Brandon and Wald /24/.

2.2 ETCHING OF CRYSTALS

Etching is widely accepted as a powerful tool for the detection and characterisation of crystal defects, especially dislocations. Although a number of general principles have been formulated over the years, etching techniques are still based on a qualitative and empirical basis.

The method of etching consists in immersing the crystal in a

suitable medium which may be a pure liquid, a solution or a gas. Small pits nucleate and grow at the emergence points of dislocations. Dislocation etchants are different for specific crystals and there is no hard and fast rule to find out the dislocation etchant for a specific crystal.

2.2.1 METHODS OF ETCHING

Different methods exist for the successful etching of a crystal. Some of the well accepted methods are thermal etching /25/, chemical etching /26/, solution etching /27/, preferential oxidation /28/, electrolytic etching /29/, cathodic sputtering /30/ and hydrothermal etching /31/.

2.2.2 THEORIES OF ETCHING

Different theories of dissolution exist in literature which may be used to explain the etching phenomenon. As the work reported in this thesis is on organic crystals, an attempt is made to summarise the existing theories of dissolution relating to nonmetallic crystals. Among the different theories of dissolution, thermodynamic and topochemical theories deal with the formation of dislocation etch pits on crystal surface. Heimann /32/ has provided a comprehensive account of the different types of theories.

The topochemical adsorption theories express the dissolution

rate in terms of chemical reactions on crystal surface /32, 33/. Enhanced dissolution caused by preferred adsorption of a reactant at the dislocation sites leads to etch pit formation. The enhanced dissolution at dislocation sites is due to the strain associated with dislocations. Better contrasting pits are produced by the more absorbing reactants. Although topochemical theories explain the etch pit formation in crystalline substances which involve the formation of reaction products, serious limitations arise from the facts that each etching system has to be treated independently and the details of the adsorption process are not very clear.

The energy localized in the vicinity of a dislocation lowers the free energy required for the nucleation of a cavity of unit depth in the surface at the site of the dislocation. This decrease in free energy causes the preferred dissolution of the surface at the emergence points of dislocations. This is the basis of the thermodynamic theories of dissolution. The free energy change with the formation of a mono-molecular pit at the dislocation site is given by

$$\Delta G = 2\pi r a \gamma - \pi r^2 a \Delta\mu / \nu - a E_d \quad (2.6)$$

where r is the radius of the cavity, a is its height, $\Delta\mu$ the change in free energy during dissolution, ν the molecular volume of the crystal, γ the specific surface free energy of an atom or molecule going from the solid surface into the solution. The change in free energy during dissolution is given by

$$\Delta \mu = -kT \ln(c/c_0) \quad (2.7)$$

where c_0 is the saturation concentration of the material in an etching medium and c is the actual concentration at the dislocation site. The localised energy per unit length at a dislocation, E_d , is given by

$$E_d = \alpha G b^2 / 4\pi (r_1/r_0) \quad (2.8)$$

in Schaarwachter's theory /34/, where α is a constant equal to about 1.5 or 2 for screw or edge dislocations respectively, G is the shear modulus, b is the magnitude of the Burgers vector, r is the outer radius of the strained region of the crystal, r_0 is the radius of the dislocation core beyond which elasticity theory holds. The maximum free energy change is

$$\Delta G_n = p \Delta G_s \quad (2.9)$$

$$\text{where } p = (1 - \alpha q G b / 4\pi \nu)^2 \quad (2.10)$$

$$\text{and } \Delta G_s = \pi E^2 a^{-2} / m \quad (2.11)$$

with the value of constant $q \approx 0.1$. Since the value of G/ν^2 for the same plane of similar type of crystals is almost a constant /35/, the value of p decreases with an increase in the hardness of the crystal.

The rates of dissolution along the dislocation line, v_n , and along the surface, v_s , are given by /34/ as

$$v_n = a \nu \exp [-(\Delta G_n + \Delta H) / kT] \quad (2.12)$$

$$v_s = \sigma \times \beta \nu \exp [-\Delta H / kT] \quad (2.13)$$

where ν is a frequency factor, ΔH the free energy change for a molecule

going from the crystal surface into the solution, a the monomolecular pit height, $\sigma = 1 - c/c_0$ the undersaturation, x_s is the mean displacement of an atom diffusing from a kink site to an adsorbed position, $\beta \leq 1$ is a factor which accounts for the hindrance of the motion of ledges in the presence of an impurity. The quantity $k^* = \beta x_s / a$ is defined as the ledge mobility factor. For large undersaturation the pit slope is obtained by the relation

$$v_n/v_s = 1/k^* \exp(\pi p a \nu^2 / \Delta\mu kT) \quad (2.14)$$

The parameters which determine the pit slope in equation (2.14) are k^* , $\Delta\mu$, ν and p . Smaller values of k^* , p and ν and a large value of $\Delta\mu$ lead to the formation of pits with greater contrast.

2.2.3 RELIABILITY OF A DISLOCATION ETCHANT

There are a number of methods to check the reliability of an etchant. One of the methods is to introduce a known number of dislocations into a crystal by bending it to a given radius of curvature and to compare the calculated and the observed dislocation densities [36]. This method is not suited for many nonmetallic crystals. The mirror image correspondence of etch patterns on matched cleavages provides another simple test for a dislocation etchant. This is perhaps the most widely used method to prove the reliability of an etchant in the case of crystals having a cleavage plane. If crystals can be obtained in thin plates, a one to one correspondence of etch pits on opposite sides can be a proof for the reliability of an etchant.

One to one correspondence of pits on successive layers and etching of grain boundary are also well accepted as definite proofs for a dislocation etchant. A comparison with an independent method such as decoration, X-ray topography etc. can be used to establish a dislocation etchant for a crystal. Dash /37/ has shown that decorated dislocation line corresponds with every etch pit in the case of silicon. B. Van der Hoek et al. /38/ has shown that the number of etch pits is roughly equal to (and often even higher than) the total number of dislocations revealed by Lang topography on the same face of potash alum and has shown the correlation between etch pits and dislocations.

2.2.4 INFORMATION OBTAINABLE FROM ETCHING

Since dislocation etching produces etch pits at the emergence points of dislocations, dislocation sites can be ascertained from etching. The etch pits give a measure of dislocation densities. Since the etch pits have certain depth they may also give some indication concerning the direction of dislocation lines /39, 40/. Gradual removal of the surface layers alternated with etching is a powerful technique for exploration of the spatial configuration of dislocations /41, 42/. Movement of dislocations can be easily observed by etching technique. A flat bottomed pit results if a dislocation moves out of a pit produced by a first etching. This is because further etching only develops the pit laterally. The etching technique is of special importance for the study of dislocation motion as etch pits do not

pin dislocation very much. Dislocation loops, helices, spirals and half-loops can be easily observed by etching /43, 44/. Tracks due to fission fragments and debris left by moving dislocations also are etched. Dislocations parallel to and close to the surface are etched as grooves /45/.

Etching technique can be applied to a number of dislocation problems. One of the important problems solved by etching is the experimental determination of the stress velocity relationship for individual dislocations by Johnston and Gilman /46/. The distribution of dislocations in slip traces and deformation bands can be revealed by etching and deductions concerning the deformation process, glide planes, dislocation density, distribution etc. can be made. Pileups against boundaries, sub-boundaries and intersection points of glide traces are often observed /47/. Dislocation multiplication and movement can be studied by etching technique. Johnston and Gilman /48/ have employed etching to study the mechanism of multiplication of dislocations in deformed lithium fluoride. Etch pit studies have contributed considerably in elucidating the origin of dislocations in melt grown crystals /49/. Systematic etch pit studies in germanium and silicon crystals have been helpful to devise methods to eliminate dislocations in them /50/. Etching has illustrated convincingly the mechanism of polygonization /51/. The displacement of dislocations in a direction perpendicular to their glide planes has been demonstra-

ted by Gilman and Johnston /52/ by etching before and after heat treatment. Radiation hardening of a crystal can be accurately measured by comparing the distance travelled by dislocations under the influence of a constant load. The rosette patterns associated with an indentation can be easily revealed by etching. The relation between the initiation of cracks and pile ups of dislocations has been studied extensively by etch pits /53/. In polar crystals positive and negative dislocations are distinguishable by etching. Dislocations accompanying electrical breakdown, surface pits due to vacancy condensation etc. can be successfully observed by the simple etching technique. Etching is also used for the study of grain boundaries /54, 55/, stratigraphical patterns /56, 57/, striations /58, 59/, twinning /60/, stacking faults /59, 61/, inhomogeneity in growth and crystallinity /59, 62/, microdefects, cloud defects, precipitates, inclusions, impurity centers etc. /63-67/, strain fields and microplasticity characteristics /68, 69/, orientation determination of crystal faces and growth directions and postulation of crystal structure models /70-73/, fracture studies /74/, magnetic domains /75/ etc. Etching is the only technique for detecting nucleation and subsequent growth of dislocations around precipitates in certain crystals /67/. Resolution of defects better than that obtained by X-ray techniques is reported by some authors /58, 68, 73, 78/. Combined with other direct dislocation observation techniques such as electron microscopy /77, 78/, X-ray topography /79, 80/, decoration /81, 82/ etc., etching has been successfully used for defect studies.

REFERENCES

1. W.T.READ, " Dislocations in crystals ", (Wiley, N.Y, 1953).
2. A.H. COTTRELL, " Dislocations and plastic flow in crystals ",
(Oxford university press, Oxford, 1953).
3. J.FRIEDEL, " Dislocations ",
(Pergamon Press, Addison Wesley, London, 1964).
4. W.G.JOHNSTON, " Progress in ceramic science ",
(Pergamon press, N.Y., 1962)
5. K.SANGWAL, J. Mater. Sci. 17(1982)2227.
6. R.GEVERS, Nature 171(1953)171
7. L.PRANDTL, Z. Angew. Math. Mech. 8(1928)85.
8. E.OROWAN, Z. Physik 89(1934)614.
9. S.AMELINCKX, " The direct observation of dislocations ",
(Academic press, N.Y., 1964).
10. W.K.BURTON et al., Phil. Trans. Roy. Soc. A243(1951)299.
11. L.J.GRIFFIN, Phil. Mag. 43(1952)651.
12. S.AMELINCKX and E.VOTAVA, Nature 172(1953)538.
13. R.GEVERS et al., Naturwissenschaften 39(1952)448.
14. F.H.HORN, Phil. Mag. 43(1952)1210.
15. S.AMELINCKX, Nature 169(1952)580.
16. G.BASSETT, Phil. Mag. 3(1958)1042.
17. A.R.LANG, Acta Cryst. 12(1959)249.
18. J.NEWKIRK, J. Appl. Phys. 29(1958)995.
19. B.H.KEAR et al., Phil. Mag. 4(1959)665.
20. P.B.HIRSCH et al., Phil. Mag. 1(1956)677.

21. W.BOLLMANN, Phys. Rev. 103(1956)1588.
22. T.MITSUISHI et al., Proc. Japan Acad. 27(1951)86.
23. M.DRECHSLER, Z. Metallk 47(1956)305.
24. G.BRANDON and W.WALD, Phil. Mag. 6(1961)1035.
25. A.A.HENDRICKSON and E.S.MACHLIN, Acta Met. 3(1955)64.
26. A.R.PATEL and A.V.RAO, J. Cryst. Growth 47(1979)213.
27. K.SANGWAL and J.N.SUTARIA, J. Mater. Sci. 11(1976)2271.
28. F.W.YOUNG and A.T.GWATHEMY, J. Appl. Phys. 31(1960)225.
29. P.A.JACQUET, Acta Met. 2(1954)770.
30. G.K.WEHNER, J. Appl. Phys. 29(1958)217.
31. N.K.GUPTA and P.N.KOTRU, Cryst. Res. and Tech. 16(1981)457.
32. R.B.HEIMANN, " Auflösunf von Kristallen ",
(Springer-Verlag, Wein, N.Y., 1975)
33. K.SANGWALL, J. Mater. Sci. 15(1980)237.
34. W.SCHAARWACHTER, Phys. Status Solidi 12(1965)375.
35. K.SANGWAL, Cryst. Res. Technol. 17(1982)K21.
36. F.L.VOGEL, Acta Met. 3(1955)95.
37. W.C.DASH, " Dislocations and mechanical properties of
crystals ", (John-Wiley, N.Y.,1957).
38. B.VAN DER HOEK et al., J. Cryst. Growth 61(1983)181.
39. A.R.PATEL, Physica 27(1961)1097.
40. B.J.MEHTA and J.R.PANDYA, Surface Technology 15(1982)141.
41. S.AMELINCKX et al., Phil. Mag. 2(1957)48.
42. K.TAKAGI et al., J. Cry. Growth 48(1980)19.
43. G.G.MURADYAN et al., Sov. Phys. Crystallogr. 26(1981)352.

44. E.LENDVAY, J. Cry. Growth 59(1982)375.
45. E.B.GOROKHOV, Izv. Aka. Nau. SSSR, Neorg.
Mater. 18(1982)885.
46. W.G.JOHNSTON and J.J.GILMAN, J. Appl. Phys. 30(1959)129.
47. Y.T.CHOU and R.W.WHITMORE, J. Appl. Phys. 32(1961)1920.
48. W.G.JOHNSTON and J.J.GILMAN, J. Appl. Phys. 31(1960)632.
49. E.BILLIG, Proc. Roy. Soc., A235(1956)37.
50. W.C.DASH, J. Appl. Phys. 30(1959)459.
51. S.AMELINCKX and R.STRUMANE, Acta Met. 8(1960)312.
52. J.J.GILMAN and W.G.JOHNSTON, J. Appl. Phys. 27(1957)1018.
53. R.J.STOKES et al., Phil. Mag. 3(1958)31.
54. P.C.CAI et al., J. Less-Com. Metals 90(1983)37.
55. W.T.READ and W.SHOCKLEY, Phys. Rev. 78(1950)275.
56. N.K.GUPTA and P.N.KOTRU, Ind. J. Pure and Appl. Phys. 19(1981)156.
57. A.R.PATEL and K.N.GOSWAMI, Acta Crystallogr. 15(1962)47.
58. G.T.BROWN et al., J. Mater. Sci. Lett. 1(1982)253.
59. P.GOLDBERG, J. Appl. Phys. 32(1961)1520.
60. M.S.JOSHI and B.T.BHOSKAR, Ind. J. Pure and
Appl. Phys. 20(1982)601.
61. M.S.ABRAHAMS and C.J.BUIOCCHI, J. Appl. Phys. 36(1965)2855.
62. T.INOVE et al., J. Cryst. Growth 55(1981)307.
63. M.TAJIMA, Jpn. J. Appl. Phys. 16(1977)1453.
64. K.TSUKAMOTO et al., J. Cryst. Growth 57(1982)412.
65. G.A.ANDREEV and V.A.KLIMOV, Sov. Phys. Solid State 23(1981)2058.
66. K.SANGWAL and M.SZURGOT, J. Cryst. Growth 58(1982)467.
67. S.R.GHADEKAR and B.T.DESHMUKH, Phys. Lett. 95A(1983)321.

68. B.DAM and W.J.P.VANENCKEVORT, J. Cryst. Growth 51(1981)607.
69. I.G.BERZINA and I.B.BERMAN, Sov. Phys. Crystallogr. 9(1964)202.
70. G.A.WOLFF et al., Zeit. für Electrochemie 61(1957)101.
71. L.YANG et al., Pract. Met. 20(1983)194.
72. I.SHIH and C.H.CHAMPNESS, J. Cryst. Growth 56(1982)169.
73. A.KOMA et al., Phys. Status Solidi 40(1970)239.
74. L.YANG and L.QUCHUN, Acta Metall. Sinica 13(1977)194.
75. J.D.STEPHENSON, Phys. Status Solidi a39(1977)89.
76. B.B.GOROKHOV, Izves. Akad. Nauk SSSR,
Neorg. Materialy 18(1982)885.
77. T.V.SAMOILOVA et al., Sov. Phys. Solid State 11(1969)966.
78. T.V.SMOILOVA and B.I.SMIRNOV, Sov. Phys. Solid State 23(1981)1351.
79. S.J.CZYZAK et al. J. Appl. Phys. 33(1962)180.
80. B.V.HOEK et al., J. Cryst. Growth 61(1983)181.
81. G.G.MURADYAN et al, Sov. Phys. Crystallogr. 26(1981)352.
82. G.A.ANDREEV and V.A.KLIMOV, Sov. Phys. Solid State 23(1981)2058.

CHAPTER THREE
DEFORMATION AND FRACTURE

Hardness, toughness and brittleness are three important mechanical parameters on which the reliability of a material for engineering applications hinges. While hardness and toughness are parameters for quantifying deformation and fracture processes of a solid, brittleness is a measure of the relative susceptibility of the material to these competing mechanical processes. Indentation technique has been accepted as the most convenient and accurate technique for the scaling of these parameters. The present chapter deals with the basic theory and techniques for the evaluation of hardness, toughness and brittleness.

3.1 INDENTATION STRESS FIELDS

The knowledge of the stress fields within the loaded system is necessary for any theory of indentation hardness and fracture. The stress field is related to the nature of the contact zone and the factor determining the boundary conditions for the field is the shape of the indenter. Two classical elastic indentation fields involve the idealized point indenter and the spherical indenter. In an isotropic, linear elastic half-space subjected to

a normal point load P , the solutions for the stress field assume the simple general form /5/

$$\sigma_{ij} = (P/\pi R^2) [f_{ij}(\phi)]_{\gamma} \quad (3.1)$$

when expressed in terms of the curvilinear co-ordinates, where R is the radial distance from the point of contact, $[f_{ij}(\phi)]_{\gamma}$ is an independent angular function which is itself a function of Poisson's ratio γ . In the case of a spherical indenter loaded into a flat specimen, the complete stress field solution is of the form

$$\sigma_{ij}/p_0 = [g_{ij}(\rho/a, z/a)]_{\gamma} \quad (3.2)$$

where p_0 is a constant nearly equal to \bar{H} , the hardness, ρ the actual distance of the point from the contact circle, 'a' is the radius of the circular elastic contact, z is the distance of mutual approach, γ is the Poisson's ratio and g_{ij} is a function of ρ/a and z/a which is a function of γ . For indenters of regular geometry such as Vickers', the stress field about the contact site has polar components of the form

$$\sigma_{ij} = Hf_{ij}(\theta, a/r) \quad (3.3)$$

where f_{ij} are dimensionless coordinate functions, 'a' a characteristic dimension of the indenter, H the hardness and θ and 'r' polar co-ordinates of the point.

3.2 HARDNESS

Hardness usually implies resistance to deformation which in turn denotes the ability of one body to resist penetration by another. When a sharp indenter is loaded onto a flat surface of a material it leaves an impression on the surface. Hardness is an indicator of the irreversible deformation processes which characterize the test material. There are three types of hardness measurements which depend upon the manner in which the hardness test is conducted, namely, 1) scratch hardness, 2) dynamic hardness and 3) indentation hardness. With scratch hardness measurement, various materials are rated on their ability to scratch one another. Hardness is measured in Mohs scale, in which ten standard minerals are arranged in the order of their ability to be scratched. In another type of hardness test the depth and width of the scratch drawn by a diamond stylus under a definite load gives the hardness /1/. In dynamic hardness measurements, the indenter is dropped on the specimen surface. The energy of impact is the measure of the hardness. Hardness is also measured in terms of the height of rebound as in the case of Shore scleroscope.

3.2.1 INDENTATION HARDNESS TESTS

Brinell hardness

The Brinell hardness test consists in indenting the surface of the solid with a ball at a definite load and for a definite time.

The diameter of the indentation is measured by a low power microscope after removal of the load. The Brinell hardness number (BHN) is expressed as the ratio of the load to the surface area of the indentation.

$$\text{BHN} = P / (\pi D/2)(D - \sqrt{D^2 - d^2}) \quad (3.4)$$

where P is the applied load in kg, D the diameter of the ball in mm and 'd' is the diameter of the indentation in mm. As a rule, the BHN of a material is constant only for one applied load and diameter of ball. Owing to elastic recovery, anomalous behaviour such as piling up or sinking in occurs affecting the hardness value.

Mayer hardness

In Mayer hardness (MH) test, the hardness is measured as the ratio of the load and the projected area of indentation.

$$\text{MH} = P / \pi r^2 \quad (3.5)$$

where P is the applied load in kg, 'r' the radius of indentation. MH is less sensitive to the applied load than Brinell hardness. For a cold-worked material the MH is essentially constant and independent of load.

Vickers Hardness

The Vickers hardness (VH) test makes use of a diamond pyramid for indentation. The pyramid has a square base and an included angle

of 136° between opposite faces of the pyramid. Vickers hardness number (VHN) is defined as the load divided by the surface area of the indentation, which is measured from microscopic measurements of the lengths of the diagonals of the impression. Lawn and Marshall have used indentation analysis for the determination of hardness /8/. Hardness is obtained from the relation

$$\text{Hardness (H)} = P/\alpha a^2 \quad (3.6)$$

where P is the load, a' is half the indentation diagonal and α is a constant whose value equals 2, all the quantities being in M.K.S units.

Rockwell hardness

The test utilizes the depth of indentation under constant load as a measure of hardness. A dead load is first applied to seat the specimen. Due to this the amount of surface preparation needed and the tendency for ridging or sinking by the indenter is minimum. Then the major load for indentation is applied, and the depth of indentation is automatically recorded on a dial gauge in terms of arbitrary hardness numbers.

Knoop hardness

When hardness is to be measured using small specimens Knoop indentation is found to be best suited. A Knoop indenter

is a diamond ground to a pyramidal form which produces a diamond shaped indentation with the long and short diagonals in the approximate ratio of 7:1. The depth of indentation is about one-thirtieth of the length of the longer diagonal. The Knoop hardness number (KHN) is the applied load divided by the uncovered projected area of indentation.

$$\text{KHN} = P/L^2c \quad (3.7)$$

where P is the applied load (kg), L is the length of the long diagonal (mm), and 'c' is a constant of the indenter.

Precautions

For accurate and reproducible results from the hardness measurements the following precautions are to be observed. 1) The indenter should be clean and well seated. 2) The specimen should be clean, dry and smooth. 3) The surface of the specimen to be indented should be flat and perpendicular to the indenter. 4) The thickness of the specimen should be at least ten times the depth of the indentation. 5) The spacing between indentations should be three to five times the diameter of the indentations. 6) The speed of application of the load should be standardised.

3.3 TOUGHNESS

Toughness is a convenient material parameter characterising fracture processes initiated by microcracks. Microcracking during

contact loading of brittle solids is a feature to a large number of applied phenomena. The shaping of brittle materials by drilling, grinding, cutting and abrasion; the damage and erosion of surface; fragmentation etc. are all closely related to the manner of initiation and propagation of microcracks. Central to the scientific analysis of such phenomena is the indentation test which historically evolves from a background of well founded principles. As early as 1881, Hertz gave a quantitative description of the cone shaped crack that runs around a contact circle and spreads downwards into one of the bodies at critical loading /4/. According to Griffith /5/ the crack is assumed to initiate at some dominant flaw in the specimen surface and then propagate into a characteristic cone in accordance with the requirements of an energy balance condition. Indentation methods are now widely used for the analysis of cracks and to evaluate toughness which is the widest accepted fracture parameter /3, 6, 7, 8, 9/.

3.3.1 MECHANICS OF INDENTATION FRACTURE

It is possible to determine the mechanics of the fracture configuration from the stress field beneath an indenter. Two important aspects of this problem are 1) crack initiation and 2) crack propagation. The first aspect deals with how and where do the cracks start and the second as to what path do the cracks take when once started and what determines the extent of their growth. In these two aspects, the initiation of cracks is less quantised in terms of basic material properties. Cracks initiate from flaws pre-existing or induced by

indentation process. Pre-existing flaws occur typically as micron-scale microcracks; their nature and distribution depend in a complex way on the mechanical, thermal and chemical behaviour of the material. It is possible in many cases to introduce, remove or control these flaws. Deformation introduced flaws tend to nucleate at points of stress concentration. In general, the indented specimen will be characterised by a number of flaws prior to fracture. Whether or not a given flaw becomes critical for fracture, depends on its size, position and orientation within the tensile field. When one becomes critical, this dominant flaw develops into a well defined propagating crack. The conditions which determine the extension of a well developed crack may then be expressed in terms of the total energy. For a quasistatic system this energy,

$$U = (-W_F + U_E) + U_S \quad (3.8)$$

where W_F is the work of the applied force, U_E is the elastic strain energy in the cracked body and U_S is the total surface energy of the crack walls. An energy interchange occurs between the mechanical term, $(-W_F + U_E)$, which decreases with extension, and the surface energy term which increases correspondingly. The variation of these energy terms with respect to crack area c is,

$$dU/dc = d(-W_F + U_E)/dc + dU_S/dc = -G + 2T \quad (3.9)$$

where G is the mechanical energy release rate and T is the fracture surface energy. In the case of an ideal brittle solid, where the dissipative components are zero for the work of creating new crack surfaces, T reduces to the reversible surface energy γ .

3.3.2 CRACK PATHS

An essential requisite for fracture analysis is the information regarding the prospective crack geometry. In an ideal brittle solid, for a given crack of characteristic area 'c', the relative orientation of an incremental extension δc is that which maximizes the quantity $G-2\gamma$ (where $T=\gamma$) in equation (3.9) /10, 11/. For anisotropic solids, notably single crystals, the orientation dependence of both elastic constants and surface energy is to be taken into account in determining the maxima in $G-2\gamma$.

For sharp indenters certain underlying features of the fracture behaviour are quite general and provide the basis for a working model /1/. Provided the surface does not contain severe handling damage, cracking would be expected to occur preferentially close to the contact axis. The sequence of the crack formation and subsequent crack propagation events for sharp indenters can be enumerated as follows: 1) the sharp point of the indenter produces an elastic deformation zone, 2) at some threshold, a deformation-induced flaw suddenly develops into a small crack, called the median vent, on a plane of symmetry containing the contact axis, 3) an increase in load causes further stable growth of median vent, 4) on unloading the median vent begins to close (but not heal fully), 5) in the course of indenter removal sideways-extending cracks, termed lateral vents, begin to develop, 6) upon complete removal, the lateral vents continue their extension,

toward the specimen surface and may accordingly lead to chipping.

For spherical indenters, in the absence of deformation induced nucleation centers, the fracture will initiate at a pre-existing flaw. The fracture grow by running around the contact in circular trajectories.

3.3.3 TOUGHNESS AS A FRACTURE PARAMETER

With the development of Griffith-Irwin fracture mechanics, several parameters are used to specify resistance to crack growth. Of these parameters, K_c , which represents the fracture driving force has gained the widest acceptance as a material quantity in design. Toughness identifies with the stress intensity factor for an equilibrium tensile crack and thereby takes on the form given by Lawn and Wilshaw /10/,

$$K_c = P\xi(c) = \text{constant} \quad (3.10)$$

where P is a loading parameter and ' c ' is a characteristic crack dimension (Fig.3.1). K_c uniquely determines the intensity of stress field about the crack tip,

$$\sigma_{ij} = K_c g_{ij}(\theta)/(2\pi r)^{1/2} \quad (3.11)$$

where g_{ij} are angular functions.

In terms of fracture mechanics, the toughness parameter may be interpreted physically at two levels: macroscopically, it emerges

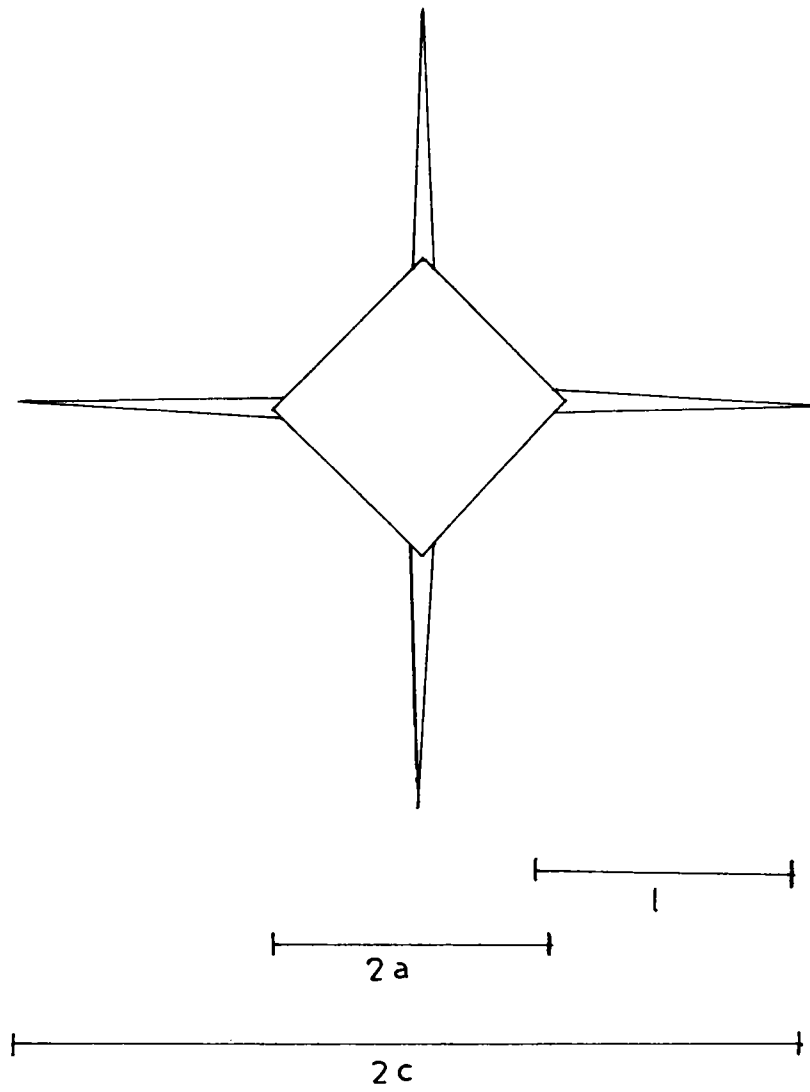


Fig.3.1 Schematic diagram showing a cracked microindentation impression.

as a composite of elastic and surface properties; microscopically, it relates to the basic non-linear separation process responsible for crack-tip extension. For a solid containing well defined crack of specific dimensions, K_c determines the fracture stress in uniform tensile loading and is accordingly a key material quantity in strength analysis. Taking the propagation stage, the well-developed median cracks extend under near center-loading conditions and accordingly satisfy the simple equation for penny-like geometry,

$$P/c^{3/2} = \beta K_c \quad (3.12)$$

where β is an indenter constant. The $c(P)$ function appropriate to initiation is much more complex; its key feature is a maximum in the load at,

$$P^* = \lambda K_c (K_c/H)^3 \quad (3.13)$$

$$c^* = \mu (K_c/H)^2 \quad (3.14)$$

where λ and μ are additional geometric constants and H is hardness. By suitably normalizing the indentation variables in the above equations, the computed functions can all be represented in a single, universal diagram. From the available Vickers data the constants are calculated and are $\beta = 7$, $\lambda = 1.6 \times 10^4$ and $\mu = 120$.

3.4 BRITTLENESS

The requirements of modern technology has caused a renewed interest in the development of strong materials. But many of the strong materials suffer from one major disadvantage; they tend to be brittle. Knowledge of the factors which determine brittleness is by and large

empirical. Brittleness is said to measure the relative susceptibility of a material to two competing mechanical responses, deformation and fracture /3/. A number of useful parameters have been devised for quantifying both deformation and fracture properties separately. But little effort has been made to combine such parameters into a common description. The crack models /12, 13/ which consider the local response of the structure about an equilibrium crack, represent the most important attempts in this direction. In these models, brittleness is tied up with the relative values of the ideal reversible surface energy and actual work of fracture. The concept is of more academic than practical importance. Another basic idea stems from the realization that a suitable indentation pattern can provide simultaneous information on deformation and fracture properties of a given material /14, 15/. Based on this basic idea Lawn et al. /3, 16, 17/ have proposed the ratio of hardness to toughness as a simple index to brittleness with a view to establish a convenient basis for material classification. The ratio of H/K_c has dimensions of (distance)^{-1/2}. A definite physical significance is attached to this factor in the indentation problem /16-19/. H/K_c reflects on the relative scales of the deformation and fracture zones about a sharp-contact site and thereby introduce a size effect into the competitive mechanical responses.

This brittleness concept is amenable to routine experimentation. All the information needed for a determination of the brittleness index is contained in a single, well developed Vickers indentation

pattern. Detailed analysis of the deformation/ fracture mechanics of the indentation process provide equilibrium relations for the characteristic dimensions 'a' and 'c' in terms of load P as

$$P/a^2 = \alpha H \quad (3.15)$$

$$\text{and } P/c^{3/2} = \beta K_c \quad (\text{for } c \gg a) \quad (3.16)$$

where H and K_c are hardness and fracture toughness; α and β are constants. Combining the above equations

$$H/K_c = (\beta/\alpha a^{1/2}) (c/a)^{3/2} \quad \text{for } c \gg a \quad (3.17).$$

Thus brittleness may be evaluated from scale measurements alone, without even specifying the load.

REFERENCES

1. B.R.LAWN and M.V.SWAIN, J. Mater. Sci. 10(1975)113.
2. E.B.BERGSMAN, ASTM Bull. 176(1951)37.
3. B.R.LAWN and D.B.MARSHALL, J. Amer. Ceram. Soc. 62(1979)347.
4. H.Hertz, J. Reine Angew. Math. 92(1881)156.
5. A.A.GRIFFITH, Phil. Trans. Roy. Soc. Lond. A 221(1920)163.
6. K.NIIHARA et al., J. Mater. Sci. Lett. 1(1982)13.
7. A.ARORA et al., J. Non. Cryst. Solids 31(1979)415.
8. T.P.DABBS et al., J. Am. Ceram. Soc. 63(1980)224.
9. J.LANKFORD, J. Mater. Sci. 16(1981)1177.
10. B.R.LAWN and T.R.WILSHAW, " Fracture of brittle solids",
(Cambridge university press, Cambridge, 1975)
11. F.C.FRANK and B.R.LAWN, Proc. Roy. Soc. Lond. A 299(1967)291.

12. A.KELLY et al., *Philos. Mag.* 15(1967)567.
13. J.R.RICE and R.THOMSON, *Philos. Mag.* 29(1974)73.
14. R.W.DOUGLAS, *J. Soc. Glass Technol.* 42(1958)145.
15. K.PETER, *Glastech. Ber.* 37(1964)333.
16. B.R.LAWN et al. *J. Mater. Sci.* 11(1976)573.
17. B.R.LAWN and A.G.EVANS, *J. Mater.Sci.* 12(1977)2195.
18. A.G.EVANS and E.A.CHARLES, *J. Am. Ceram. Soc.* 59(1976)371.
19. A.G.EVANS and T.R.WILSHAW, *Acta Metall.* 24(1976)939.

CHAPTER FOUR

EXPERIMENTAL TECHNIQUES

This chapter describes the experimental techniques used in the growth, identification of faces, specimen preparation, dislocation etching, indentation analysis, fractographic studies, dielectric measurement, spectral analysis and thermal studies of DAHC and CA single crystals.

4.1 GROWTH TECHNIQUES

The crystal growth set up for DAHC crystals is shown in Fig.4.1. It consists of a solid state constant temperature bath with an inner working chamber of volume $(37.5 \times 26.5 \times 34.5) \text{cm}^3$ and a capacity of 40 litres. The temperature is controlled by a Beckman thermometer having an accuracy of $\pm 0.01^\circ\text{C}$ below 60°C . A uniform distribution of temperature throughout the bath is effected by a multi-bladed stirrer.

To eliminate the vibration due to stirring a separate arrangement was made to hold the crystallizers containing the growth solution. The arrangement provided the facility to grow many crystals in the same run. The solution in the crystallizers was stirred by 'T' shaped stirrers connected to the shafts of variable d.c. motors.

For growing CA crystals the crystallizers were placed in hermetically sealed vessels containing water absorbants. These vessels were placed in the thermostated water bath during crystallization.

Good quality seeds of DAHC and CA were obtained by the method prescribed by Holden /1/.

4.2 IDENTIFICATION OF FACES

The faces of large crystals were identified by measuring the angles between the faces using contact goniometer of Carl Zeiss Jena which is of the type invented by Carangeot in 1780. It is the simplest instrument suitable for measuring angles of large crystals. It consists of a protactor and a rotating bar pivoted about the centre of the protactor. In the measurement of an interfacial angle the goniometer is applied to the crystal so that the edge between faces is parallel to the axis of rotation of the bar. The circular scale is divided in degrees. An auxiliary scale on which one degree is divided into twelve equal divisions provide an accuracy of 5 minutes to the angle measured. The angular measurements for small crystals were made using a two circle goniometer head attached to a spectrometer as shown in Fig.4.2. It is based on the principle of obtaining consecutive reflections of rays of light from crystal faces. A complete revolution of the crystal makes it possible to measure the angles between faces of one zone. The angle between faces of other zones can be obtained in a similar way. This goniometer arrangement allows measurements to be made with an accuracy of one third of a minute.

4.3 SPECIMEN PREPARATION

The specimens required for characterization of DAHC and CA were

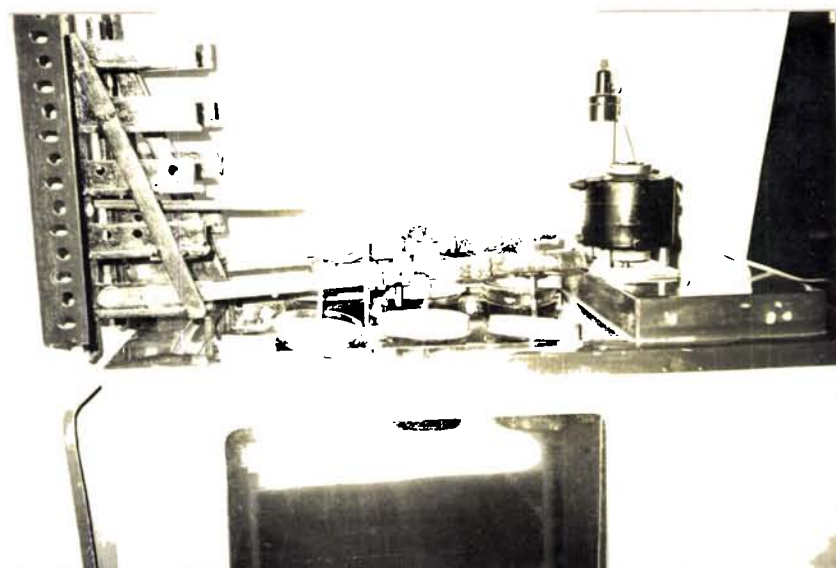


Fig.4.1 Experimental set up for the growth of DAHC single crystals.

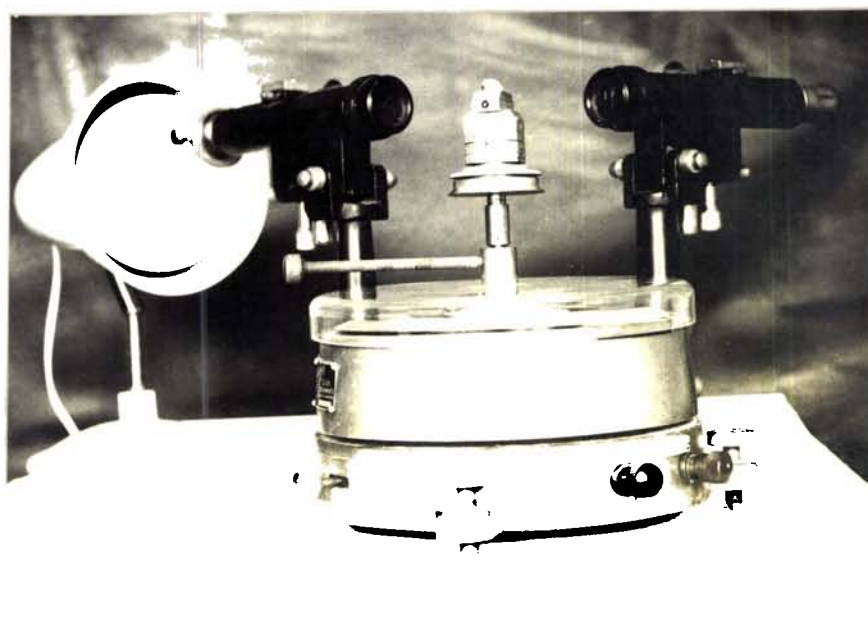


Fig.4.2 Goniometer set up for the measurement of interfacial angles.

obtained from good quality crystals. Single crystals were cut in the required form using a solvent string crystal cutting unit shown in Fig.4.3.

Description of a crystal cutter.

The crystal cutting unit consists of five parts: 1) a driving unit, 2) pressure exerting unit, 3) a wetting unit, 4) a rotating platform and 5) a movable vernier holder fitted with clips.

The driving unit consists of a variable speed d.c. motor and pulley system consisting of three pulleys fixed to a vertical frame. Two of these are cone pulleys for varying the speed of the thread. The third pulley forms a part of the wetting system.

The pressure on the crystal is exerted by increasing the tension of the cutting string. A movable guide fitted with two grooved heads, a spring load arrangement and an auxiliary movable pulley is used to increase the tension.

The wetting unit consists of a reservoir, the height of which can be adjusted using a fine screw arrangement. The volume of the solvent in the reservoir can also be varied.

A rotating platform graduated in degrees helps to cut the crystal in any desired direction. This platform can be fixed in any desired direction using a fixing screw. A vernier attachment may be used along with

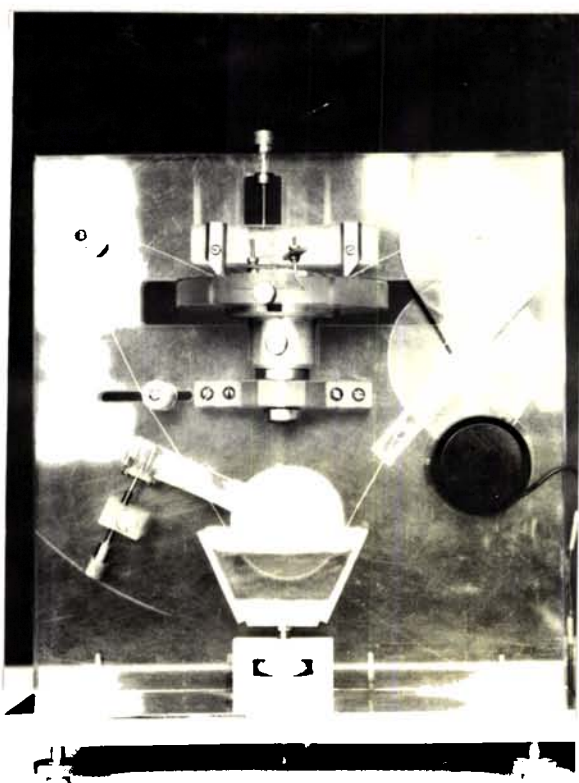


Fig.4.3 Solvent string crystal cutting unit.

the circular main scale to obtain high accuracy.

At the centre of the platform is fixed a movable scale attached to a screw head. Using the screw arrangement the crystal can be moved by a fraction of a millimeter. To keep the crystal in position specially designed locking clips are used.

The major factors that determine the perfection of the cut are, 1) the speed of the string, 2) the pressure exerted by the string on the crystal and 3) the wetting of the string. All these factors can be varied in the cutting unit described above. The optimum conditions for a perfect cut is to be found out for each specific crystal.

4.4 DISLOCATION ETCHING STUDIES

Etching of crystals was performed in special vessels by stirring the etchant at the rate of nearly 50 r.p.m. Specially designed grippers of light materials were used to handle crystals which could not be handled by metallic forceps. For very thin crystals etching was done by keeping the crystal in a net and immersing the net in the etchant. Etched crystals were studied under incident light microscope, 'Epityp 2' of Carl-Zeiss Jena. As grown crystals or cleaved crystals were used for etching studies. Small specimens and specimens for which repeated etching was not necessary, were mounted on microscopic slides using adhesive. Specimens which needed observation on both sides were placed on a special thin plate with grooves of different size and shape. For observing shallow pits, the surface of the specimens were coated with a thin film of

aluminium by vacuum evaporation.

4.5 MICROINDENTATION ANALYSIS

Hardness, toughness and brittleness of DAHC and CA crystals were evaluated by microindentation technique. Microindentation is carried out on DAHC and CA using Hanemann diamond pyramid indenter which can be attached to the Carl-Zeiss microscope. The set up for microindentation analysis is shown in Fig.4.4. The Hanemann hardness tester consists of a diamond in the shape of a quadrangular pyramid. The sides of the pyramid have a slope of 22 degrees. The bottom of the diamond which is shaped as a short bar, is mounted on a small hole drilled into the front lens. Large annular portions which are left free in the front lens is used for illumination and observation of the specimen. The indenter unit is also provided with an optical system with a scale to indicate the testing load. The objective, with the diamond is suspended from two disc springs. Any load applied to the diamond causes the suspension to activate the optical system which indicate the load observable through the eyepiece.

The eyepiece have two reticles (one of the reticles is stationary and the other movable), each of which is at right angles. The two markigs can be used to measure the diagonal length or the area of the indentation mark. Using this indenter loads as small as 0.2 gms and as large as 200 gms can be applied to the specimen during indentation.

4.6 FRACTOGRAPHIC STUDIES

Fractography is the technique developed for studying the patterns found on nascent fracture surfaces using optical microscope /2/. Nascent fracture surfaces are obtained by cleaving a crystal using a blade. For the fractographic studies of DAHC, a specially fabricated crystal cleaving unit was used by which routine cleaving can be accurately performed to get very thin slices. The set up for crystal cleaving is presented in Fig.4.5. It consists of 1) a metallic supporting frame, 2) a cleaving unit, 3) a circular platform and 4) a crystal holder. The supporting frame is made up of a horizontal base on which two vertical bars are fixed. The other ends of the bars are joined by a horizontal bar. The cleaving unit is made up of another horizontal bar which can slide freely along the vertical bars and can be stopped at any position using arresters. A sharp blade is fixed at the centre of the horizontal bar. Pressure is applied on the blade using a spring load arrangement. A scale on which the crystal rests moves under the action of a screw at the centre of the platform. The crystal is fixed with the help of locking clips specially designed for the purpose. This unit helps one to find out the pressure required to cleave a crystal.

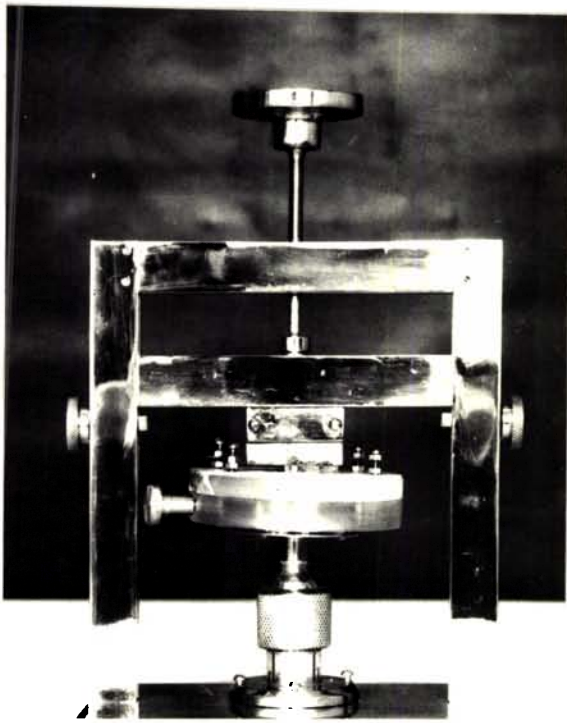


Fig.4.5 Crystal cleaving unit.

4.7 DIELECTRIC MEASUREMENT

For the measurement of dielectric constant and loss of DAHC, samples of size $(5 \times 5 \times .4) \text{mm}^3$ were cut from large single crystals using solvent string cutter described in section 4.3. These samples were then polished to obtain smooth surfaces and dried thoroughly. A uniform layer of silver paint was applied as electrodes and mounted on the holder of a dielectric cell. The cell used for the dielectric measurement is shown in Fig.4.6. It consists of an inner thin walled brass jacket which can be evacuated. This inner jacket is kept in an outer jacket containing liquid nitrogen. Heating filament is wound around this jacket which is switched on during the heating cycle. The crystal specimen is held between copper electrodes fixed on two teflon discs. The lower disc is fixed to three symmetrical rods and the upper disc slides on them and is kept pressed to the specimen with springs. Temperature measurements were made with a copper-constantan thermocouple kept in the proximity of the crystal. The thermocouple voltage was measured using a digital microvolt meter.

The experimental set up for the measurement of the dielectric constant and loss is shown in block diagram (Fig.4.7). The dielectric measurements were made by capacitance measurement of DAHC specimens placed as dielectric between two electrodes. Capacitance and loss were measured by using a 0.1% universal bridge TF 1313 A of Marconi Instruments Ltd., U.K. The frequency of the input voltage was varied

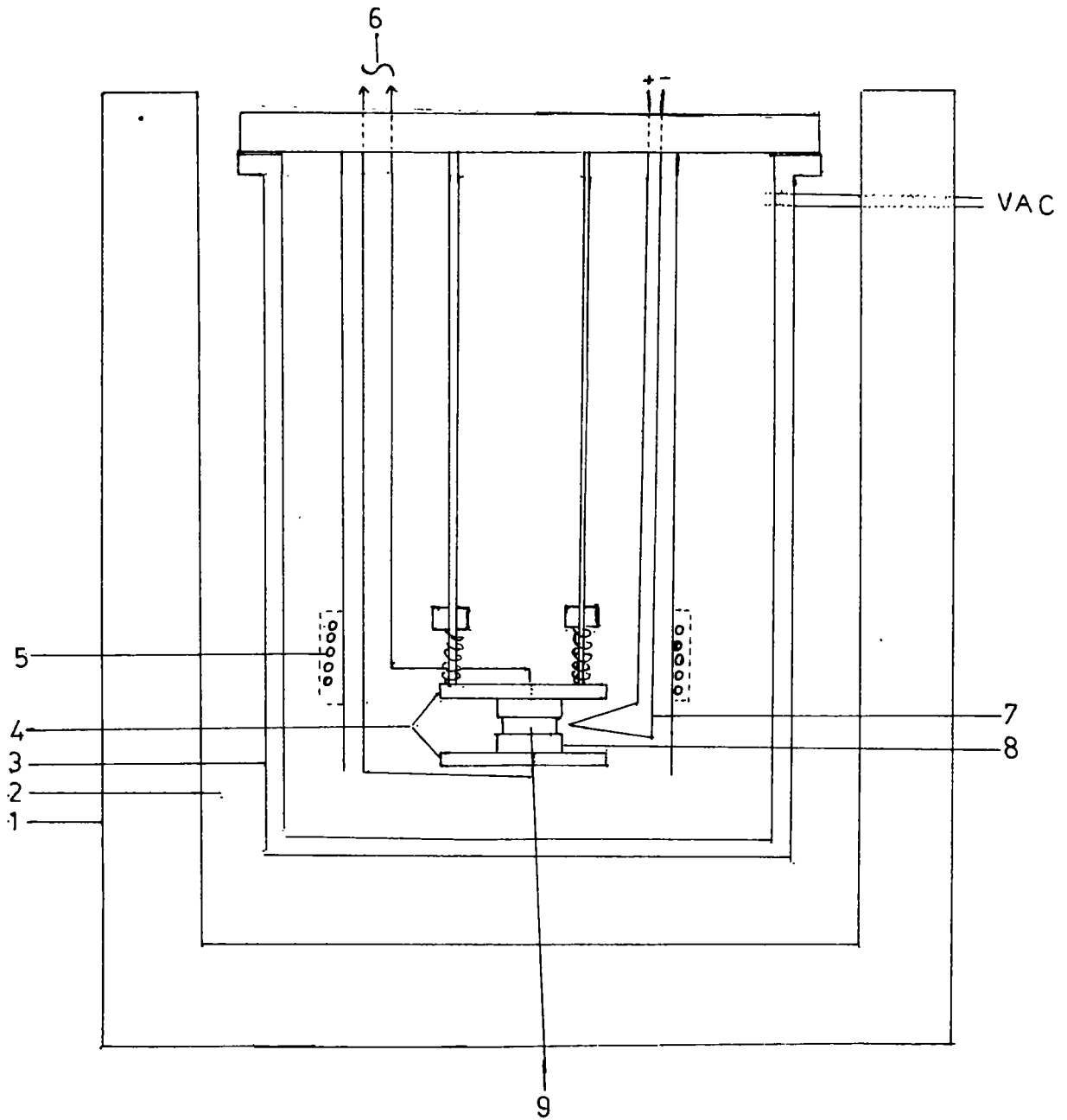


Fig.4.6 Schematic diagram of dielectric cell. 1) Outer jacket, 2) Liquid N₂, 3) Inner jacket, 4) Teflon discs, 5) Heating elements, 6) Electrode leads, 7) Thermocouple, 8) Copper electrode, 9) Specimen.

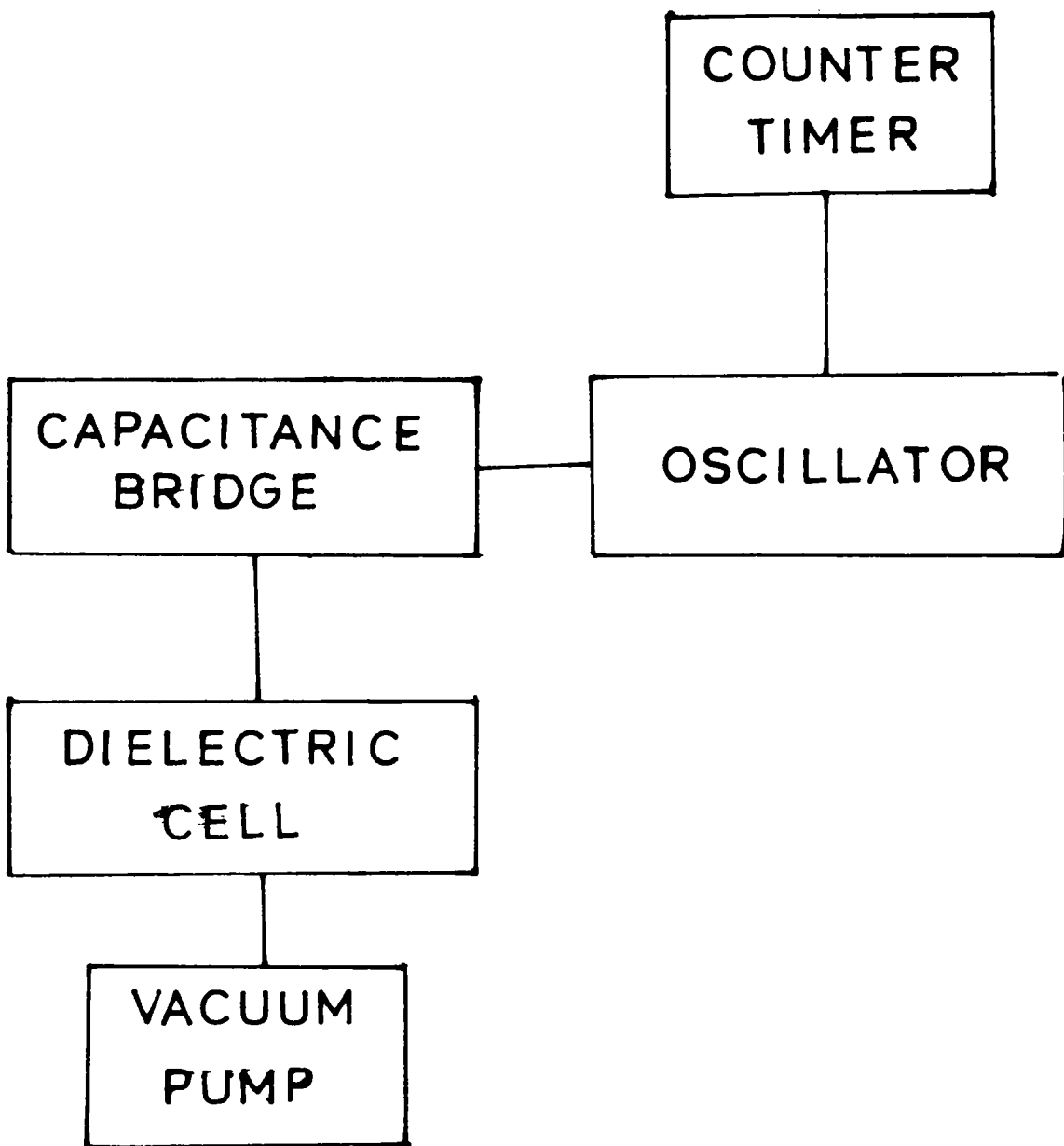


Fig.4.7 Block diagram of the experimental set up for dielectric measurements.

using a philips oscillator along with a systronic counter timer. The experiment was conducted in a vacuum of the order of 10^{-2} Torr.

4.8. SPECTRAL AND THERMAL STUDIES

The IR spectrum of DAHC has been recorded at room temperature on Perkin-Elmer 599 spectrophotometer. This double beam IR spectrometer gives good ordinate accuracy and constant response down to 0% transmission. Low noise facility helps improved microsampling and is also helpful when working with accessories and poorly transmitting samples.

The success of a spectroscopic investigation depends on the preparation of suitable samples. In the case of DAHC, crystalline samples could not be used due to their strong absorbance of IR rays. Transmission was almost zero percent for 0.5mm thick samples. Thinner samples were susceptible to cracking. Hence mull and disc techniques were used for the preparation of the samples. In the mull technique a few good quality crystals were finely powdered in a grinding mill so that the mean particle size is below the IR region wavelength. This was further treated in a glazed porcelain mortar. This very fine powder was mixed with the required quantity of nujol. The mixture was pasted on a NaCl window for spectroscopic analysis. In the disc technique a perfect crystal was powdered with thoroughly dried KBr. About 1 gm of the mixture was used to make a pellet and using this the spectrum was obtained.

The UV spectrum was recorded on a double beam spectrophotometer, Shimadzu UV-190 having a wavelength drive capability with a Czerny--Turner grating monochromator, covering a wavelength range 195 to 860 nm with a 2nm band width. The double beam optics ensure a flat base line with +/- 2% T. It can be converted to a recording spectrometer by hooking up an external recorder, having low noise, low drift and high stability. The specific features include linear absorbance, linear transmittance and direct concentration read out. The UV spectrum of DAHC was recorded in doubly distilled water.

The thermal analysis of DAHC and CA crystals were carried out using a DSC, Perkin-Elmer 2. The samples were sealed in Al sample pan and heated at the rate of 20^oK/min in dry nitrogen atmosphere and DSC scanning was done on DAHC and CA from room temperature upto the melting points of these crystals.

REFERENCES

1. A.HOLDEN and P.SINGER, Crystals and crystal growing, (Doubleday and Company Inc., N.Y. 1960)
2. C.A.ZAPFFE and C.O WORDEN, Acta Cryst. 2(1949)377.

CHAPTER FIVE

GROWTH AND MORPHOLOGY OF DAHC AND CA SINGLE CRYSTALS

5.1 INTRODUCTION

Love and Patterson /1/ have grown DAHC single crystals by a layering technique. In this technique, the aqueous citrate solution was layered under either ethanol or acetone, i.e. under hydrophilic solvents in which citrate salt is nearly insoluble.

CA is reported to crystallize as anhydrous at temperatures above 36.6°C and as monohydrate below this temperature /2/. The rate of growth of CA in aqueous solution has been studied by NYVLT and VACLAVU /3/.

The external morphology of a crystal depends on the growth rates of the various faces and the variation of these rates with time. The growth itself is determined by internal and external factors. The internal factors affecting crystal morphology are crystal structure, the presence and distribution of dislocations and the presence of twin boundaries. The external factors are temperature, the pressure, the degree of supersaturation and undercooling, the supply of crystallizing particles (determined by their concentration and diffusion in the noncrystalline phase and the amount of stirring in this phase).

Through the study of surface structures information pertaining

to 1) mechanism and process of crystal growth, 2) the unit of growth, 3) movement of dislocations after cessation of growth and the stress history of crystals, 4) supersaturation conditions of crystal growth in different localities, 5) the prediction of possibility of polytypism, 6) new interpretation for the mechanism of contact twin formation and 9) direct observation of twinning due to stacking fault during growth and its structural interpretation can be obtained.

This chapter deals with the growth, identification of faces and study of the as grown faces of DAHC and CA crystals.

5.2. EXPERIMENTAL

Saturated solution of DAHC in doubly distilled water was prepared from 99% pure citrate powder of Sarabai M. Chemicals. Crystals were grown, layering the salt solution under ethyl alcohol and acetone in separate test tubes. The crystals obtained were small and were not found useful for morphological studies. Different concentrations of the salt solution were layered under acetone and the effect of concentration on the initiation of nucleation and the number of crystals obtained after a period of two weeks were observed.

Crystals used for the present investigation were grown by slow evaporation at constant temperature using saturated salt solution. Good quality seeds were suspended either at the bottom or centre of

the crystallizer containing the salt solution. Crystals were also grown in a mixture of alcohol and water where the ideal solubility condition for crystal growth from solution was achieved /5/.

99.5% pure citric acid obtained from E. Merck,(India) Ltd., was further purified by recrystallization using doubly distilled water. Using this a saturated solution was prepared and CA crystals were grown by slow evaporation in constant temperature bath by seeding the solution. The angles between the faces of the crystals of DAHC and CA were measured using goniometers described in chapter four. The as grown faces of these crystals were studied using the microscope described earlier.

5.3. RESULTS AND DISCUSSION

Fig. 5.1 shows DAHC crystals grown in a test tube in which the solution is layered under ethyl alcohol. The nucleation is spurious and a number of crystals grow at the interface of the salt solution and the alcohol layer. The effect of solution concentration on initiation of nucleation, the number of crystals and the quality of the crystals after a period of two weeks in acetone layering are presented in table 5.1. In solutions of concentration less than 3.6 N, nucleation was slow and crystals with well developed faces were obtained. Some of the crystals contained inclusions (Fig. 5.2). Large and perfect crystals were grown during a period of two weeks by slow evapora-



Fig.5.1 DAHC crystals growing in a test tube. (x4)

TABLE 5.1. Effect of solution concentration on initiation of nucleation, the number of crystals and the quality of crystals obtained after a period of two weeks.

Sl. No.	Solution concentration (Normality)	Initiation of nucleation (Hrs.)	Number of crystals after two weeks	Quality of crystals
1	4.87	4	100	Tiny, imperfect
2	4.68	4	100	"
3	4.51	5	100	Small, imperfect
4	4.36	6	100	"
5	4.21	8	100	Small
6	4.07	12	50	"
7	3.94	14	40	Medium
8	3.82	28	20	"
9	3.71	32	15	"
10	3.59	40	13	$(7 \times 5 \times 1) \text{mm}^3$
11	3.49	52	12	$(8 \times 5 \times 2) \text{mm}^3$
12	3.40	62	10	$(8 \times 5 \times 2) \text{mm}^3$ faces developed

tion of saturated salt solution (Fig. 5.3). The crystals were transparent. A crystal growing from a suspended seed in a crystallizer is shown in Fig. 5.4. DAHC crystals grown from a mixture of water and ethyl alcohol are shown in Fig. 5.5.

Typical CA crystals obtained by slow evaporation are shown in Fig. 5.6.

From the goniometric measurements and the crystallographic data /1/, the prominent faces of DAHC were identified. Crystals generally grow in tabular form, the largest face being the (001). The prominent faces of a typical crystal are schematically represented in Fig. 5.7. Some of the crystals obtained by slow evaporation of saturated solution having other external morphologies are shown in Fig. 5.8 and their schematic representations are given in Fig. 5.9.

Crystallographic data from Burns and Iball /6/ and the goniometric measurements were used to identify the prominent faces of CA crystals. The schematic representation of a typical crystal obtained is shown in Fig. 5.10. A modified habit that is seen is also shown schematically in Fig. 5.11.

The shape of a crystal is usually determined by the relative rates of advance of close-packed faces. Close-packed faces grow relatively slowly since atoms can only be added at kink sites, while high



Fig.5.4 DAHC crystals growing from a suspended seed in a crystallizer.
(x2)

Fig.5.5 DAHC crystals grown from a mixture of water and ethyl alcohol.

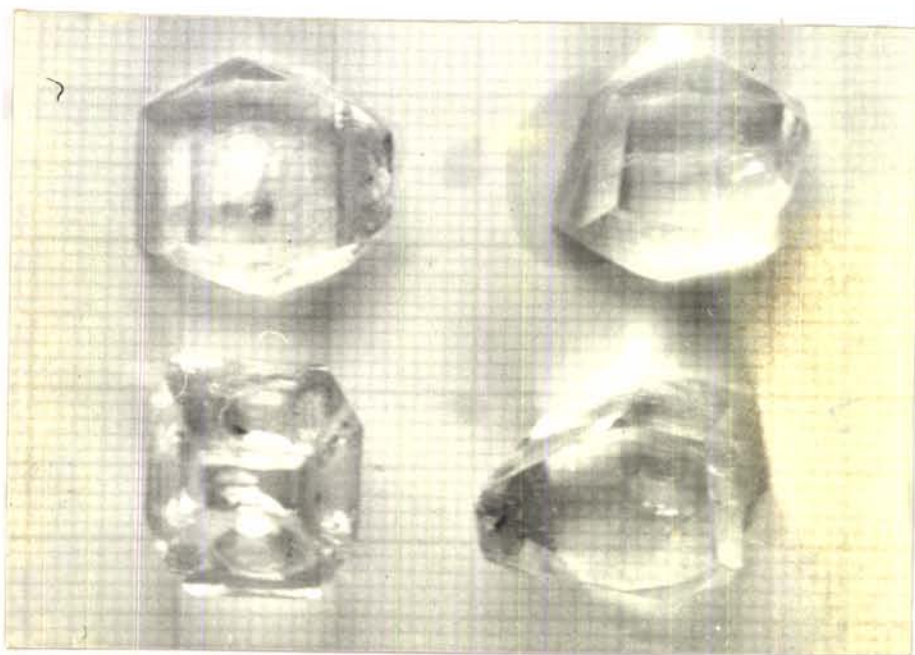


Fig.5.6 CA crystals grown by slow evaporation.

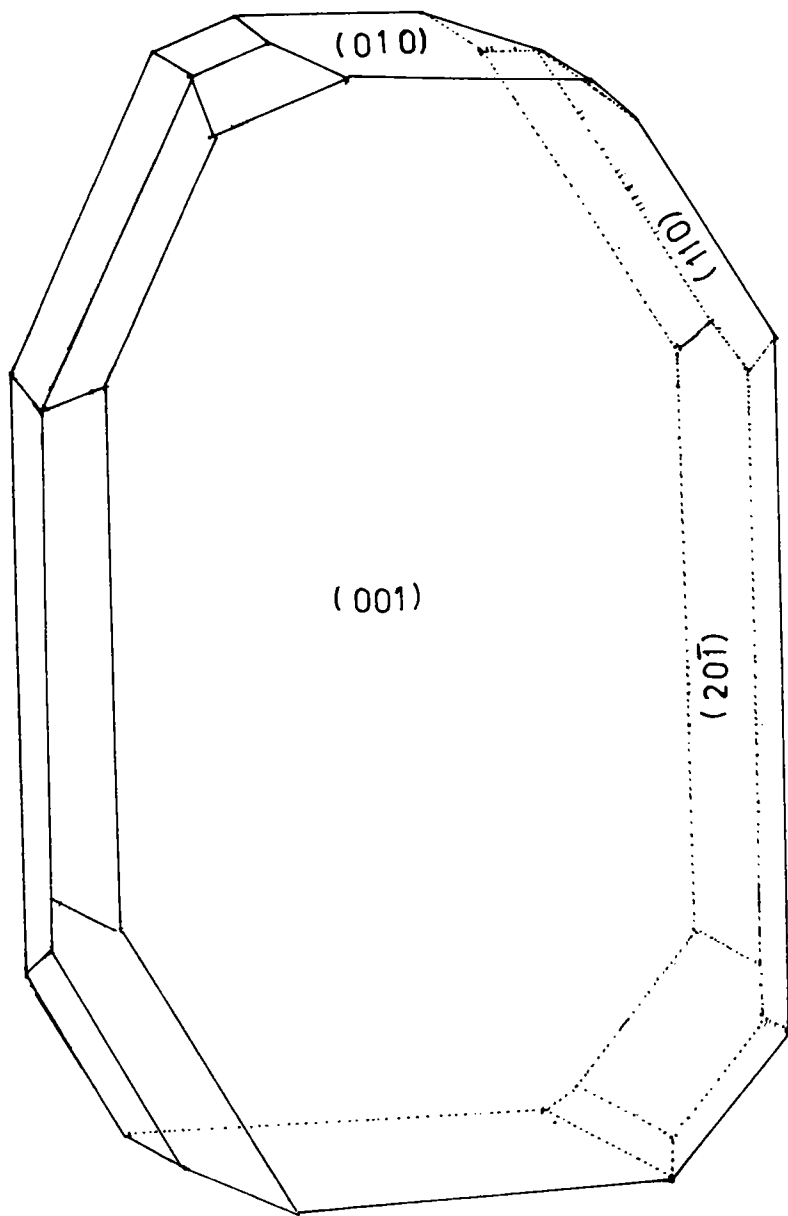


Fig.5.7 Schematic diagram of a DAHC crystal showing the prominent faces.

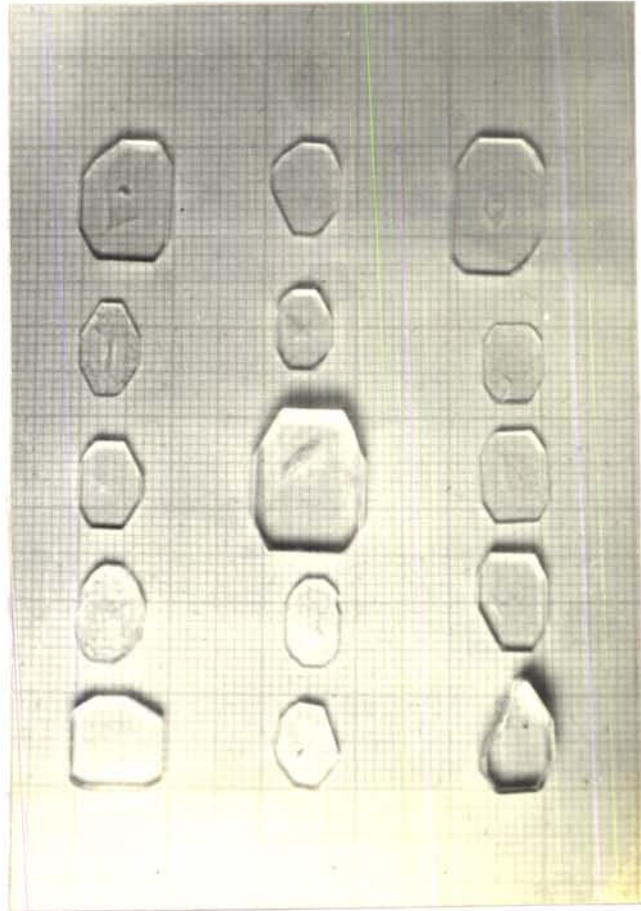


Fig.5.8 DAHC crystals exhibiting different external morphologies.

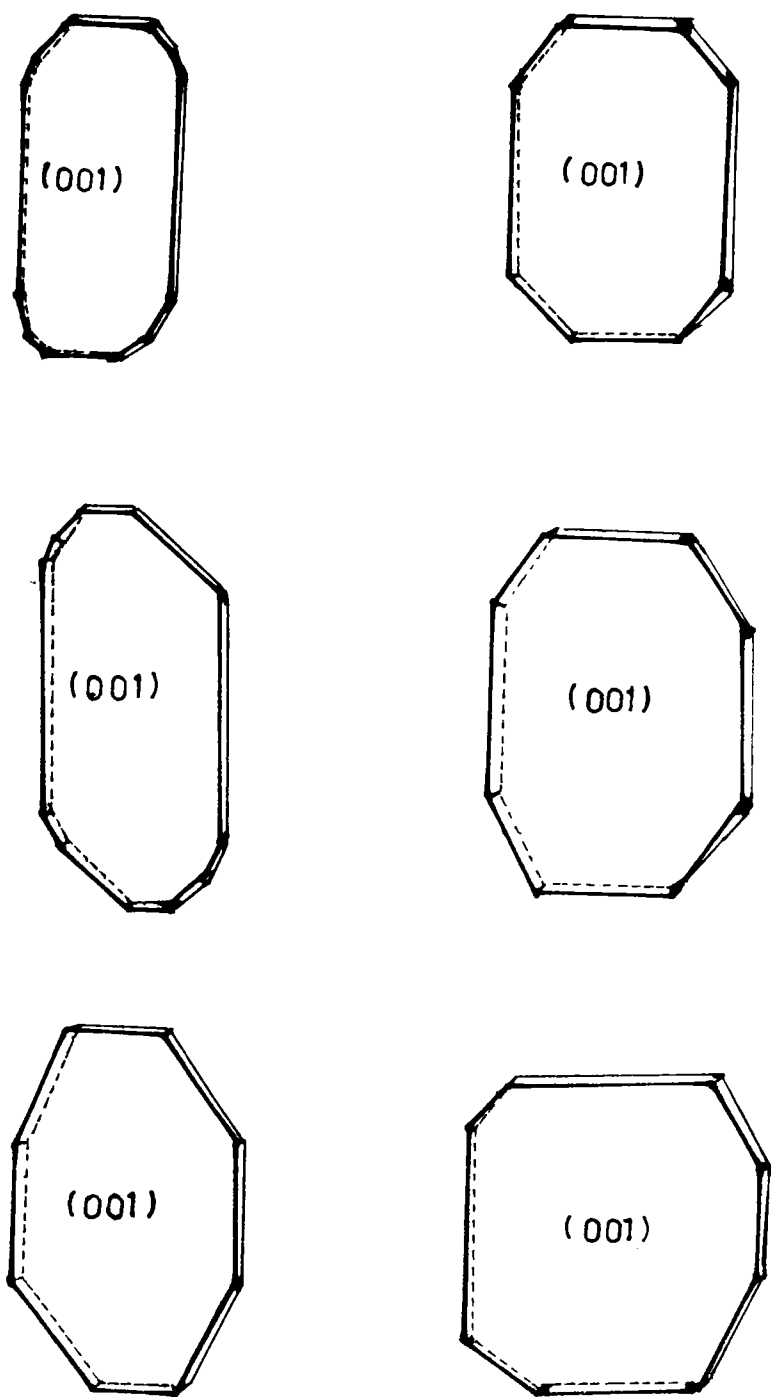


Fig.5.9 Schematic representation of DAHC crystals with different external morphologies.

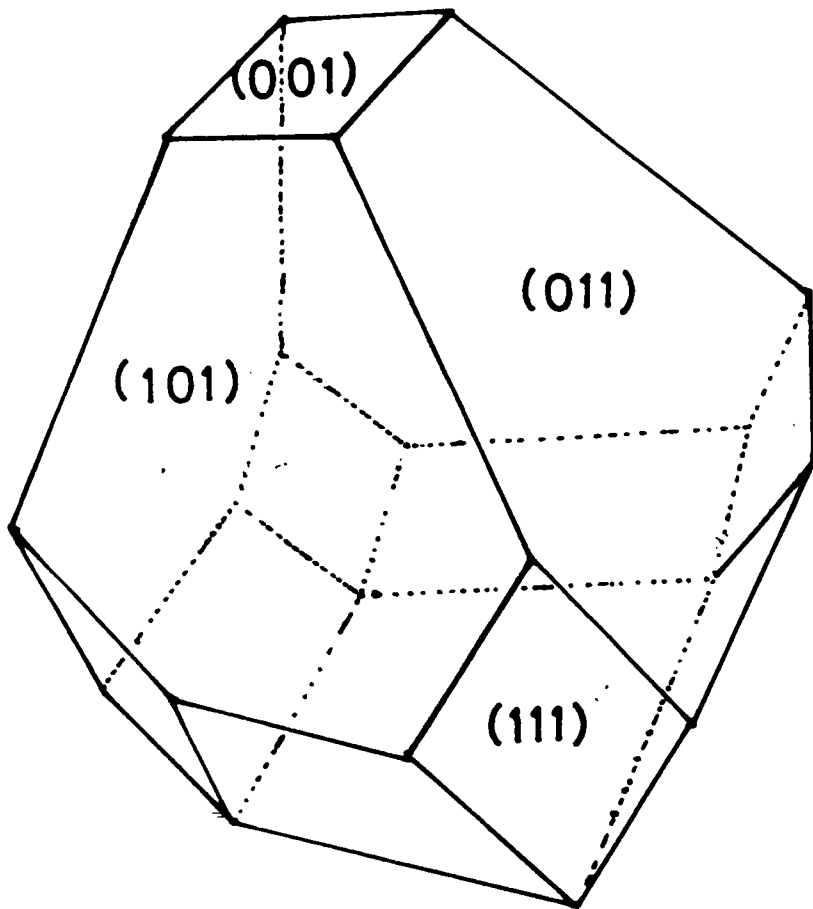


Fig.5.10 Schematic diagram showing the prominent faces of a CA crystal.

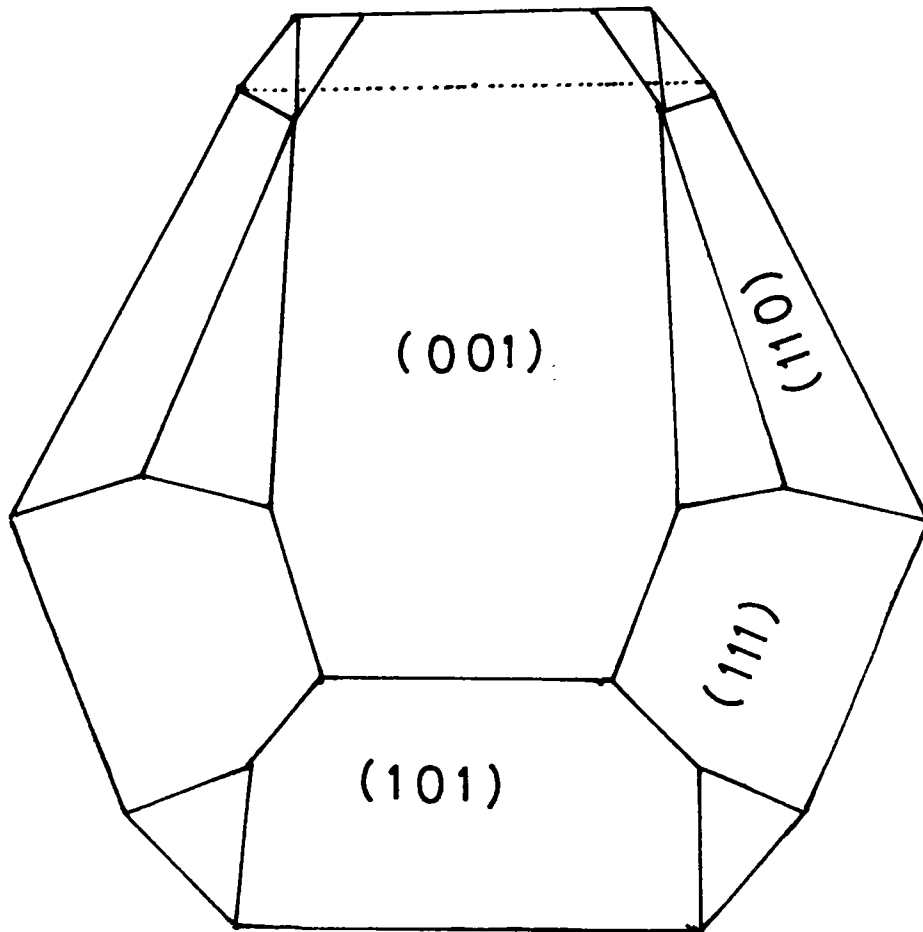


Fig.5.11 Schematic diagram of a CA crystal showing a modified habit.

index faces grow more rapidly. During growth the high index faces advance rapidly and disappear, the close-packed faces determining the growth rate. At extremely low growth rates when the solution and the crystal are nearly in equilibrium the shape should be determined by the requirement that the total surface energy of the crystal be as small as possible.

Crystals of different shapes are grown from the same stock solution. Therefore, the most important factor that has affected the modification of habit is probably the difference in the supply of crystallizing particles to the crystals growing at different regions. Variation in supersaturation and the presence of impurities are also found to be factors affecting habit modification in DAHC and CA crystals.

There are two ways in which the growth of a plane crystal face occur for real crystals, i.e. 1) by means of two dimensional nucleation and 2) by screw dislocation mechanism. Microscopic observations of the as grown faces of crystals show that layer growth by means of two dimensional nucleation is active in the growth of DAHC and CA crystals.

5.4. CONCLUSIONS

During the growth of DAHC crystals by layering technique, spurious nucleation can be controlled by reducing the concentration of the salt solution. Slow evaporation method from aqueous solution gives

good quality large DAHC and CA single crystals. DAHC can also be grown from a mixture of water and ethyl alcohol. The prominent faces in these crystals obtained have been identified by goniometric measurements using the available crystallographic data. Microscopic observations have shown that both DAHC and CA crystals grow by the two dimensional nucleation mechanism.

REFERENCES

1. W.E.LOVE and A.L.PATTERSON, Acta Crystallogr. 13(1960)426.
2. S.LESZCZYNSKI, " Crystallization in chemical industry ",
(Panstwowe Wyd. tech, Warszawa, 1956)
3. J. NYVLT and V. VACLAVU, Collection Czechoslov.
Chem. Commun. 37(1972)3664.
4. I. SUNAGAVA, "Crystal growth and characterization,
(Proc. ISSCG-2 Spring School Japan, Oxford, 1975).
5. J.J.GILMAN, " The art and science of growing crystals ",
(John-Wiley and Sons, N.Y., 1963).
6. D.M.BURNS and J.IBALL, Acta Cryst. 7(1954)137.

CHAPTER SIX

DISLOCATION ETCHING STUDIES OF DAHC AND CA SINGLE CRYSTALS

6.1. INTRODUCTION

Since dislocations are known to affect the plastic, electric, magnetic, piezoelectric, dielectric, etc properties of crystals considerably /1-4/ it is of paramount importance to assess their dislocation content before any study of the properties is undertaken. Microscopy of etched surface is applied to dislocation studies in crystals irrespective of whether they are conductors /5, 6/, semiconductors /7, 8/ or insulators /9, 10/.

In this chapter, to begin with, a comparative study of the different methods for the observation of dislocations is made and it is shown that the dislocation etch method is the most convenient and widely used technique. The results of dislocation etch studies made on DAHC and CA crystals are then presented and discussed.

6.2. EXPERIMENTAL

Chemical resistance of DAHC to a number of compounds were studied and a few potential etchants were identified. Propionic acid was found to be a reliable dislocation etchant for the (001) and (110) faces of DAHC and the (101) face of CA crystals. The time of etching to

produce good etch pits for the etchant was obtained by trial and error. Lateral etch rate was measured using the micrometer screw eye piece attached to the microscope which is described in section 4.4. Etching of DAHC crystals were done in a mixture of acetic acid and benzene at various temperatures to obtain the activation energy. NaOH solution was used to wash away a thin layer of etched crystal in successive layer etching. DAHC crystals were also etched in formic acid, acetic acid and methyl alcohol.

6.3. RESULTS AND DISCUSSION

6.3.1. PRESENT STATUS OF DISLOCATION STUDIES

The increasing importance of dislocation studies in crystals can be clearly understood from the number of papers published on dislocations in recent years (Fig. 6.1). The graph shows that one out of every hundred papers published in physics deals with dislocations. The result of a comparative study of the different direct methods for observation of dislocations with regard to the frequency of their occurrence is presented in Fig.6.2. This study clearly establishes the importance of etching method (also expressed by many others) as the simplest /11, 12/, most convenient /13, 14/ and widely accepted /15, 16/ technique. The percentage distribution of etching studies in conductors, semiconductors and insulators is shown in Fig.6.3. This shows that the etch pit technique is a powerful tool for disloca-

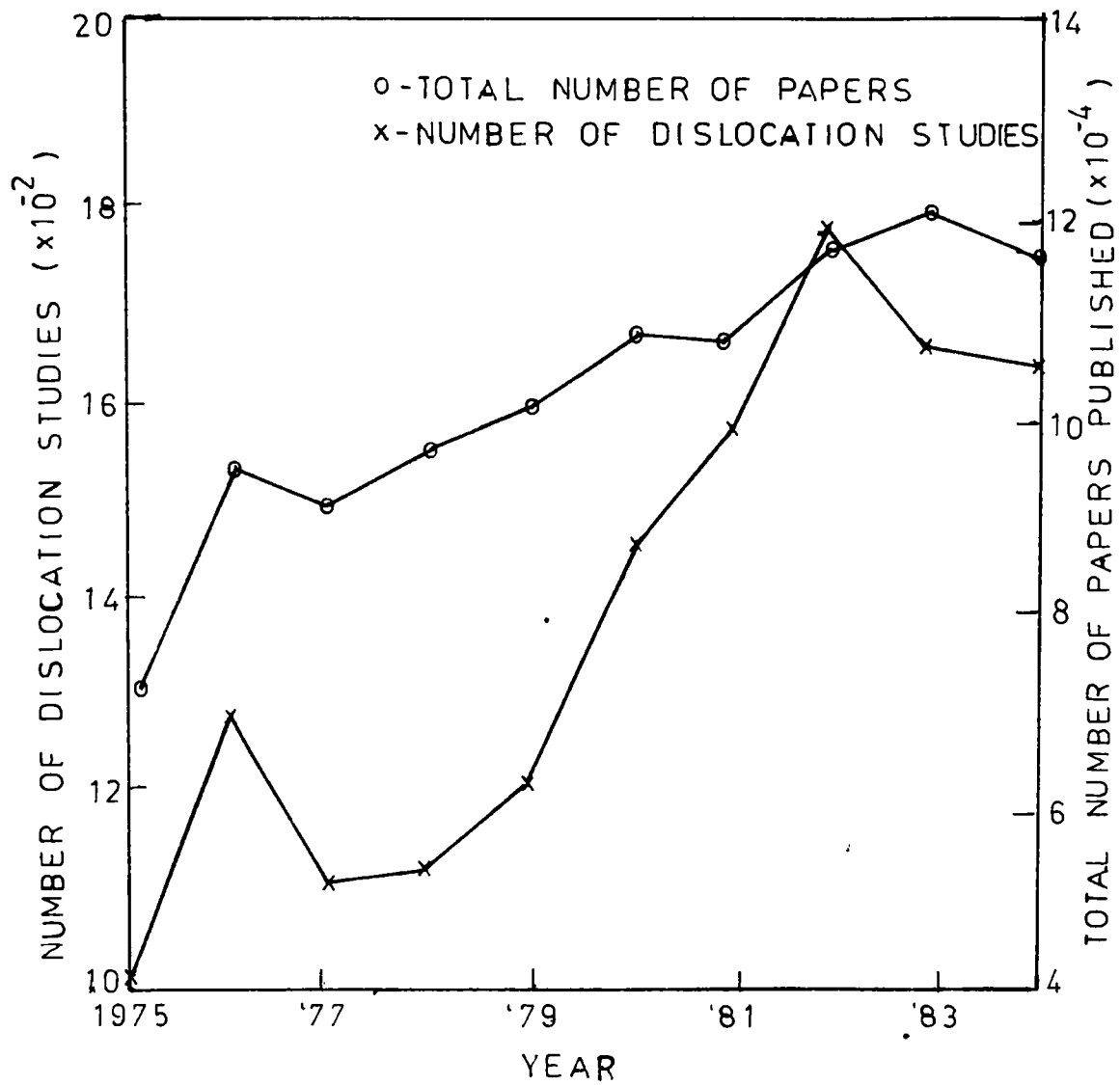


Fig.6.1 Total number of papers published and the number of dislocation studies from the year 1975-1984.

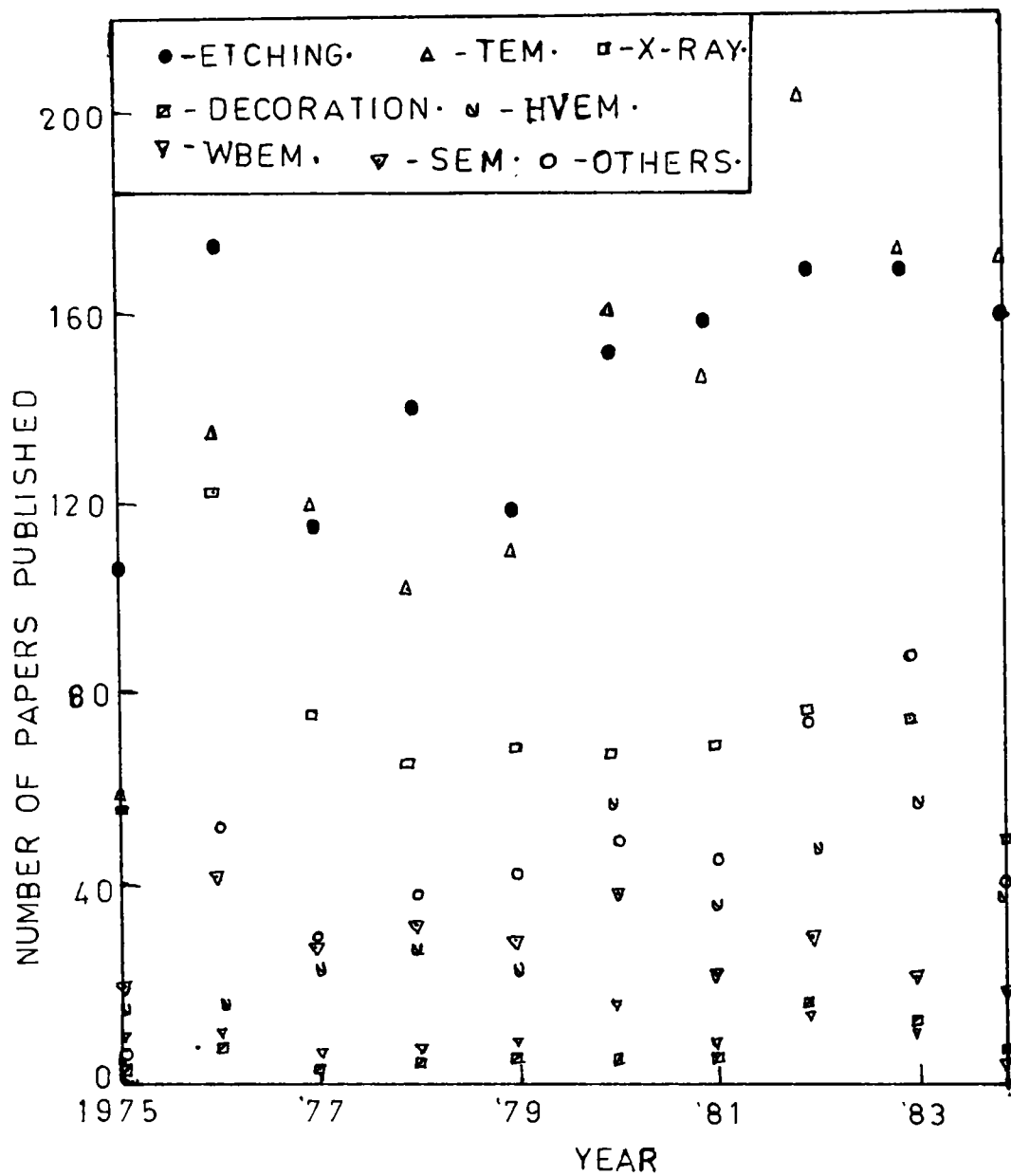


Fig.6.2 Etching compared with other direct methods of dislocation observation.

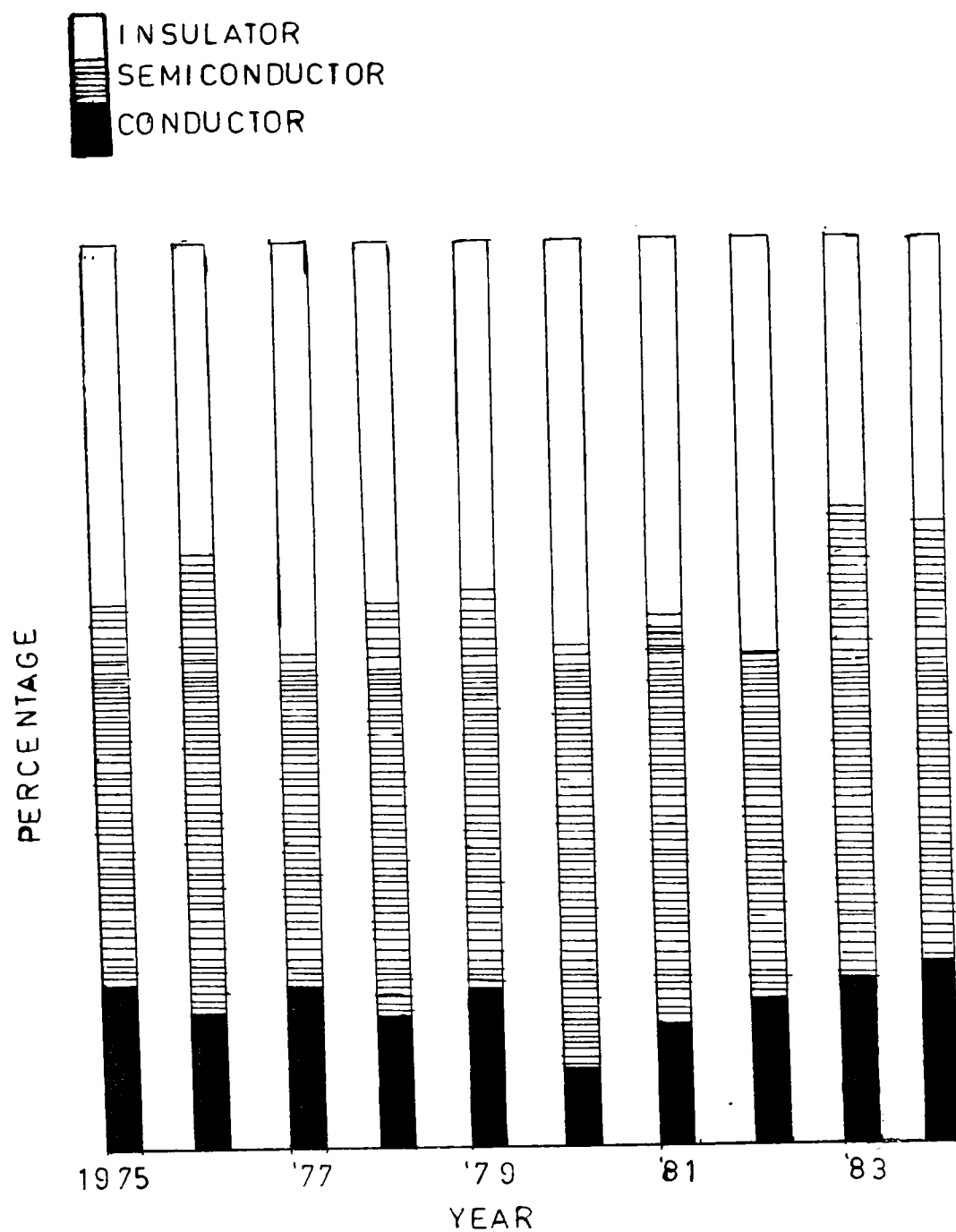


Fig.6.3 Percentage distribution of etching studies on conductors, semi-conductors and insulators.

tion studies in all types of crystals.

6.3.2. ETCHING OF DAHC CRYSTALS

Chemical resistance of DAHC to a number of compounds at room temperature is presented in table 6.1. Nitric acid, formic acid, acetic acid, propionic acid and methyl alcohol are found to be potential etchants for (001) face of DAHC. Propionic acid is shown to be a good dislocation etchant for (001) surface by repeated etching (Fig.6.4), successive layer etching (Fig.6.5) and grain boundary etching (Fig.6.6). The average pit density is found to be of the order of $2 \times 10^2/\text{cm}^2$. On repeated etching, the etch pits increase in dimensions keeping their number and shape the same. Additional pits that appear on successive layer etching in Fig.6.5b is due to dislocation loops. In the grain boundary, the pits are not equispaced. This implies unequal spacing of dislocations forming the boundary. Such irregularly spaced dislocations are due to imperfectly polygonised boundaries or boundaries under stress.

Etch features

Dislocation density of most specimens is low. However regions of high dislocation density forming clusters of pits are sometimes observed (Fig.6.7). These are due to the presence of impurities. The clusters of pits often vanish on successive layer etching thereby

Table 6.1. Chemical resistance of DAHC

System	Concentration	Time(secs)	Observation
HNO ₃	70%	20	Etch pit formation
H ₂ SO ₄	98%	30	Attacked, film formation
HCl	35.6%	30	No reaction
HI	55%	15	Attacked, film formation
HF	39%	10	Attacked, film formation
HCOOH	98%	15	Etch pit formation
CH ₃ COOH	60%	10	Etch pit formation
CH ₃ CH ₂ COOH	99%	15	Etch pit formation
HOH	Triply distilled	2	Washed
CH ₃ OH	32.4%	20	Etch pit formation
CH ₃ CH ₂ OH	95%	20	No reaction
C ₆ H ₆	78%	60	No reaction
CH ₃ C ₆ H ₅	92%	60	No reaction
C ₅ H ₅ N	79%	60	No reaction
NaOH	Saturated	10	Washed
KOH	Saturated	10	Washed



(a) Fig.6.5 (b)

Fig.6.5 (a) Etch pits on the (001) face of a DAHC crystal. (x500)

(b) The same area in (a) after successive layer etching. (x500)

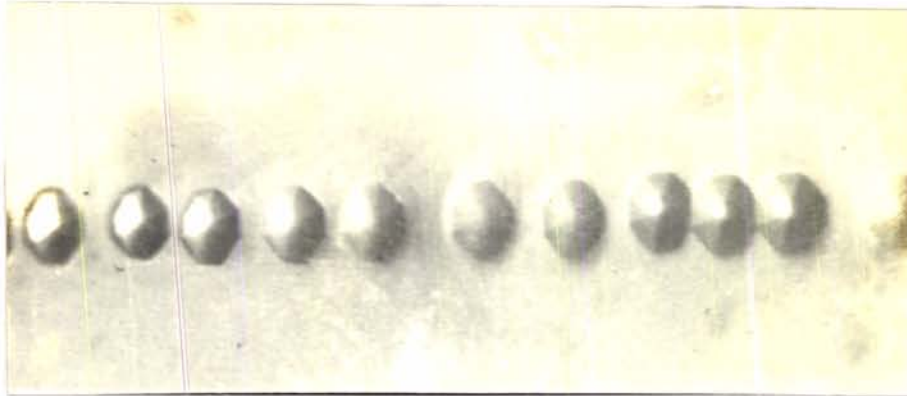


Fig.6.6 An etched grain boundary on (001) surface of a DAHC crystal. (x500)

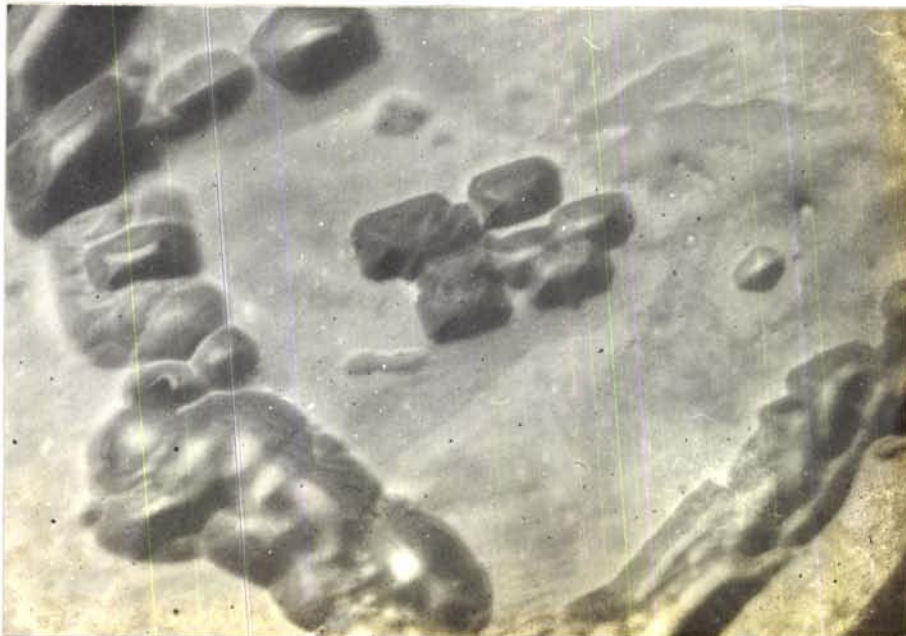


Fig.6.7 A cluster of pits observed on (001) surface of a DAHC crystal. (x120)

showing that they do not originate from the seed of the crystal. Microscopic foreign particles are sometimes observed at such sites indicating the chance of impurity origin of such pits.

Paired rows of pits as seen on (100) surface of strontium-barium niobate /17/ due to an array of dislocation loops or spiral has also been observed and is shown in Fig.6.8. Etching also reveals helices (Figs.6.9a,b) as has been observed in certain crystals /18, 19/. Dendrite like structures (Figs.6.10a,b) extending to a few millimeters are sometimes seen on (001) face. After a few cycles of successive etching such structures disappear.

Another interesting feature observed on etched (001) face is evenly spaced arrays of pits along $[010]$ direction (Fig.6.11) with maximum spacing of about 3.6×10^{-3} cm and minimum of about 1.3×10^{-3} cm.

Evidence of movement of dislocations in the crystal is occasionally observed (Fig.6.12). It is seen from Fig.6.13 that propionic acid is capable of revealing slip lines produced on (001) face, after application of a shear stress.

Successive layer etching

The spatial distribution of dislocations can be studied by etch-

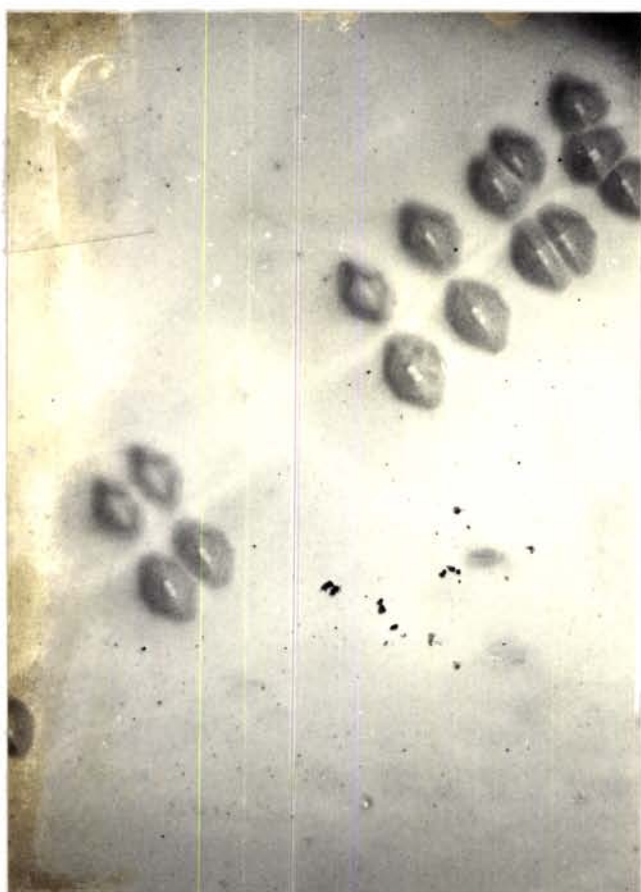
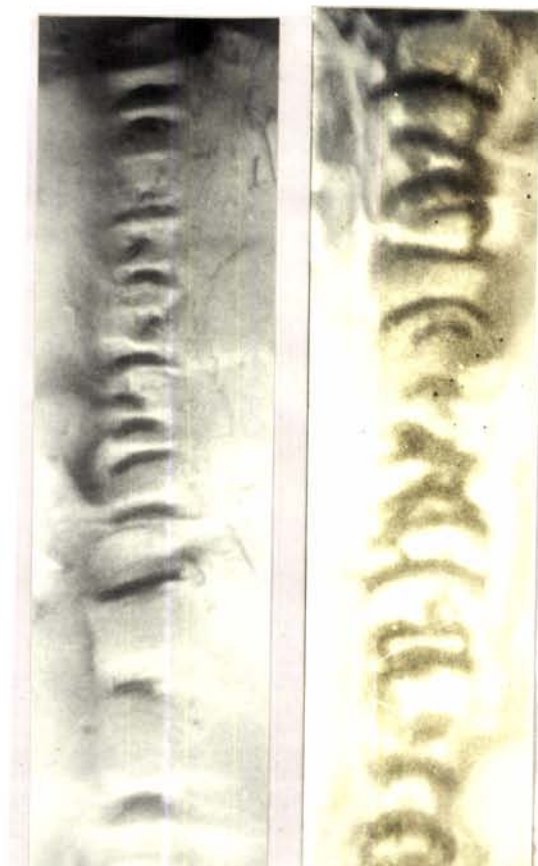


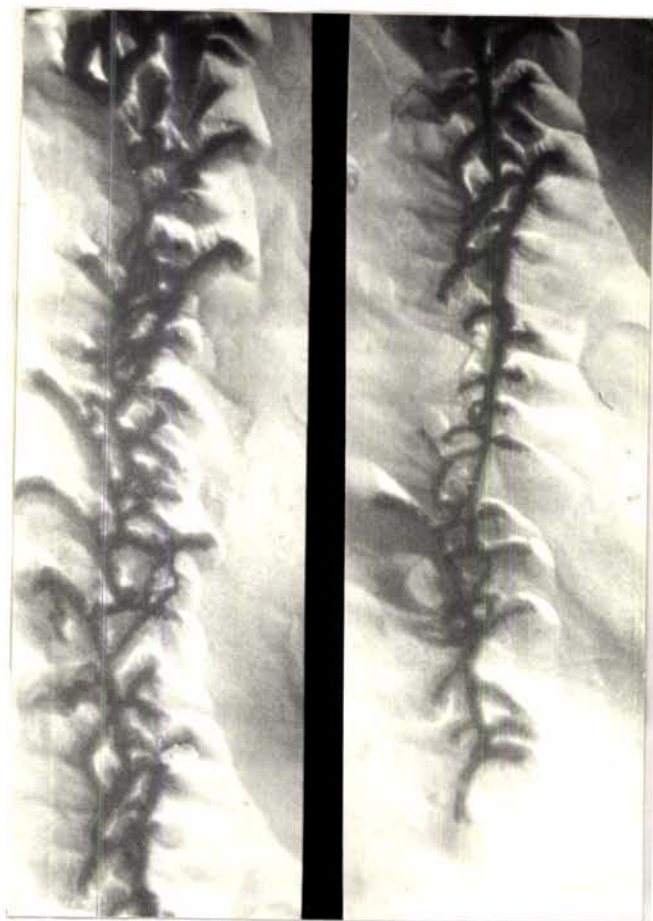
Fig.6.8



(a) Fig.6.9 (b)

Fig.6.8 Dislocation loops on (001) face of DAHC.(x120)

Fig.6.9 (a), (b) Dislocation helices on (001) face of DAHC. (x120)



(a) Fig.6.10 (b)

Fig.6.10 (a), (b) Dendrite - like structures observed on (001) surface of DAHC. (x120)



Fig.6.11 Array of pits along $[010]$ direction on (001) face of DAHC. ($\times 360$)



Fig.6.12 Etch pattern indicating movement of dislocations in DAHC. (x500)



Fig.6.13 Slip lines on (001) surface of DAHC. Etching time 30 secs. (x500)

ing successive layers. This technique is said to be favourable with low dislocation density materials /20/. Most of the crystals of DAHC have low dislocation density, hence etching method is suitable for revealing the spatial distribution of dislocations. From etching crystals of thickness of nearly 1mm, one to one correspondence of etch pits is often not observed on both sides. This fact suggests that there are loops, helices or branching of dislocations. Such a crystal was etched layer by layer and photomicrographs were taken until a one to one correspondence of etch pits was obtained. Analysis of the micrographs of the different layers confirmed the presence of loops, helices and branched dislocations. Dislocation loops were also observed around inclusions in successive layer etching.

Types of pits observed

Fig.6.14 shows a typical etched surface where a variety of pits are observed on (001) face of DAHC etched with propionic acid. Some of the different types of pits observed are, a) octagonal pits with corners rounded off (A-type, deep pits), b) flat bottomed pits (B--type), c) elliptical assymmetric pits (C-type) and d) small pits (D--type). Almost all the pits are oriented in the $\overline{010}$ direction.

Successive layer etching of (001) surface of DAHC with propionic acid reveals that octagonal pits are associated with dislocations which extend into the crystal more or less perpendicular to the sur-

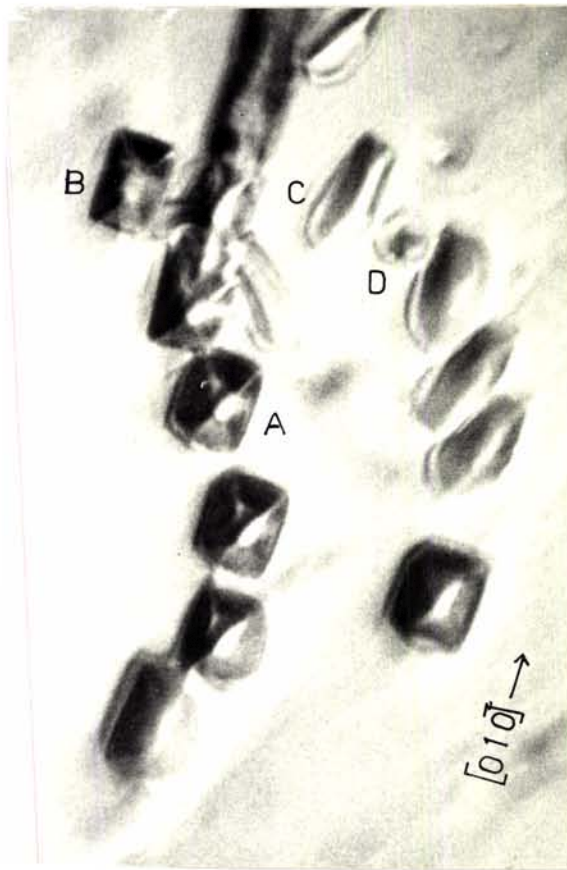


Fig.6.14 Etched (001) surface showing different types of pits. (x600)

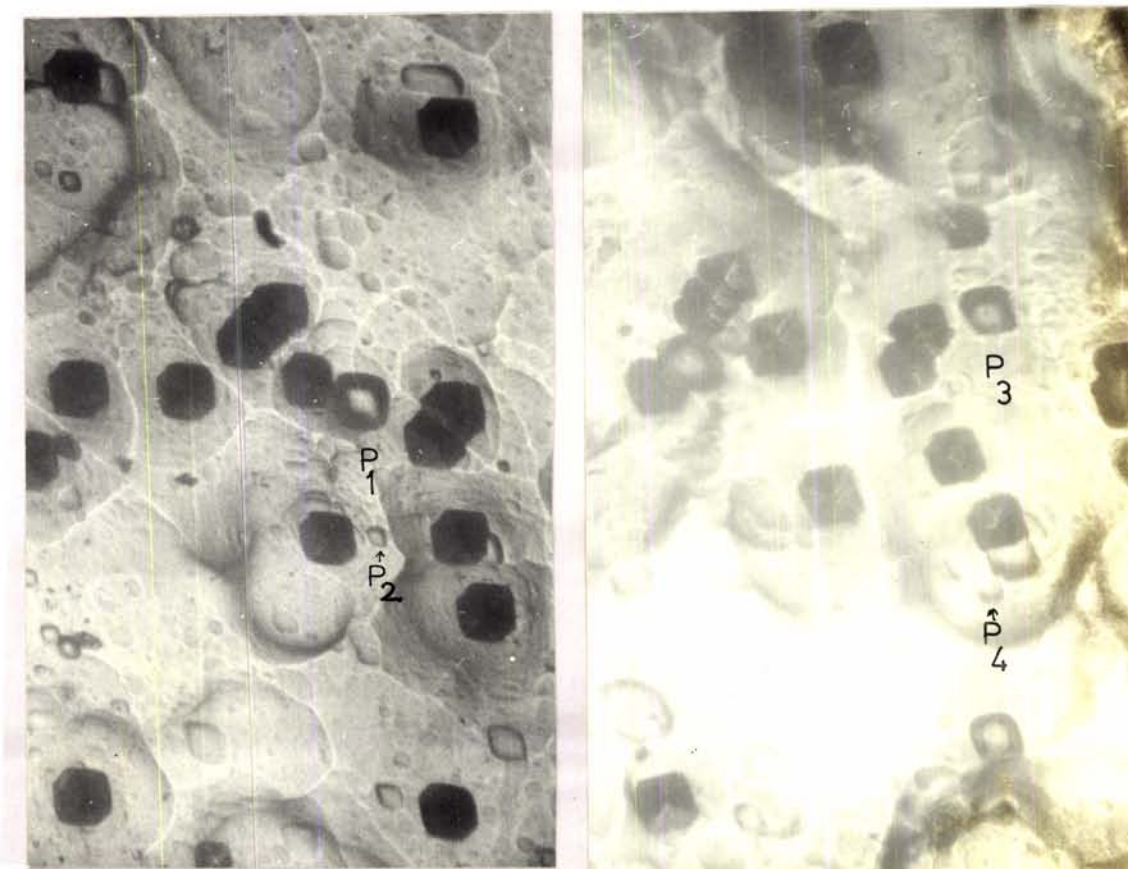
face. The flat bottomed and shallow pits appear and disappear on successive layer etching indicating that they are due to dislocations which extend only a few molecular layers. Such shallow pits are due to small dislocation loops. Figs.6.15a,b show the same area before and after successive layer etching respectively. The elliptical asymmetric pits are associated with inclined dislocations. The small pits are produced by thermal stresses and small defects.

Kinetics of etching

Fig.6.16 gives lateral etch rate along $[010]$ direction versus mean distance from the centre of the deep and shallow pits. The etch rate decreases with distance from the dislocation line as the stress associated with dislocation decreases with distance. The lower etch rate for the shallow pits supports the view that these pits are associated with small dislocation loops. From the relation for the rate of dissolution along the surface [21],

$$v_t = \sigma x_s \beta \nu \exp \left[\frac{-\Delta H}{kT} \right] \quad (6.1)$$

where x_s is the mean displacement of an atom diffusing from a kink site to an adsorbed position, $\beta \leq 1$ is a factor which accounts for the hindrance of the motion of ledges in the presence of an impurity, ν is a frequency factor, $\sigma = 1 - c/c_0$ is the undersaturation where c_0 is the saturation concentration of the material in an etching medium and c is the actual concentration at the dislocation site, T is the absolute temperature, k is Boltzman's constant and ΔH is the free



(a)

Fig.6.15

(b)

Fig.6.15 (a) An etched (001) surface of DAHC. (x120)

(b) Same area in (a) after successive layer etching. Flat bottomed pits such as P_1 and shallow pits such as P_2 in (a) is not seen here, while new pits such as P_3 and P_4 appear. (x120)

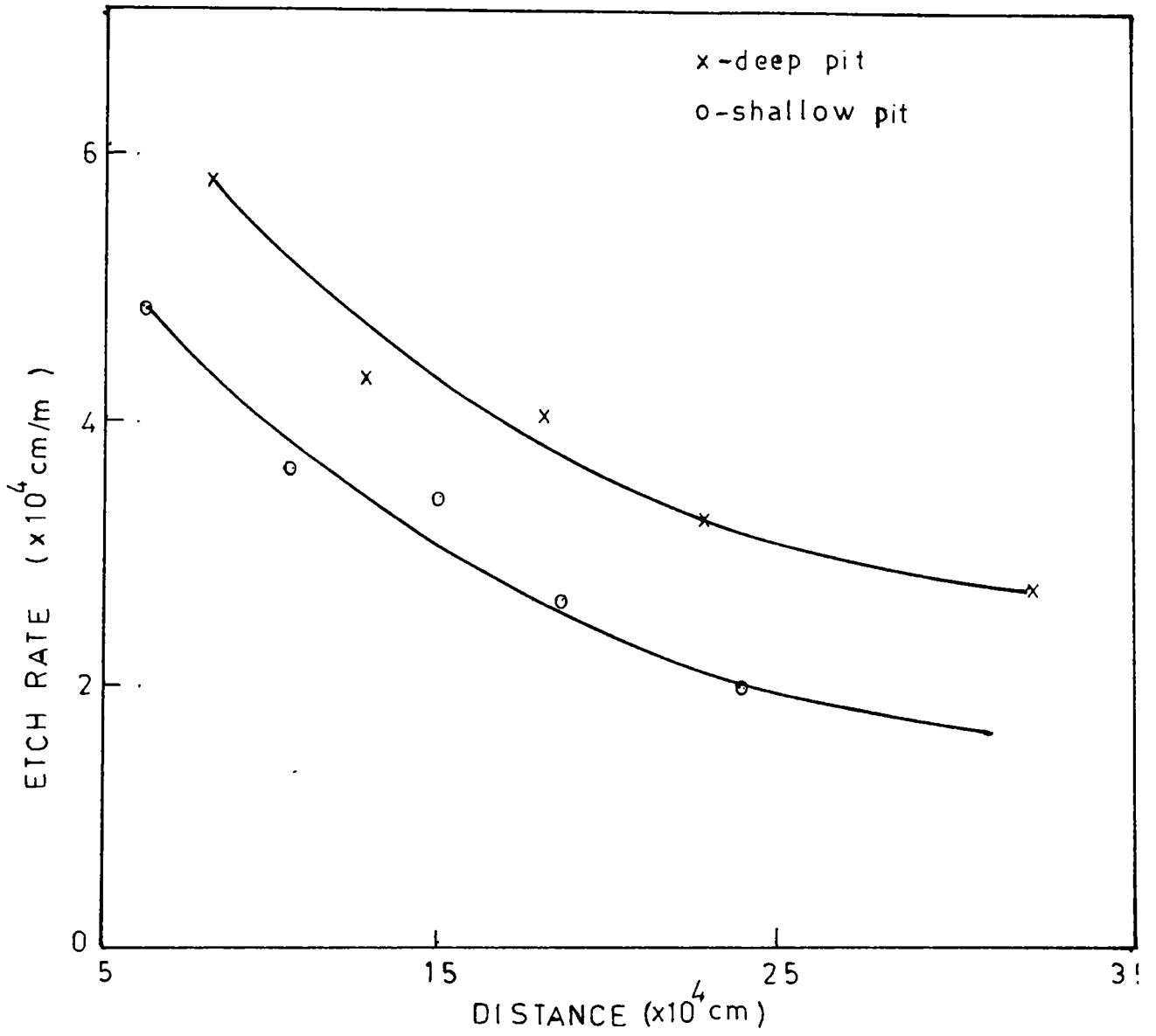


Fig.6.16 Plot of lateral etch rate along $[010]$ direction versus mean distance from the centre of the pits.

energy change for a molecule going from crystal surface into solution, one can find the mean difference in elastic strain energy associated with a molecule at the deep pit site and the shallow pit site by introducing a strain energy term in ΔH . It is assumed that σ , x_s , ρ and v have the same value in the case of both types of pits. Fig.6.17 shows the relation between this difference in strain energy and the time of etching. The strain energy difference remains constant in the initial stages of etching and then increases sharply showing that the strain energy due to the dislocations at the shallow pit site decreases considerably beyond a certain etching time.

The activation energy for the etching process is obtained if the free energy change ΔH for a molecule going from the crystal surface into the etching solution can be calculated. This was obtained by etching the (001) face of DAHC using a 10M benzene solution of acetic acid, which was found to be a reliable etchant. Etching experiments were performed at various temperatures. From the lateral etch rate data along $[010]$ and $[100]$ directions for the deep pits, a graph is drawn taking $\ln v_t$ along the y-axis and $1/T$ along the x-axis. The graph obtained is a straight line (Fig.6.18). From the slope of the graph, the free energy change for a molecule during etching of the crystal is found to be equal to 0.659 ev. The etch rate along the two directions $[010]$ and $[100]$ is determined by the frequency factor by which the molecules goes from ledge positions into the solution and therefore the ratio of the frequency factor along the two direct-

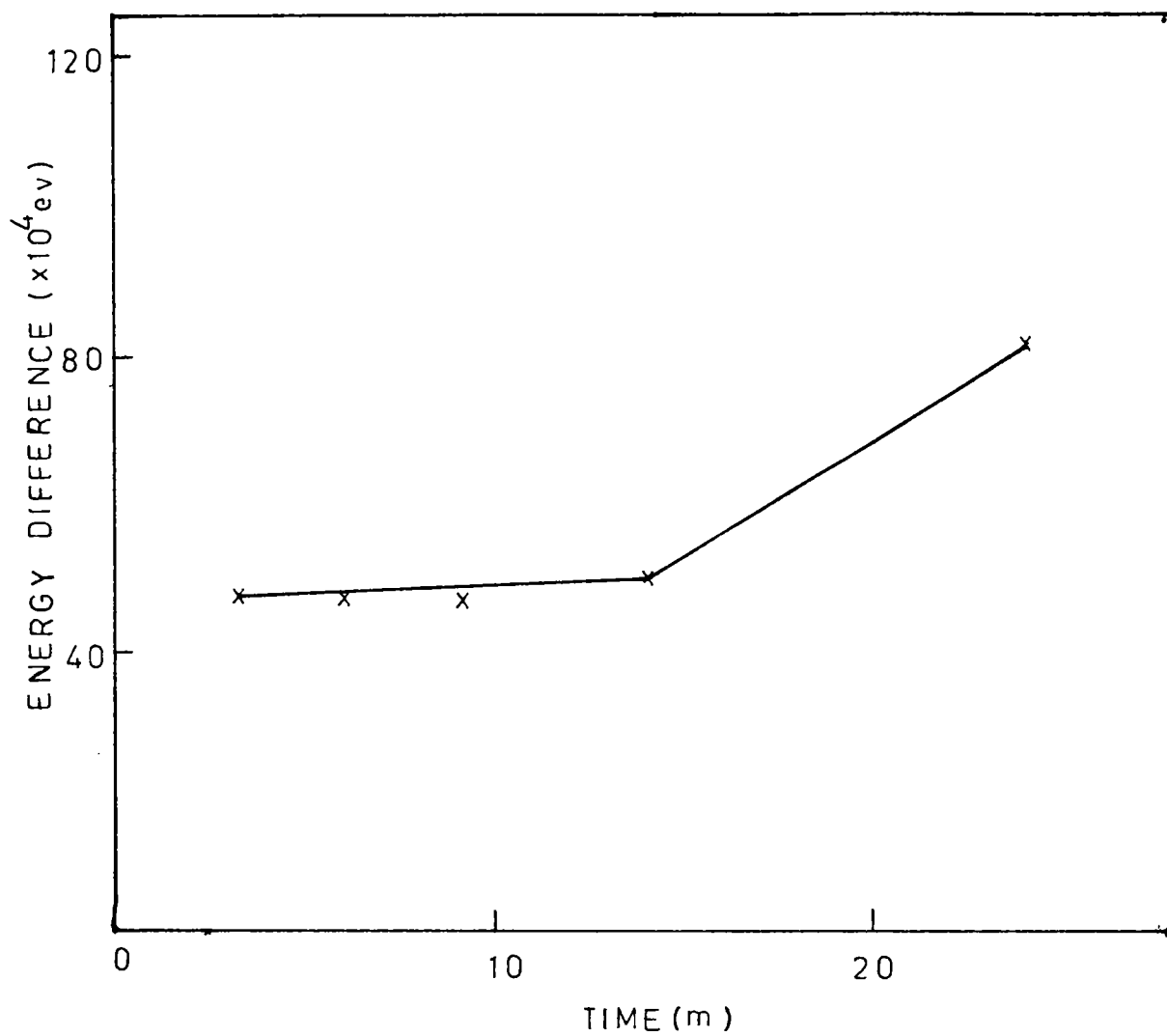


Fig.6.17 Plot showing the relation between the difference in strain energy between the deep and shallow pits versus time of etching.

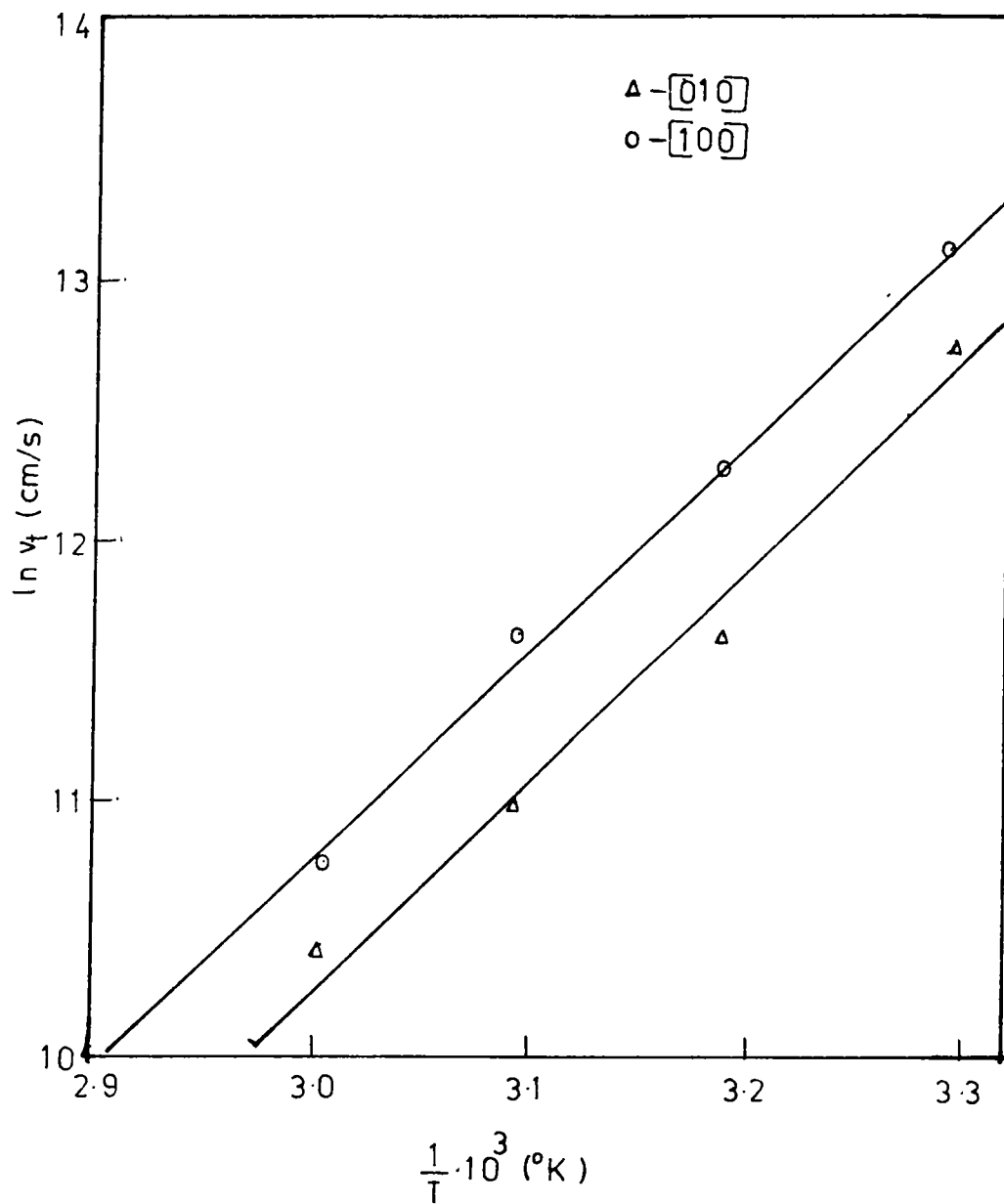
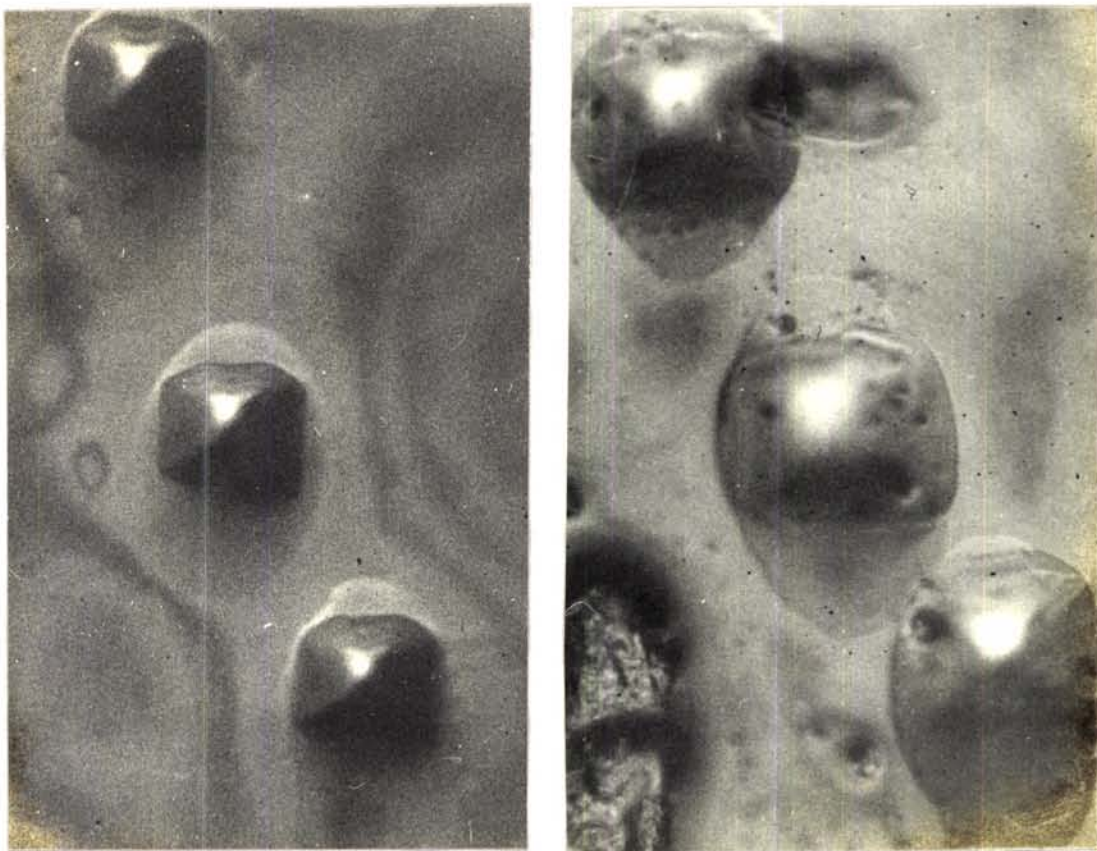


Fig.6.18 Graph showing lateral etch rate along $[010]$ and $[100]$ direction versus inverse of absolute temperature.

ions can be obtained from the difference in etch rate along these directions. The ratio of the frequency factor along $[010]$ and $[100]$ directions on (001) face is found to be around the value 1.65.

Comparison of etchants

It is an accepted fact that although an etchant may show dislocation sites for a specific crystal, all the dislocations are not necessarily etched by a particular etchant. Some etchants may reveal edge dislocations and some screw dislocations /22, 23/. Certain etchants reveal fresh/aged dislocations /24/. In the case of polar crystals it has been shown that the two types of dislocations differing in their signs behave differently during etching /25/. Positive and negative dislocations in copper appear as light and dark pits /26/. In short, an etchant may act differently for different types of dislocations and thus different etchants may be required to bring out all types of dislocations in a crystal. Formic acid (Figs.6.19a,b), acetic acid (Figs.6.19c,d) and methyl alcohol (Figs.6.19e,f) are shown to be other dislocation etchants for (001) face of DAHC by repeated etching. The morphology of the pits observed during etching with formic, acetic, propionic acids and methyl alcohol etchants is clearly seen in Figs.6.20, 6.21, 6.22 and 6.23 respectively. The factors affecting the morphology of etch pits /27-35/ can be summarised as 1) concentration and composition of the etchant or inhibitor, 2) etching conditions such as dynamic or static, 3) temperature of the etchant, 4)



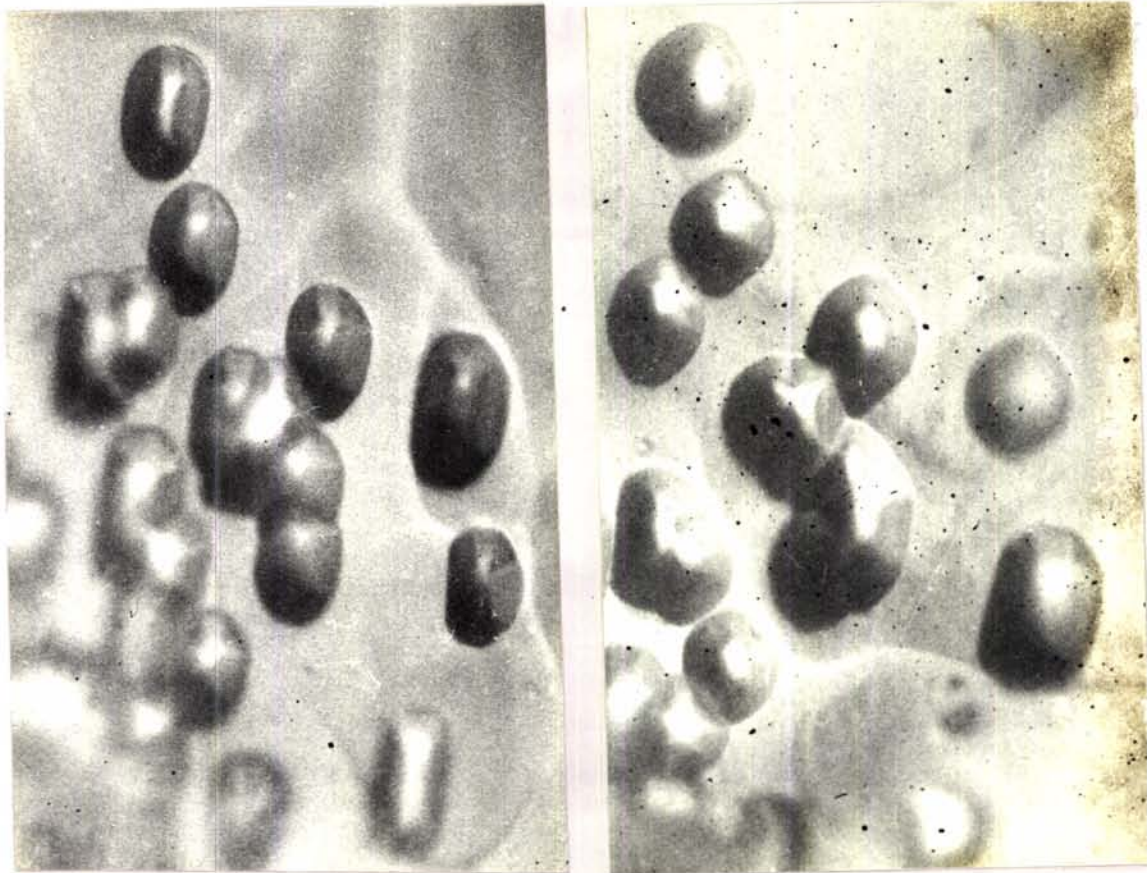
(a)

Fig.6.19

(b)

Fig.6.19 (a) (001) surface of DAHC etched in formic acid. (x150)

(b) Same area after repeated etching. (x150).



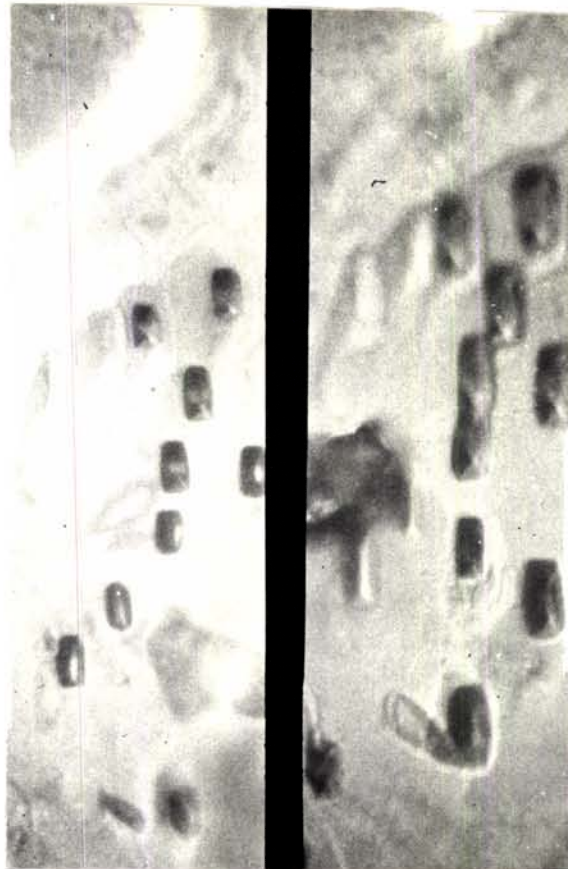
(c)

Fig.6.19

(d)

Fig.6.19 (c) (001) surface of DAHC etched in acetic acid. (x150)

(d) Same area after repeated etching. (x150)



(e) Fig.6.19 (f)

Fig.6.19 (e) (001) surface of DAHC etched in methyl alcohol. (x150)

(f) Same area after repeated etching. (x150)



Fig.6.20

Fig.6.20 A typical etch pit on (001) surface of DAHC. Etchant - formic acid. (x700)



Fig.6.21

Fig.7.21 Another etch pit. Etchant - acetic acid. (x700)

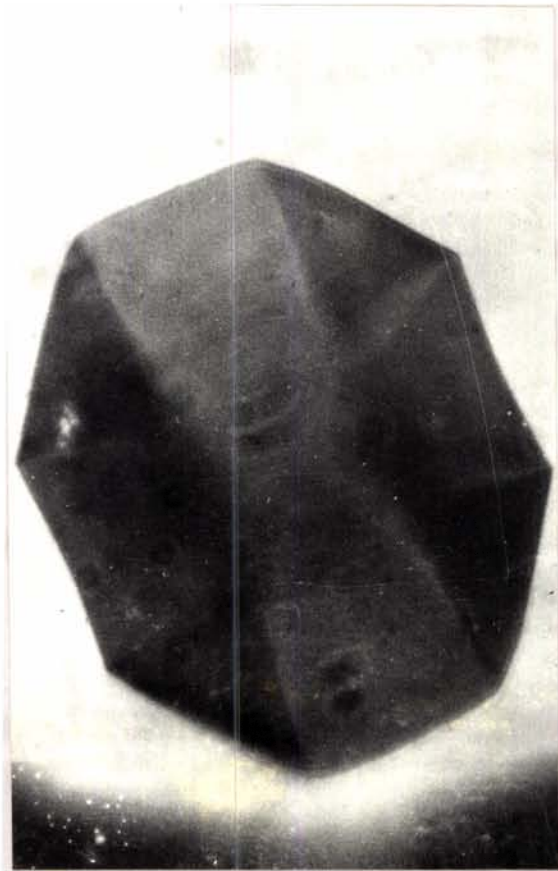


Fig.6.22

Fig.6.22 A typical etch pit on (001) surface of DAHC. Etchant - propionic acid. (x700)



Fig.6.23

Fig.6.23 Another etch pit. Etchant - methyl alcohol. (x700)

stability and inhibition capability of structurally different complexes present in the etching medium, 5) inhibitive action of reaction products, 6) nature of dislocations, 7) etching time, 8) symmetry of the etched plane, 9) energy associated with etched defects, 10) magnitude and sign of dislocation Burgers vector and 11) solubility of the crystal in a solution.

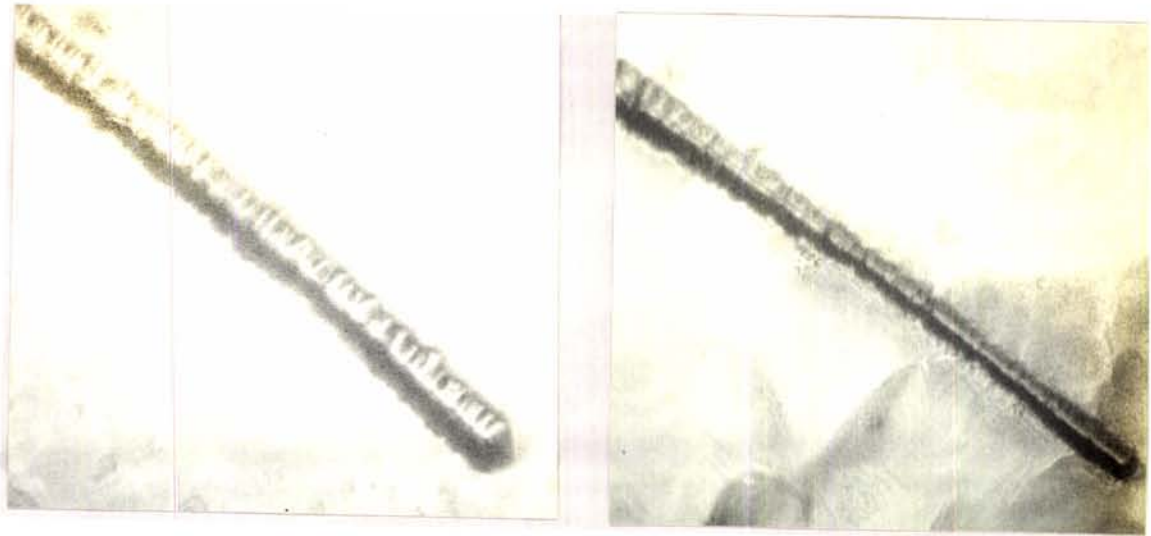
Fig.6.24a shows a grain boundary etched with formic acid for 10 secs. This is again etched in acetic acid for 15 secs after washing away a thin layer of the crystal (Fig.6.24b). Another layer under the same area is again etched in propionic acid for 30 secs. and shown in Fig.6.24c. Figs.6.25a,b,c show the junction of a grain boundary successively etched in formic acid, acetic acid and methyl alcohol for 20 secs each respectively.

Etching of (110) cleavage face

Propionic acid is a good dislocation etchant for the (110) cleavage face as revealed by the mirror image correspondence of etch pits on matched cleavages (Figs.6.26a,b). The mean density of dislocations intersecting (110) face is found to be around $6 \times 10^3/\text{cm}^2$.

6.3.3. ETCHING OF CA CRYSTALS

Formic acid, acetic acid, propionic acid and methyl alcohol



(a)

(b)



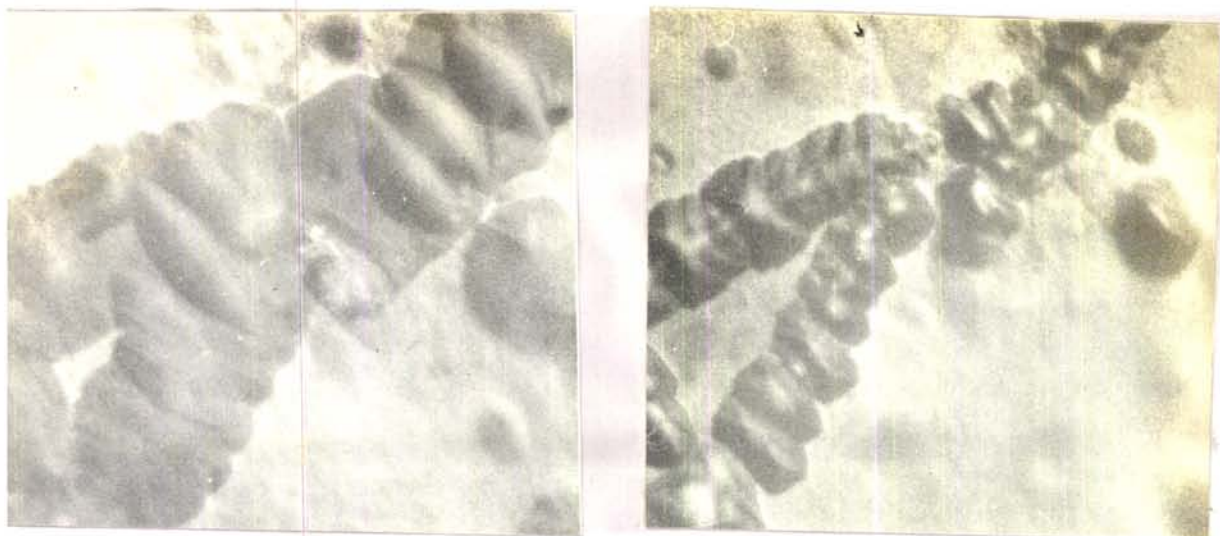
(c)

Fig.6.24

Fig.6.24 (a) A grain boundary etched in formic acid. (x120)

(b) Area in (a) etched in acetic acid after surface removal. (x120)

(c) Area in (b) etched in propionic acid after further surface removal. (x120)



(a)

(b)



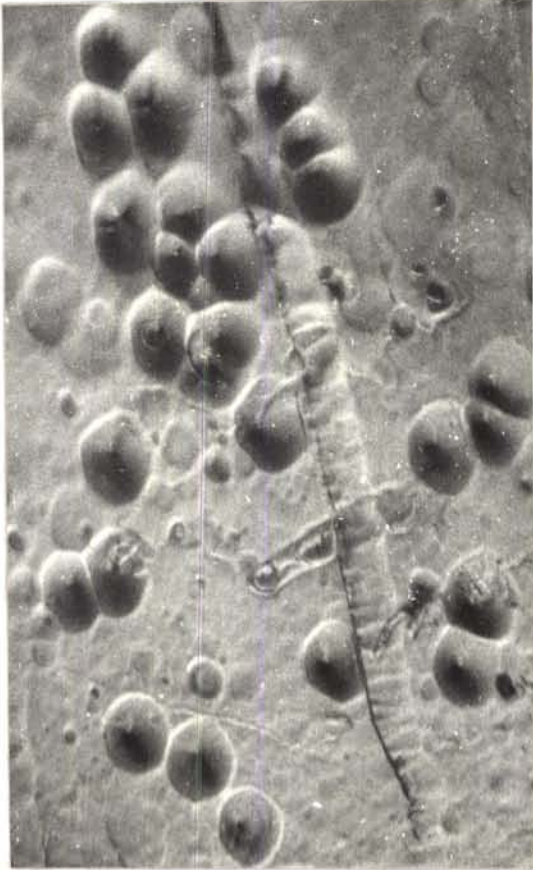
(c)

Fig.6.25

Fig.6.25 (a) Junction of a grain boundary etched in formic acid. (x150)

(b) Area in (a) etched in acetic acid after surface removal. (x150)

(c) Area in (b) etched in methyl alcohol after further surface removal. (x150)



(a)

Fig.6.26

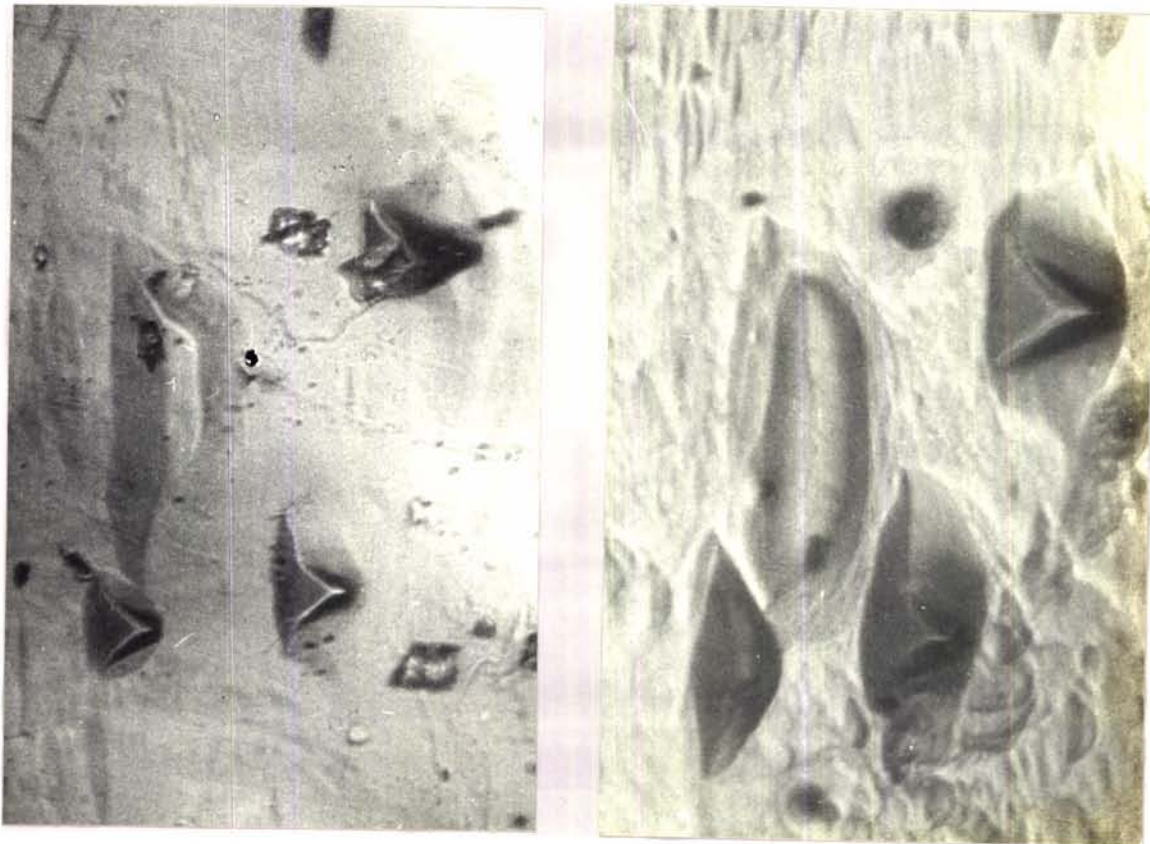
(b)

Fig.6.26 (a), (b) Matched cleavage faces of DAHC etched in propionic acid. (x200)

were found to be potential etchants for the (101) face of CA crystals also. Propionic acid is shown to be a reliable dislocation etchant for the (101) face. Fig.6.27a shows the (101) surface etched for 10 secs. This is repeatedly etched for 10 more secs and the etch pits are found to increase in size and depth without increase in number (6.27b). The reliability of the etchant was further confirmed by successive layer etching. Fig.6.28a shows another etched surface. The same surface has been etched after removing a thin layer (Fig.6.28b). NaOH solution was used for removing a thin layer from the crystal surface. It can be seen that there is a one to one correspondence of pits in successive layer etching. The mean density of dislocations intersecting the (101) surface is around $2 \times 10^3/\text{cm}^2$. A typical etch pit under high magnification is shown in Fig.6.29. The shape of the pit can be clearly seen here. Cluster of dislocations are also observed and is presented in Fig.6.30.

6.4. CONCLUSIONS

Microscopy of etched surface is a widely accepted method for direct observation of dislocations in conductors, semiconductors and insulators. Propionic acid is a reliable dislocation etchant for the (001) face of DAHC single crystals. The mean density of dislocations intersecting the (001) face of DAHC is of the order of $2 \times 10^2/\text{cm}^2$. Propionic acid also reveals dislocation loops, helices, movement of dislocations and slip lines. Shallow pits observed during propionic



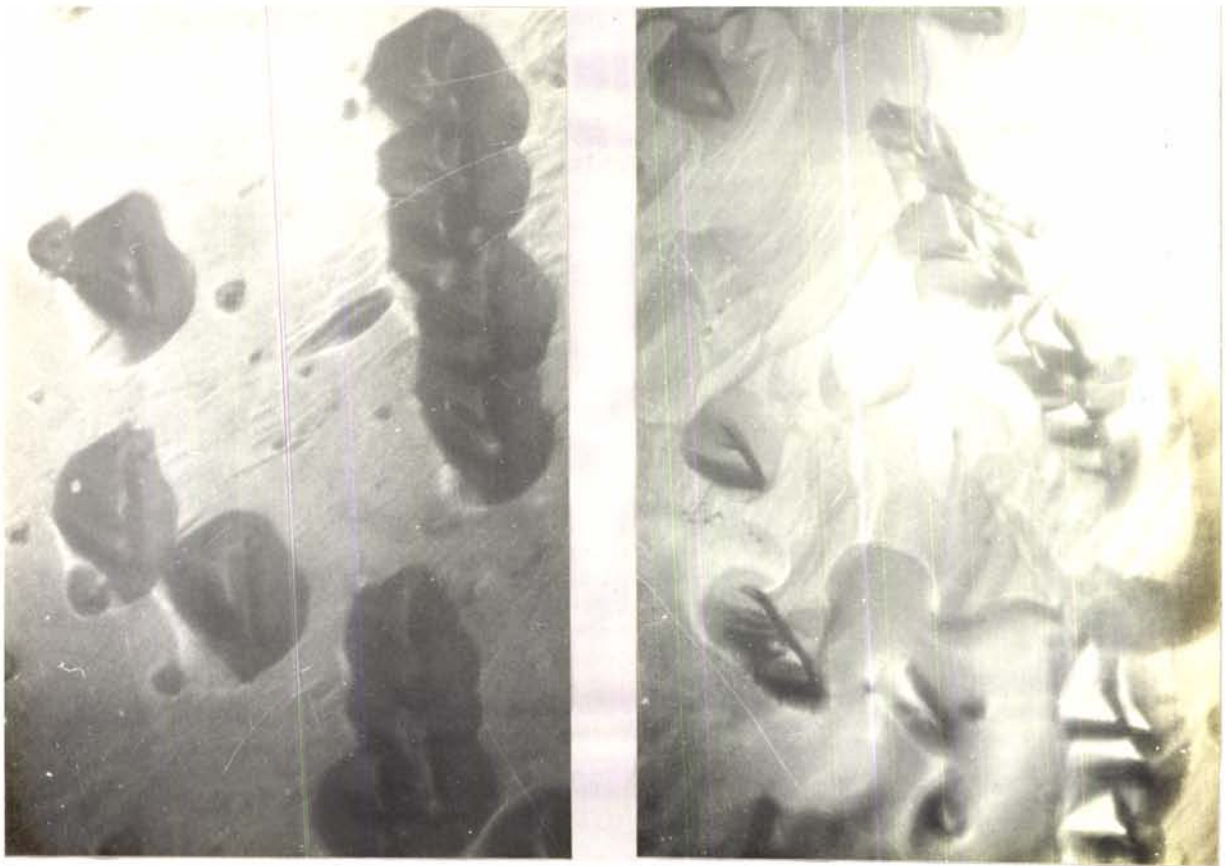
(a)

Fig.6.27

(b)

Fig.6.27 (a) (101) surface of a CA crystal etched in propionic acid.
(x120)

(b) The area in (a) after repeated etching. (x120)



(a) Fig.6.28 (b)

Fig.6.28 (a) An etched (101) surface of a CA crystal. (x120)

(b) The area in (a) after successive layer etching. (x120)



Fig.6.29

Fig.6.29 A typical etch pit on (101) face of a CA crystal at high magnification showing the shape of the etch pit. (x700)



Fig.6.30

Fig.6.30 A dislocation cluster on (101) surface of a CA crystal. (x120)

acid etching are due to small dislocation loops. The activation energy of a molecule for the etching process is found to be 0.659 eV. Formic acid, acetic acid and methyl alcohol are other dislocation etchants for (001) face of DAHC. Propionic acid is a reliable etchant for the (110) face of DAHC. It is also capable of etching (101) face of CA crystals. The density of dislocations intersecting this surface is about $2 \times 10^3/\text{cm}^2$.

REFERENCES

1. T.S.MIKHAILOVAKAYA et al., Sov. Phys. Solid State 23(1981)1255.
2. R.Yu.LYALIKOVA et al., Ibid. 24(1982)1042.
3. A.V.ZARETSKII et al., Ibid. 25(1983)408.
4. W.D.JOHNSTON, "Defects in semiconductors II", (Symposium proceedings, Boston, USA, North-Holland, N.Y. 1983) p.453.
5. K.KAWABUCHI, J. Cryst. Growth 11(1971)92.
6. Y.IMASHIMIZU and J.WATANABE, Trans. Jap. Inst. Metals, 24(1983)1.
7. B.W.BATTERMAN, J. Appl. Phys. 28(1957)1236.
8. R.B.HEIMANN et al. J. Cryst. Growth 57(1982)48.
9. K.SANGWAL, J. Mater. Sci. 17(1982)2227.
10. J.GEORGE and P.K.SARANGADHARAN, J. Phys. D: Appl. Phys. 10(1977)1467.
11. E.B.LEIKO et al., Phys. Status Solidi. a 44(1977)285.
12. N.SAKA and T.IMURA, Phys. Status Solidi. a 19(1973)653.
13. S.N.G.CHU et al., J. Electrochem. Soc. 129(1982)352.

14. I.V.GRIDNEVA et al., Phys. Status Solidi. a 54(1979)195.
15. M.S.JOSHI et al., Ind. J. Pure and Appl. Phys. 19(1981)412.
16. S.K.ARORA and T.ABRAHAM, J. Mater. Sci. 17(1982)1723.
17. Y.ITO and Y.FURUHATA, Phys. Status Solidi. 23(1974)147.
18. E.LENVAY, J. Cryst. Growth 59(1982)375.
19. T.INOVE et al., J. Cryst. Growth 55(1981)307.
20. K.TAKAGI et al., J. Cryst. Growth 48(1980)19.
21. W. SCHAARWACHTER, Phys. Status Solidi. 12(1965)865.
22. S.MENDELSON, J. Appl. Phys. 32(1961)1579.
23. F.W.YOUNG, J. Appl. Phys. 32(1961)192.
24. J.J.GILMAN, "The surface chemistry of metals and semiconductors"
(edited by H.C.GATOS, N.Y., 1960) p.136.
25. H.C.GATOS et al., J. Appl. Phys. 32(1961)1174.
26. J.D.LIVINGSTON, Acta Metallurg. 10(1962)229.
27. T.I.PAPUSHINA et al., Izv. Akad. Nauk SSSR,
Neorg. Mater. 17(1981)823.
28. B.BORECKA and K.SANGWAL, J. Mater. Sci. Lett. 1(1982)364.
29. K.SANGWAL et al. J. Cryst. Growth 58(1982)261
30. R.J.JACCODINE, J. Appl. Phys. 33(1962)2643.
31. D.J.VAGHARI and B.S.SHAH, Ind. J. Pure and Appl.
Phys. 19(1981)1205.
32. T. SUZUKI, J. Cryst. Growth 20(1973)152.
33. K.SANGWAL, J.Mater. Sci. 17(1982)3598.
34. K.SANGWAL and A.A.URUSOVSKAYA, J. Cryst. Growth 41(1977)216.
35. H.NISHIKAWA, Jpn.J.Appl.Phys. 12(1973)1647.

CHAPTER SEVEN

MICROINDENTATION ANALYSIS OF DAHC AND CA SINGLE CRYSTALS

7.1. INTRODUCTION

In this chapter, the microindentation analysis of DAHC and CA single crystals, to evaluate the hardness, toughness and brittleness and to study the variation of these quantities with load is presented. The nature of the cracks in these crystals is also analysed.

7.2. EXPERIMENTAL

DAHC crystals were indented on the as grown $[00\bar{1}]$ face with the indenter diagonal along $[01\bar{0}]$ and $[10\bar{0}]$ directions, and on the cleavage $[11\bar{0}]$ face with the indenter diagonal along $[11\bar{0}]$ and $[00\bar{1}]$ directions. These indentations were made on dislocation free regions using the Hanemann microhardness tester Model D32 described in chapter four.

A number of samples ($\approx 10\text{mm} \times 3\text{mm} \times 2\text{mm}$) were indented and corresponding to different loads in the range of interest, at least ten indentations were made and the average diagonal length of the indentations were obtained for each load. At first the load was applied for a time $T = (t_s + t)$, where $t_s = 5\text{secs}$ is the sinking time of the pyramid, varying the actual load resting time from 5 secs to 300 secs at constant load. The permanent impression for these and subsequent

trials were measured after a time lapse of 30 min to allow for any elastic recovery. Since the area of the impression did not bear any observable dependence on loading time for the constant load used, t was taken as 15 secs for all subsequent trials.

To study the nature of the threshold crack on $[00\bar{1}]$ and $[\bar{1}1\bar{0}]$ faces, the indented specimens were viewed under optical microscope for different loads from 0.5 g to the point when well developed cracks formed. The indented surface was also observed after etching with a suitable etchant to detect the initiation of the crack. To confirm the above observations, another set of indentations in the same load range was made and the surface studied under the microscope after gradual removal of the surface.

CA crystals were also indented on the $[\bar{1}0\bar{1}]$ surface with the indenter diagonal along $[01\bar{0}]$ and $[\bar{1}0\bar{1}]$ directions and the deformation and fracture were studied as in the case of DAHC crystals.

7.3. RESULTS AND DISCUSSION

7.3.1. DAHC CRYSTALS:

The variation of hardness with load of DAHC is given in Fig.7.1. Values of load upto 12.5 g are used for hardness measurements, since the incidence of cracking does not seem to influence the deformation

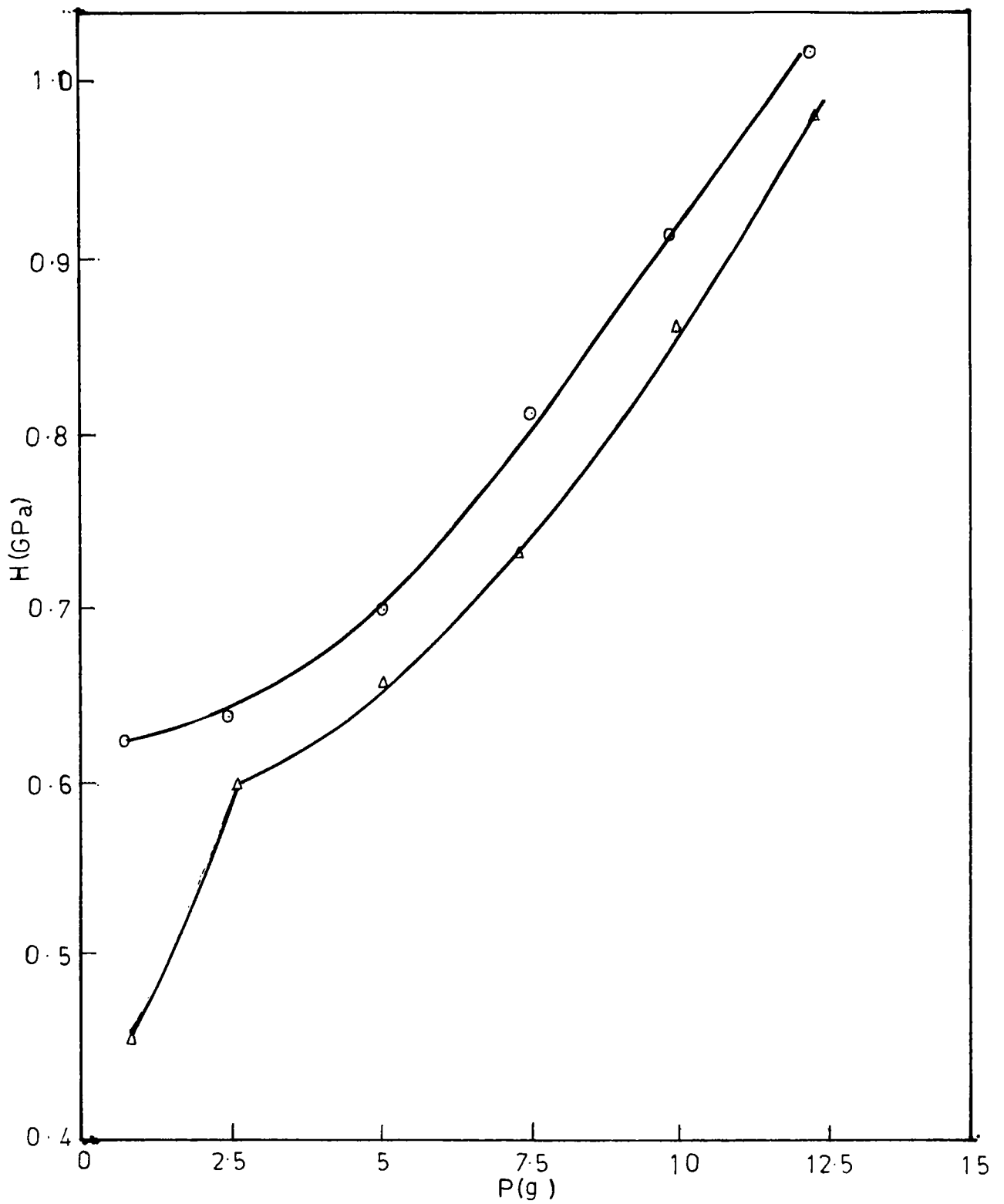


Fig.7.1 Variation of hardness with load for DAHC crystals.

Δ , (001) face; \circ , (110) face.

mechanics as long as the impression remains reasonably well defined and the crack does not extend considerably compared to the impression diagonal /1/. The special feature of the variation is the sharp increase in hardness with increase in load. The major contribution to the increase in hardness with load in DAHC is attributed to the high stress required for homogeneous nucleation of dislocations in the small dislocation free regions indented /2/. Also in the case of DAHC, microcracks ($c < a$) appear below 12.5 g. Thus a part of the applied stress is utilized for nucleation and propagation of these cracks and does not contribute to any increase in deformed area beneath the indenter, resulting in an increase in hardness value.

For loads greater than about 12.5g the cracks are large compared with the impression diagonal, and hence the toughness parameter comes into play. The plot of P against $c^{3/2}$ for loads upto 25g, where the slope suddenly changes, is shown in Fig.7.2. Loads beyond 25g were not used for the evaluation of toughness as chipping of material occurs sometimes above this load. Niihara /3/ has suggested the Palmqvist crack length l (Fig.3.1) instead of the median crack length c in the low load region for the evaluation of fracture toughness, and recommends l/a as a more appropriate normalization parameter than c/a for toughness evaluation. But in the case of DAHC single crystal, for loads above 12.5g well developed median cracks are formed (Fig.7.-3) although $c/a \approx 2$ to 5. The preference of c over l in the present case is further supported by Lankford /4/ who has shown that c/a norm-

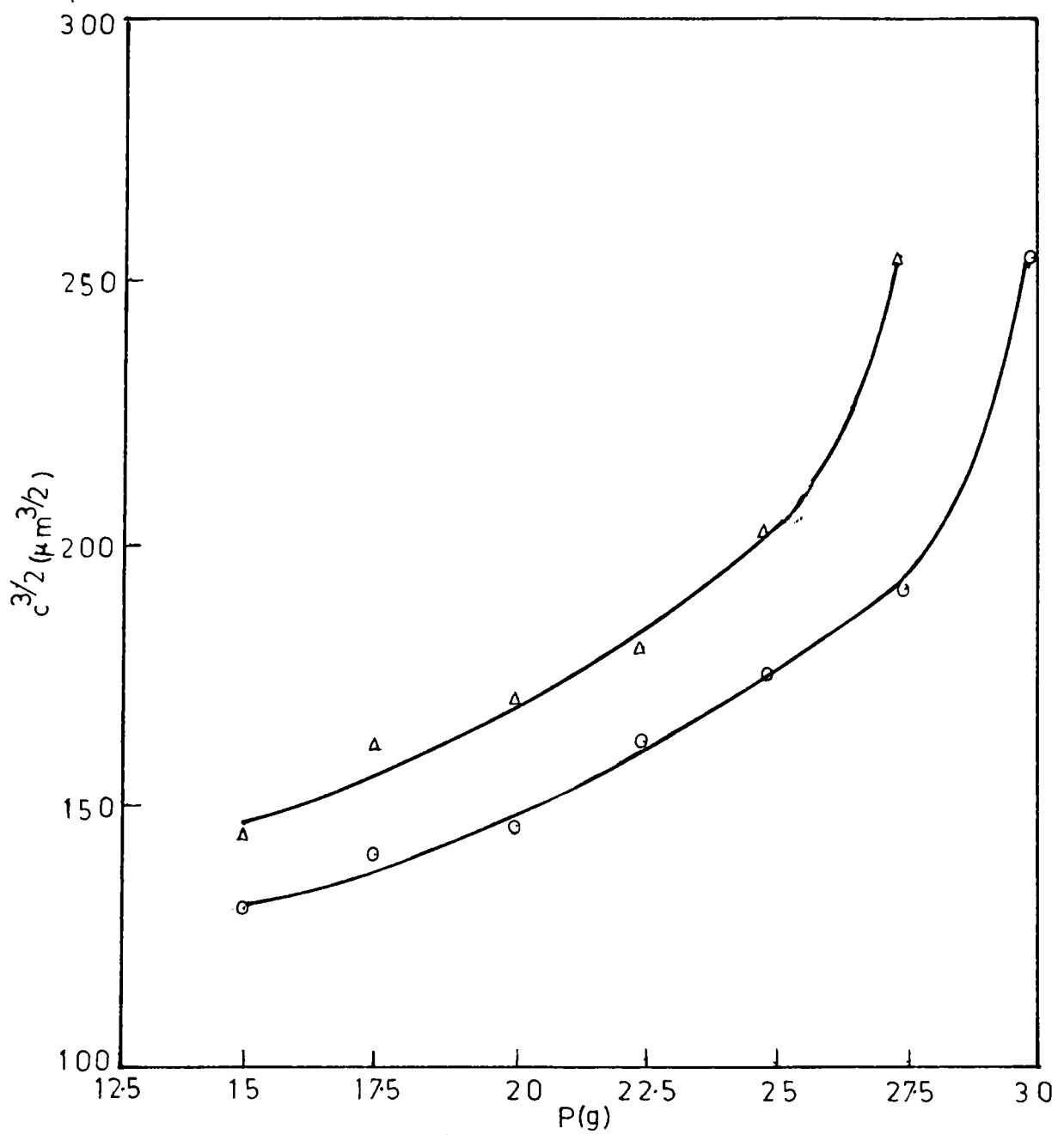


Fig.7.2 Variation of 3/2 power of semicrack length with load.

Δ , (001) face; o, (110) face.

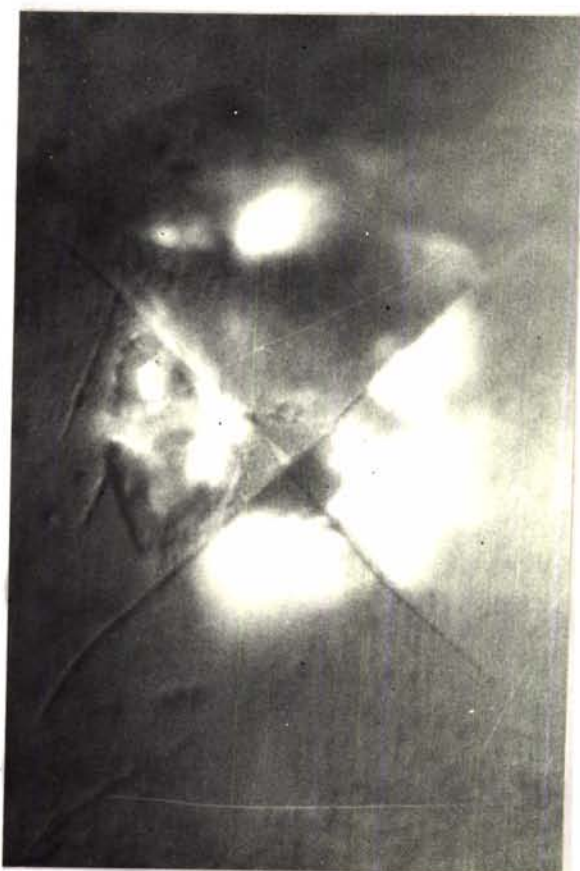


Fig.7.3 Sample indentation mark at a load above 12.5g on (001) face of DAHC showing half penny configuration around the indentation mark.

alization parameter "most nearly approaches universality".

The toughness value calculated is found to increase with increase in load in a regular manner as seen from Fig.7.4. The hardness, toughness and brittleness value for (001) and (110) faces of DAHC are given in table 7.1. For the purpose of classification and comparison with the corresponding values of well known materials, the average values of hardness, toughness and brittleness for the two planes are calculated and presented in table 7.2. This procedure is justified since there is no remarkable variation in these values for the two planes investigated, and the directional dependence of hardness is negligibly small.

Chemical etching is a useful technique by which slip traces and crack system around a microindentation can be easily observed. In order to show that cracks, if they are formed due to indentation, should be visible under microscope, two indentation marks, one with visible cracks (Fig.7.5a) and the other without visible cracks (Fig.7.6a) on the (001) face were etched with a suitable etchant. The position of the cracks visible earlier in the indentation marks are now shown by the four arms at the corners (Fig.7.5b) whereas the indentation without visible cracks shows no trace of cracks (Fig.7.6b). Fig.7.7a shows two indentation marks with cracks at different loads. After removal of a surface layer the crack lines have disappeared (Fig.7.7b), which clearly indicate that the cracks are radial and originate

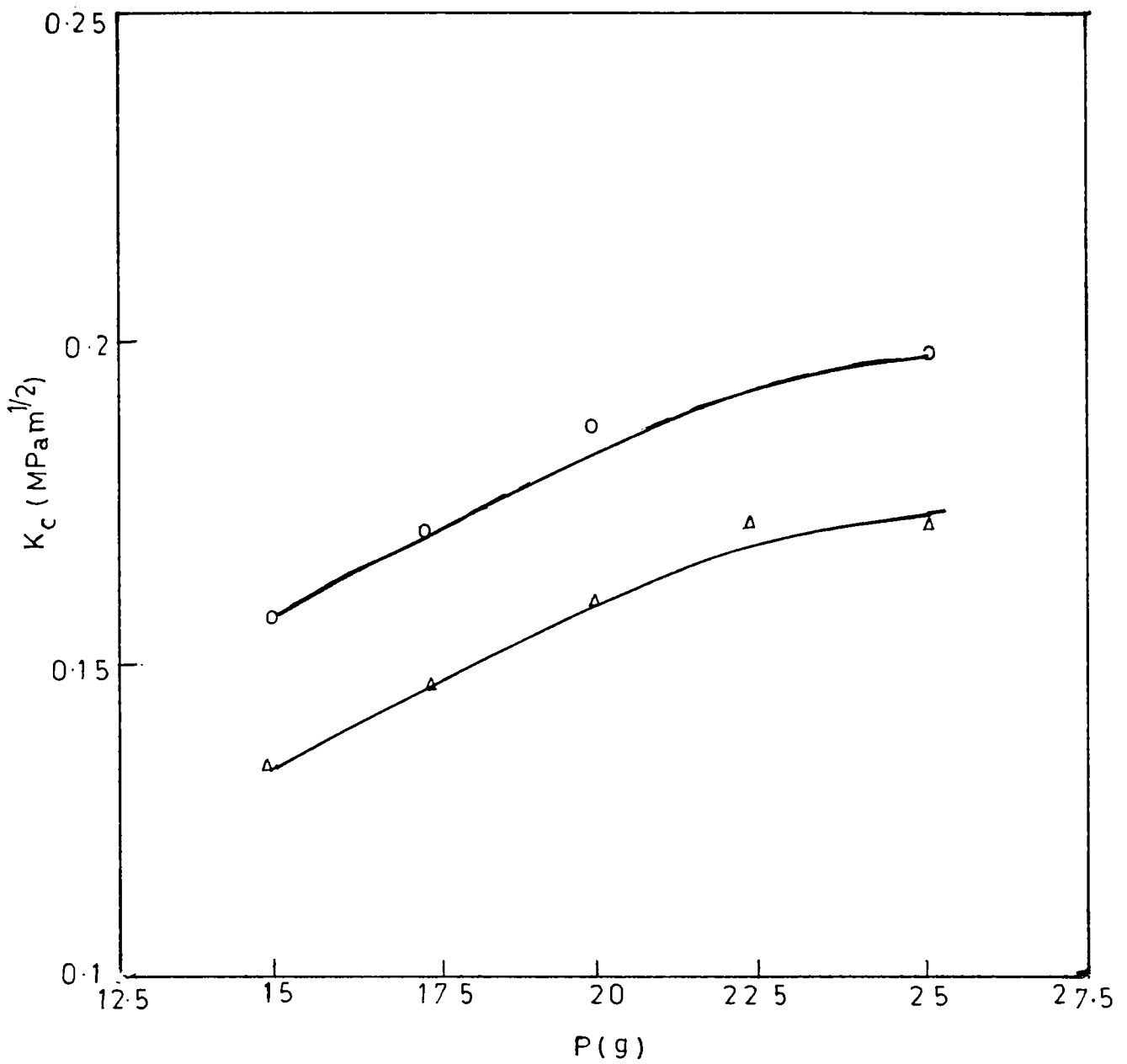


Fig.7.4 The variation of toughness with load for DAHC crystals: Δ , (001) face; o , (110) face.

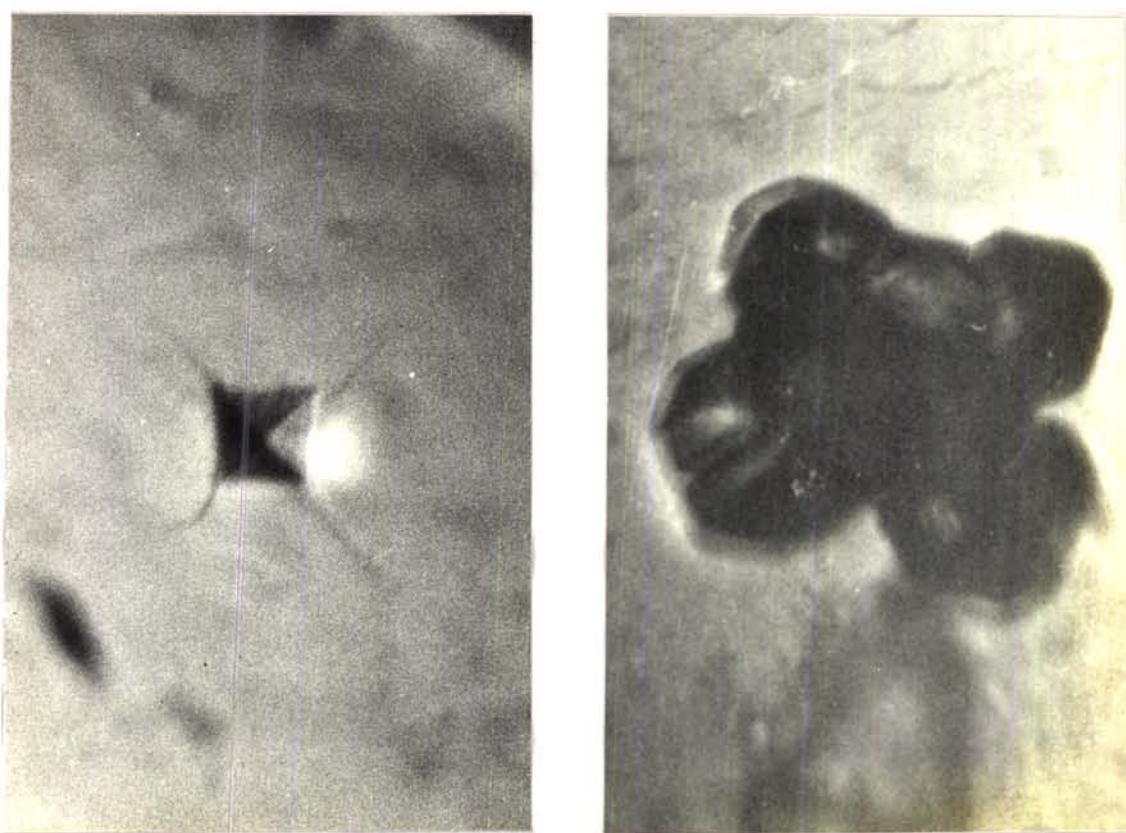
Table 7.1. Hardness, toughness and brittleness of DAHC.

Faces	Load range (g)	Hardness (GPa)	Toughness (MPa m ^{1/2})	Brittleness (μm ^{-1/2})
(010)	0.5 - 1.5	0.506		
	1.5 - 12.5	0.75		
	12.5 - 25.0		0.154	4.08
(101)	0.5 - 7.5	0.648		
	7.5 - 12.5	0.828		
	12.5 - 25.0		0.185	3.99

Table.7.2. Hardness, toughness, brittleness and threshold load and crack length values of DAHC with the corresponding values of some well known materials.

Material	Hardness (GPa)	Toughness (MPa m ^{1/2})	Brittleness (m ^{-1/2})	Threshold parameters			
				Load		Crack length	
				Th.(N)	Ex.(N)	Th.(μm)	Ex.(μm)
NaCl [#]	0.24	0.5	0.48	7.11	14.7	120.0	100.0
C ₆ H ₁₄ N ₂ O ₇	0.68	0.17	4.04	0.04	0.04	7.43	6.1
ZnSe [*]	1.1	0.9	1.2	8.0		80.0	
ZnS [*]	1.9	1.0	2.0	2.0		30.0	
Fe [*]	5.0	50.0	0.1	8x10 ⁵		12x10 ³	
MgF ₂ [*]	5.8	0.9	6.0	0.05		3.0	
SiO ₂ [*]	6.2	0.7	9.0	0.02		1.5	
Ge [#]	9.0	0.46	19.56	0.01	0.02	0.14	0.25
Si [#]	10.0	0.6	16.66	0.02	0.04	0.2	0.65
Al ₂ O ₃ [#]	12.0	4.0	3.0	0.25	0.24	5.0	3.0
Si ₃ N ₄ [*]	16.0	5.0	3.0	2.0		12.0	
SiC [#]	19.0	4.0	4.7	0.07	0.09	2.0	1.0
WC [*]	19.0	13.0	1.4	70.0		60.0	

- Data taken from Lankford /4/. * - Data taken from Lawn and Marshall /5/. Th. - Theory. Ex. - Experiment.



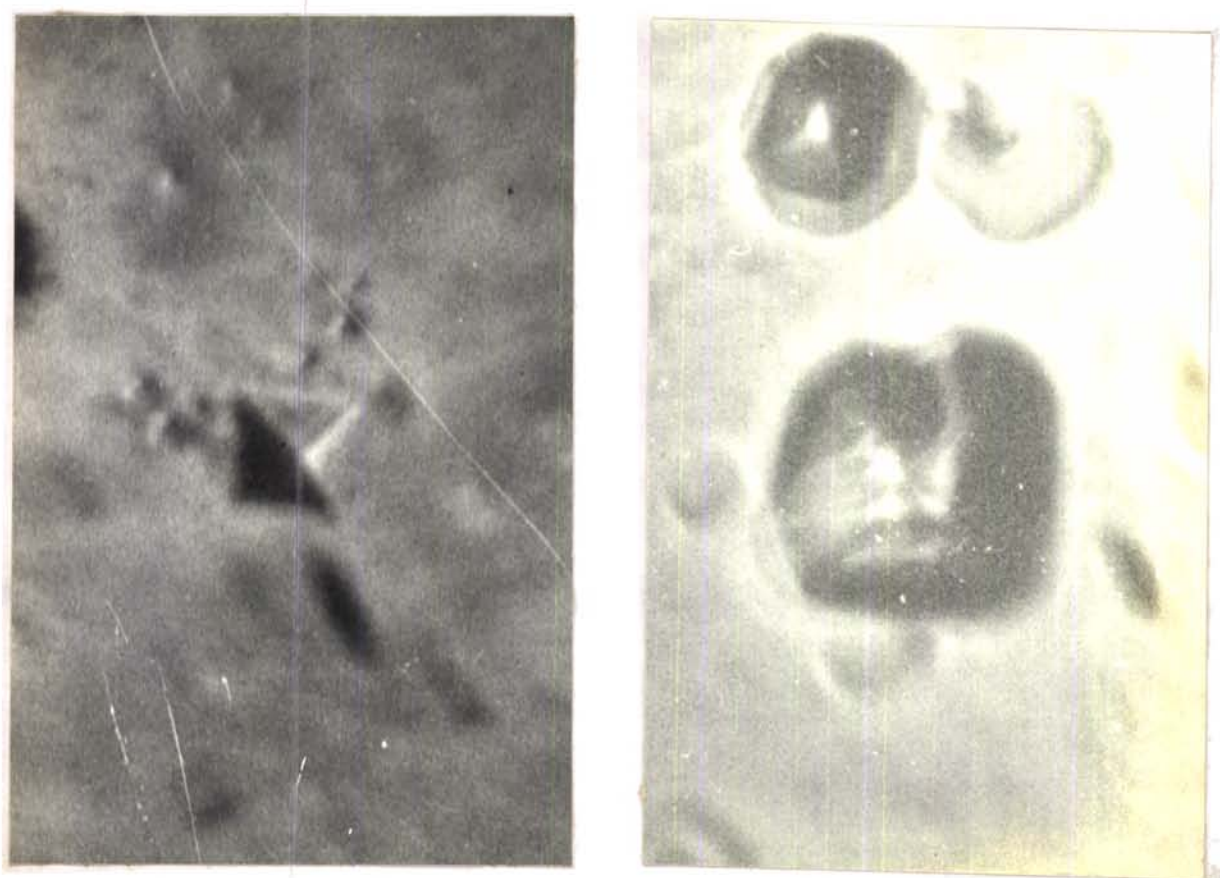
(a)

Fig.7.5

(b)

Fig.7.5 (a) An indentation mark showing the threshold cracks on (001) face of DAHC.

(b) Etch figure of indentation mark in (a) showing four arms in the directions of the cracks.



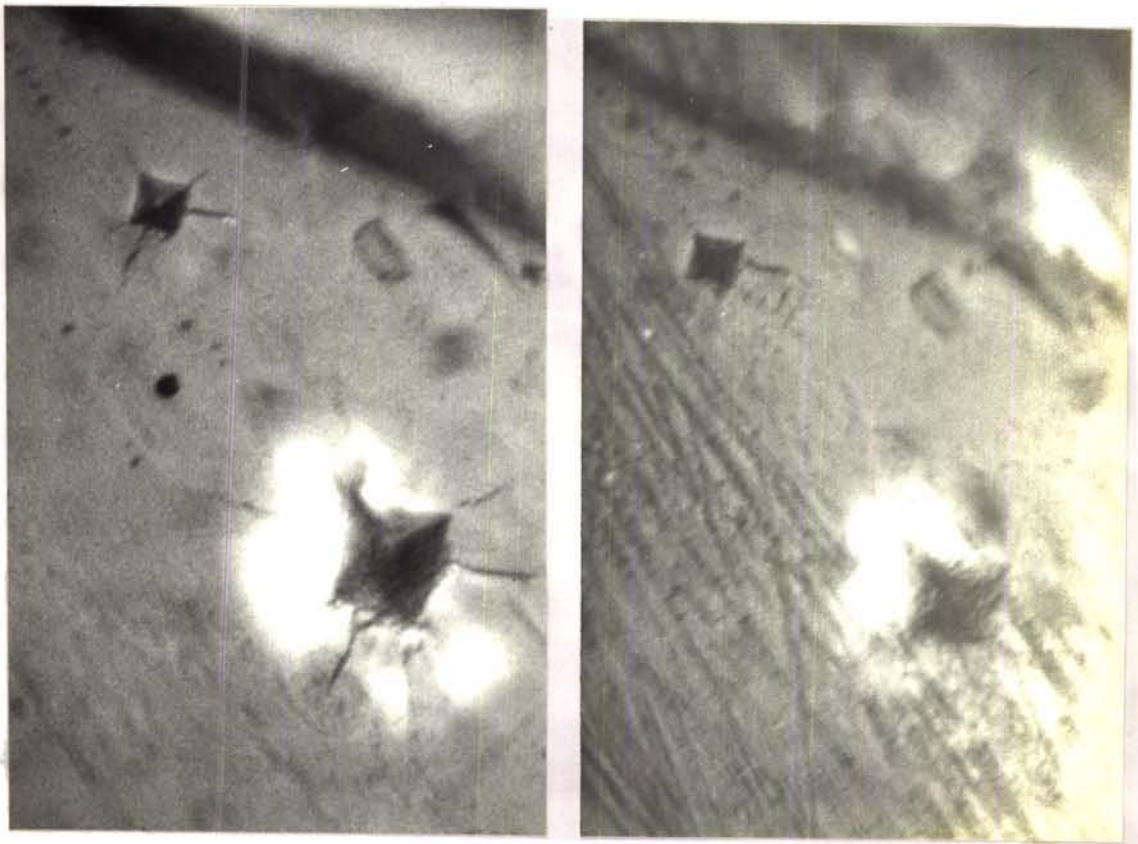
(a)

Fig.7.6

(b)

Fig.7.6 (a) An indentation mark at the threshold load without any visible crack.

(b) Etch figure of the indentation mark in (a) which verifies the absence of cracks.



(a) Fig.7.7 (b)

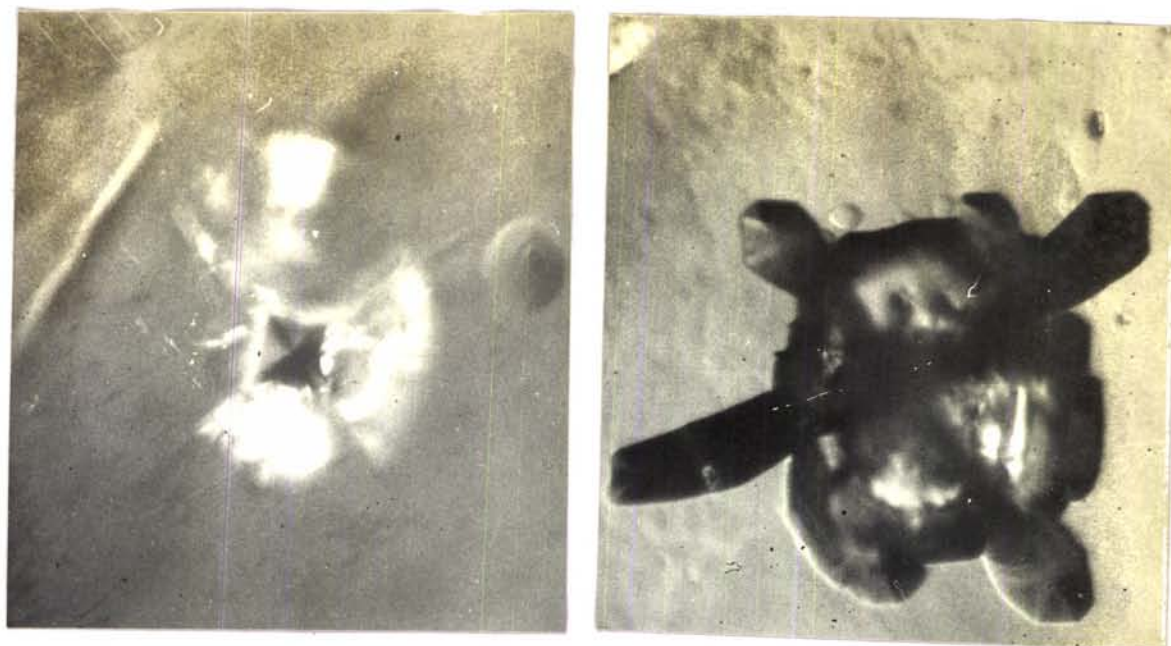
Fig.7.7 (a) Indentation marks at two different loads showing the crack system on the (001) face.

(b) The area in (a) after surface removal.

from the surface. For smaller load, only radial cracks are found indicating that a radial crack is the threshold event in crack formation in DAHC. As the load is increased lateral cracks are observed around the impression (Fig.7.8a). The lateral crack system is clearly seen in the etched pattern (Fig.7.8b). The lateral cracks seem to extend well below the plane of indentation pyramidal apex, as can be seen from Fig.7.8c, where the indentation impression is completely removed; the cracked area is still visible. At higher loads, lateral cracks take the shape of median cracks, forming a well developed half penny configuration around the indentation mark.

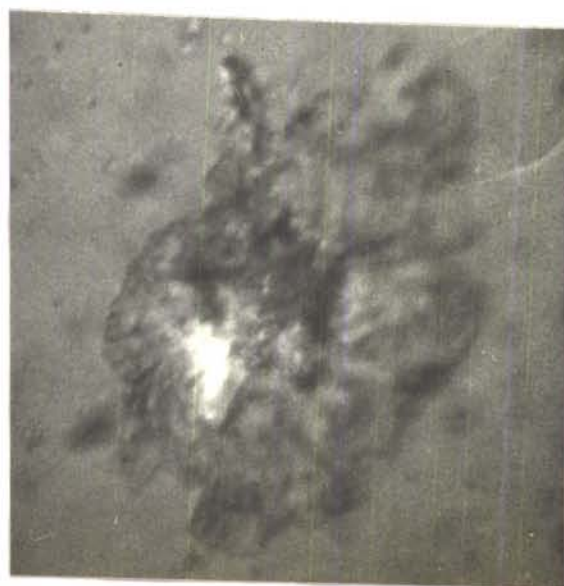
7.3.2. CA CRYSTALS

The variation of hardness with load on the (101) face of CA crystal is shown in Fig.7.9. The hardness at first slightly decreases with load reaching a minimum at around 7.5g and thereafter increases. This indicates that the deformation produced at the initial stages of loading is relatively large compared to the deformation produced by a load above 7.5g. Around this load of 7.5g cracks initiate and slowly develop. The applied load is utilized for the nucleation of dislocations which cause cracks. The variation of hardness was measured only upto a load of 12.5g as the crack length above this load was found to be large compared to the diagonal of the indentation impression. The average value of hardness is 0.588 GPa.



(a)

(b)



(c)

Fig.7.8

- Fig.7.8 (a) An indentation mark on (001) face showing lateral cracks.
(b) Etch figure of lateral cracks showing crack system clearly.
(c) The area seen in (a) after surface removal.

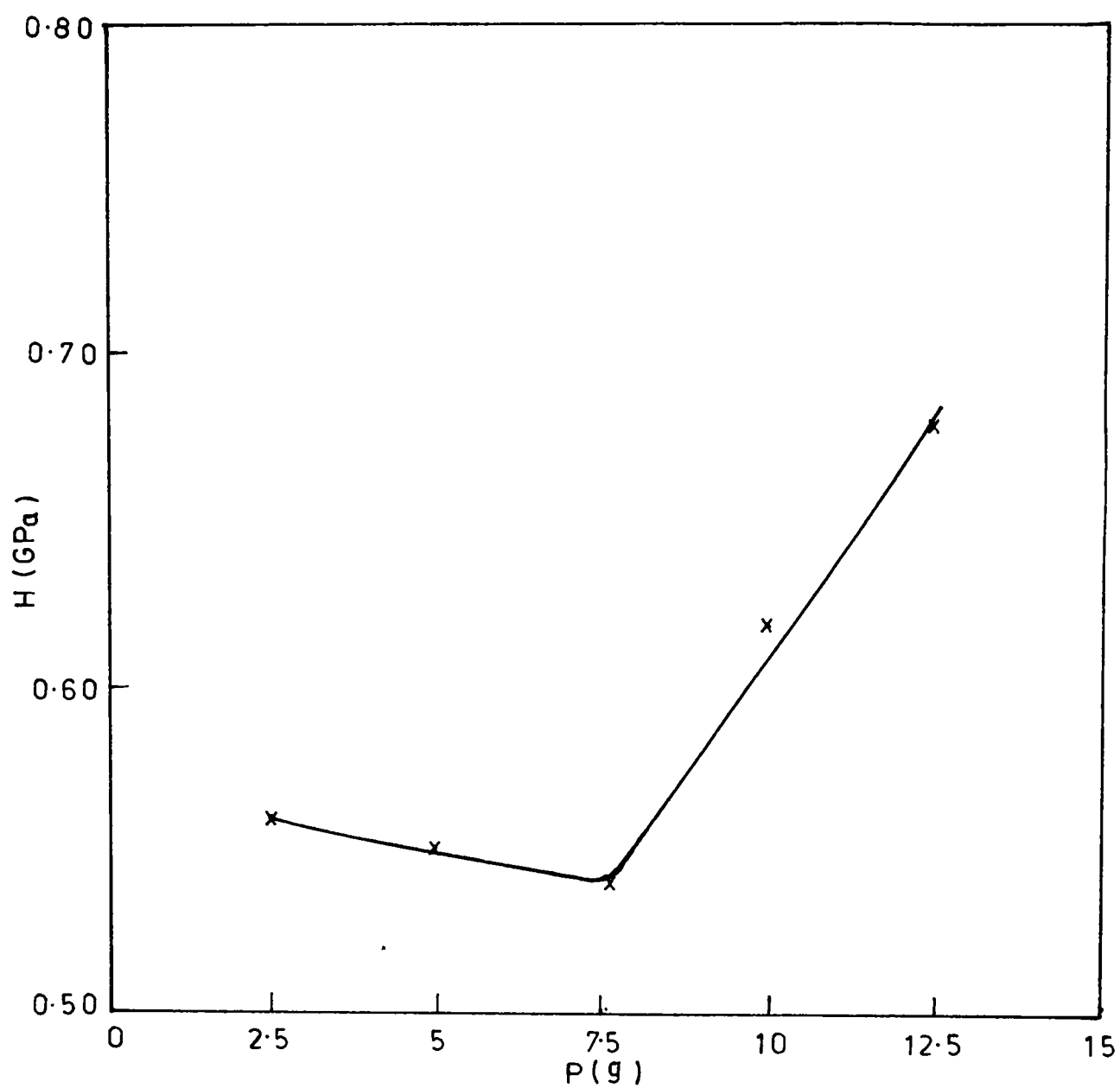


Fig.7.9 The variation of hardness with indentation load for CA crystals.

The plot of P against $c^{3/2}$ above a load of 15g is shown in Fig.7.10. The curve shows a steep increase upto 20g and thereafter slow increase upto 25g. Crack dimensions above this load were not useful as chipping of surface layers of the crystal occurred above this load. The curve shows that the increase of the crack dimension is considerably large upto 20g. Thereafter the number of cracks around the impression can be observed to increase and the loading stress is partly utilized for further nucleation of crack initiating dislocations without contributing to the increase in dimensions of the already existing cracks.

The variation of toughness with load is presented in Fig.7.11. This curve first shows a decrease in toughness value upto a load around 20g and thereafter an increase upto 25g in full agreement with the above results. The mean value of toughness is $0.132 \text{ MPa m}^{1/2}$ and the brittleness of CA is found to be $4.48 \mu \text{ m}^{-1/2}$.

In Fig.7.12 is seen an indentation mark with small cracks on (101) surface of CA crystal for low loads. These cracks disappear on removing a thin layer from the surface (Fig.7.13) showing that the crack has not extended deep into the crystal. This indicates that the initial cracks on (101) surface of CA crystals are radial. As the load is slowly increased lateral crack patterns appear around the indentation mark. This on further loading takes the pattern of a well developed median crack. A typical crack system on (101) face for a

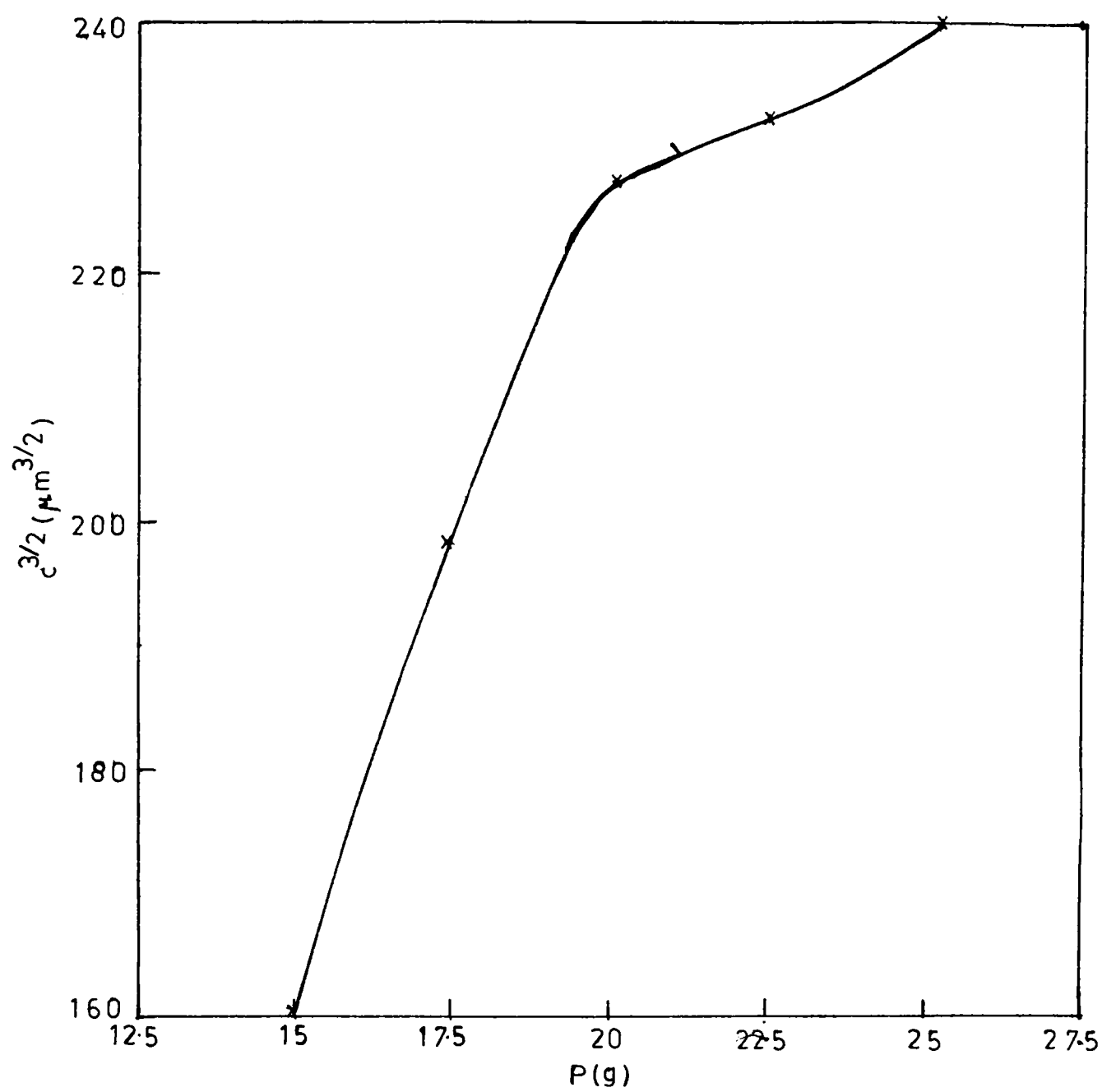


Fig.7.10 The variation of $3/2$ power of semi-crack length with load for CA crystals.

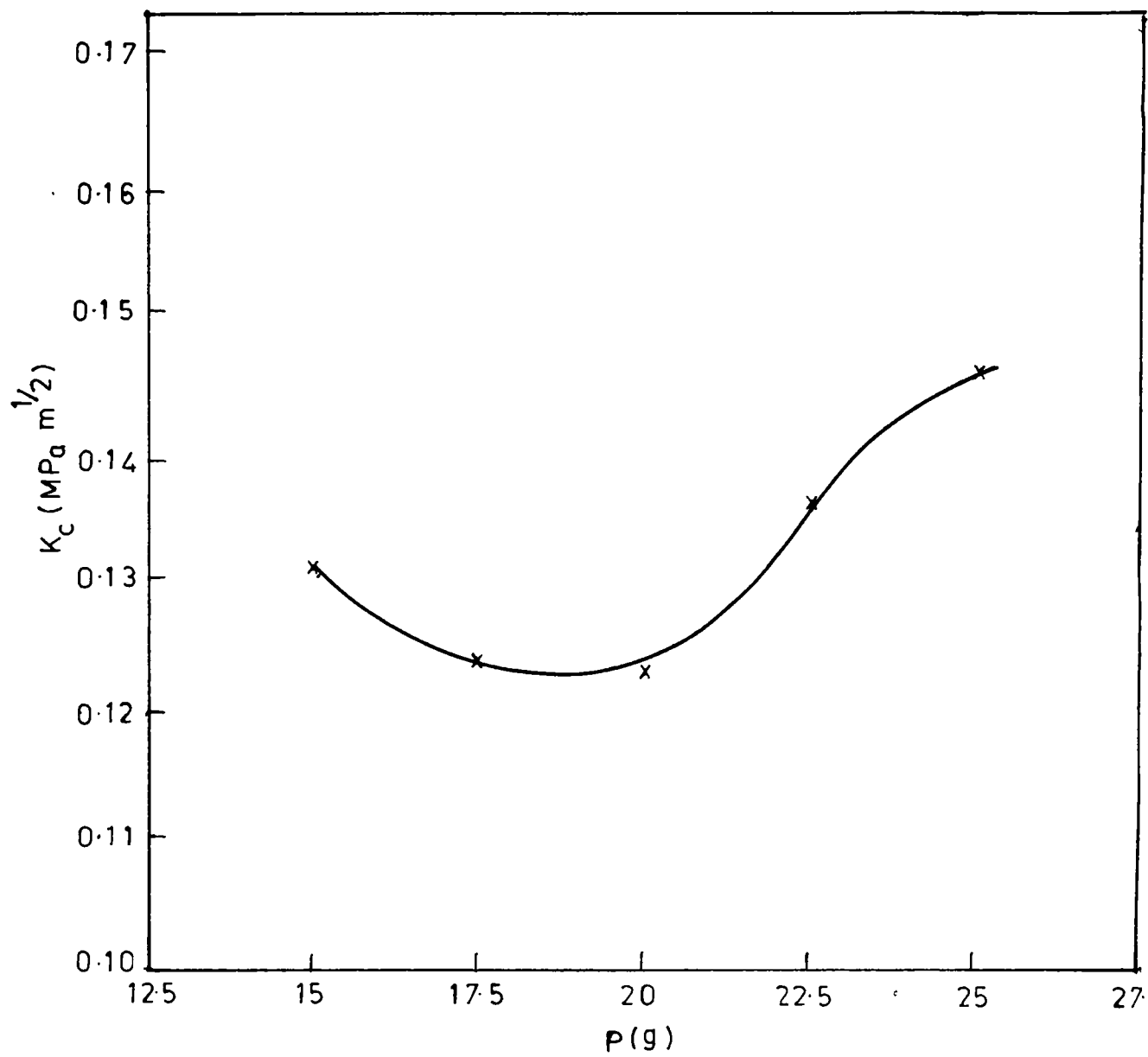


Fig.7.11 The variation of toughness with load for CA crystals.



Fig.7.12 An indentation mark on (101) surface of a CA crystal showing small cracks.

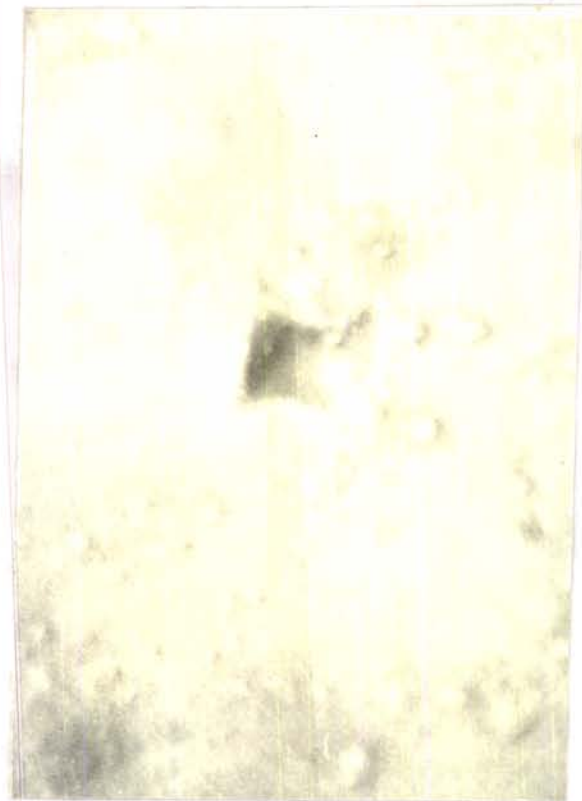


Fig.7.13 An indentation mark on (101) surface of a CA crystal after surface removal. Small cracks are absent.

load of 25g is shown in Fig.7.14. The cracks are found to have extended well beneath the apex of the indentation mark as seen from the residual impression at the indented area after surface removal (Fig.7.15).

7.4. CONCLUSIONS

Hardness, toughness and brittleness values of DAHC crystals are found to be 0.688 GPa, $0.17 \text{ MPa m}^{1/2}$ and $4.04 \mu \text{ m}^{-1/2}$ and that of CA crystals are 0.588 GPa, $0.132 \text{ MPa m}^{1/2}$ and $4.48 \mu \text{ m}^{-1/2}$ respectively. The hardness and toughness of these crystals are found to vary with load. The threshold crack in these crystals is found to be radial. The radial crack system develops into lateral and median pattern as the load is increased step by step.

REFERENCES

1. A.ARORA et al., J. Non. Cryst. Sol. 31(1979)415.
2. N.GANE and J.M.COX, Philos. Mag. 22(1970)881.
3. K.NIIHARA, J. Mater. Sci. Lett. 2(1983)221.
4. J.LANKFORD, ibid. 1(1982)493.
5. B.R.LAWN and D.B.MARSHALL, J. Amer. Ceram. Soc. 62(1979)347.



Fig.7.14 A well developed crack system on (101) surface of a CA crystal.

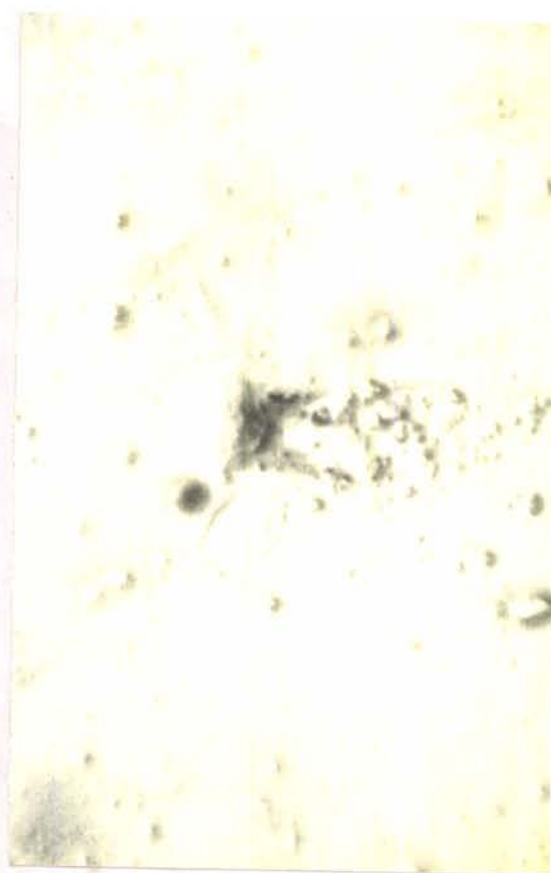


Fig.7.15 Residual impression of a well developed crack system on the (101) surface of CA crystal.

CHAPTER EIGHT

FRACTROGRAPHIC STUDIES OF DAHC CRYSTALS

8.1. INTRODUCTION

Fractography is the technique developed in the middle of this century in metallurgical fields for studying the patterns found on nascent fracture surfaces using optical microscope. It has been applied /1, 2, 3/ to cleavages of nonmetallic crystals to demonstrate its usefulness in disclosing deformation and cleavage mechanisms and in displaying intracrystalline structures, particularly imperfection structures. This technique is useful to obtain numerous informative patterns which serve to distinguish crystal types, to reveal the history of growth of the individual crystal, and to provide direct visual evidence for the mosaic constitution of the solid state. By using a special fractographic stage, Zapffe /1/ studied a number of specimens and the specific structures observed on them. He has shown that a detailed information of 1) the imperfection structure of the crystal, 2) the crystallographic mechanisms involved in deformation and fracture, 3) the path of the cleavage traverse as influenced by crystallography, imperfection structures and local stress resolutions and 4) other phenomena relating to both intergranular and intragranular characteristics of the grain or crystal, can be obtained from fractographic studies.

This chapter deals with the basic theory of cleavages described

in terms of dislocations, the important patterns observed on cleavages, stress necessary for cleavages and the study of cleavages of DAHC using fractographic techniques.

8.2. CLEAVAGE OF CRYSTALS

The cohesion of crystals is not identical in all directions. It may be strong in some directions and weak in certain other directions. Thus, many crystals break almost exclusively along certain planes known as cleavage planes on crushing or grinding. The most striking example of such a cleavage is provided by mica. Minerals like chrysotile have more than one cleavages.

Cleavage planes are always planes of high reticular density of atomic or molecular packing and large interplanar spacing. The cohesion is strong in the plane and weak at right angles to the plane. Cleavage planes thus have generally simple indices.

Cleavage of a crystal is usually represented by classical elastic theory. Describing cleavage in terms of dislocations play an important role in relation to the appearance of cleavage steps.

Cleavage requires large energy necessary to create two free surfaces. Thus it cannot be produced instantly over a large surface. It propagate from point to point in the form of a crack starting from

an initial point. The edge of the crack, joining the cleaved surfaces, can be considered as an edge dislocation. These edge dislocations in a sense, climb in the cleavage plane perpendicular to their Burgers vectors, creating the crack in their wake. Since the movement of the lips of the crack is continuous, there is a continuous distribution of these dislocations on the lips. Cleavage can thus be produced if a sufficient number of lattice dislocations climb along the same plane without diffusion.

8.2.1 CLEAVAGE STEPS

Cleavage prefers close packed planes which have smaller surface energy. The surfaces of the cleavage faces are not perfectly smooth but present a system of steps very nearly parallel to the cleavage direction. These steps often converge to form higher steps or patterns called river patterns. They are said to be due to the forest of dislocations which pierce the cleavage plane /4/. This is supported by numerous experimental evidences /5, 6/. A large number of new steps automatically form when the edge of the crack goes through a sub-boundary. The microscopic steps are formed by a combination of much smaller elementary steps. These steps generally take up a curvilinear shape running parallel to one another and normal to the successive positions of the crack tip. This occurs if the surface tension of the step is fairly isotropic as it reduces the step energy to a minimum. The leading crack dislocation which opens the crack must be loc-

ally in equilibrium with a step at a triple point. Sometimes, the steps run in a zigzag manner along close packed crystallographic directions. For this to occur the step energy spent that way is less than if the steps were straight but a noncrystallographic direction.

8.2.2. RIVERS

The presence of steps produces a frictional force on the tip of the crack and as a result the average surface energy to be produced per unit area of cleavage plane increases. This slows down the crack propagation and explains the convergence of steps into rivers. If the distribution of steps is not perfectly uniform, the crack tip will lag behind the rest at some regions of the crack because they have to create more steps. The curvature assumed at the tip of the crack in these regions makes the neighbouring steps converge. The convergence of the steps towards some regions of the tip of the crack continues until all the steps of a region are combined into a large step. For slowly moving cracks two steps of atomic height should meet at an angle θ ,

$$\theta = \gamma_s / \mu b \quad (8.1)$$

where γ_s is the step surface tension, μ is the shear modulus and b the magnitude of Burgers vector. Two steps meet to form a step of height $2b$ or to annihilate depending on whether their signs are the same or opposite. This may lead to the formation of multiple steps. It is shown that multiple steps should coalesce at the same rate as

the ordinary steps.

When a cleavage crack crosses a grain boundary it takes a larger number of similar steps resulting from the crossing of the parallel dislocations of the boundary. Neighbouring steps run a distance of 5 to 10 times their initial distance before coalescing. The course of the steps oscillates but they meet at an angle nearly equal to 12 degrees.

A cleavage has less well marked rivers when developing through a crystal, especially if it is brittle. The rivers are optically visible some distance away from the origin of the crack. The rivers are made up of steps of both signs. The rivers which are farther apart coalesce less quickly and new ones continually form so that their average distance is of the order of a few microns. The heights of rivers do not increase rapidly with distance but sometimes decrease and actually stop. This is due to the coalescence of steps of both signs.

8.3. STRESS NECESSARY FOR CLEAVAGE

The cleavage can be considered to be produced when the lips of a crack are displaced by a distance which is of the order of interatomic distance. The surface energy required for the creation of the two surfaces is $2\gamma \approx \mu b/5$ per unit area, where γ is the surface free energy, μ is the shear modulus and b is the Burgers vector. The tensile

stress is

$$\sigma' \approx 2\nu/b - \mu/5. \quad (8.2)$$

This is greater than the theoretical elastic limit $\mu/10$ for slip. Thus cleavage requires large stress concentrations. The necessary stress concentration can be produced by indenters, grips etc.

8.4. EXPERIMENTAL

DAHC crystals were cleaved using the technique described in chapter four. The cleaved surfaces were studied under the microscope.

8.5. RESULTS AND DISCUSSION

Fig. 8.1 is a mached nascent cleavage face of a crystal at low magnification. There are two fundamental types of patterns that can be observed on cleavage faces /9/. They are, 1) patterns determined by factors within the crystal and 2) patterns determined by the nature of the stress. This latter patterns are called hackle structures and are principally significant to the extend that they reveal the conformation of the fracturing forces as it traversed the crystal. A typical hackle pattern is shown in Fig. 8.2. No pronounced directional weakness within the crystal has played a role in determining the path of the cleavage although a slight textural flaw is indicated as a roughening of some of the hackle markings. This is due to frictional forces acting on the tip of the crack. A typical river pattern is



Fig.8.1 Matched cleavage face of DAHC crystal. (x100)



Fig.8.2 A hackle pattern observed on the cleavage face of DAHC. (x600)

shown in Fig. 8.3. It is clearly seen that the neighbouring steps run a distance of 5 to 10 times their initial distance before coalescing and they meet at an angle nearly equal to the theoretical value. The rivers which are farther apart coalesce less quickly. The height of the rivers are found to increase as more and more branches are added. Rivulets which merge with a large step that run perpendicular to them are seen in Fig. 8.4. Rivers converging to impurity centers are also found (Fig. 8.5). An etched cleavage surface containing river patterns is shown in Fig. 8.6. The rivers are not etched because their surface lie in a plane which is not etched by the dislocation etchant. Grain boundaries are also observed on cleavage faces as seen in Fig. 8.7. Radial lines known as Wallner lines which indicate the propagation of cleavage is seen as light dark bands perpendicular to the cleavage direction in DAHC (Fig. 8.8). Wallner lines are typical display of stress patterns produced by rupturing force as it traverses the crystal. The fractograph shown in Fig. 8.9 illustrates patterns which strongly present the lamellar structure.

Specific crystallographic markings are sometimes observed on cleavage surfaces. A stepped tilt boundary is shown in Fig. 8.10. Rectilinear markings showing instance of rectilinear cleavage is shown in Fig. 8.11. Steps having opposite sign which disappear on merging is shown in Fig. 8.12. Other interesting features relating to the history of the crystals are also seen on some cleavage surfaces. In Fig. 8.13 is shown a layer structure which may probably be due to

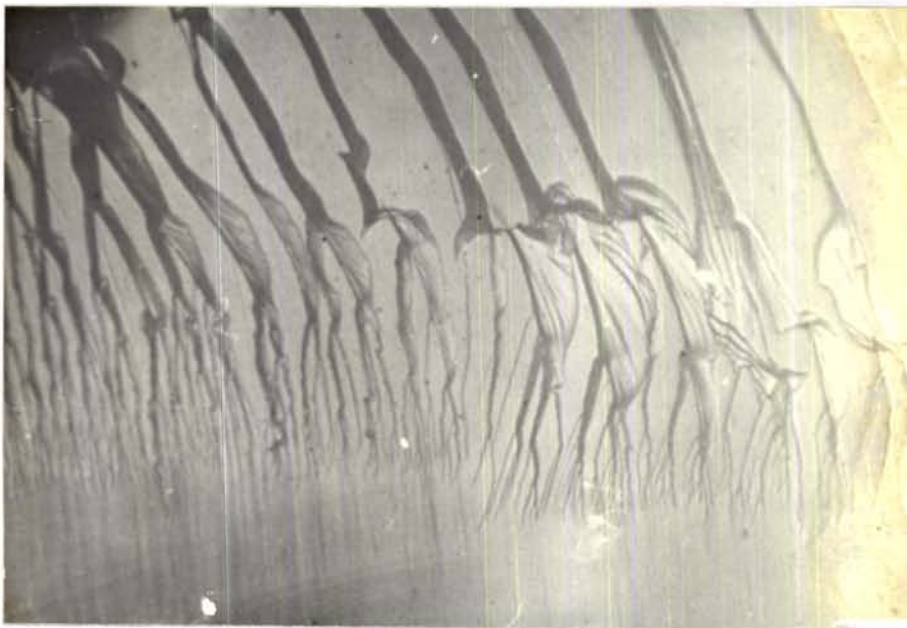


Fig.8.3 A river pattern observed on the cleavage face of DAHC. (x160)



Fig.8.4 Micrograph showing rivulets which merge with a large step that run perpendicular to them. (x100)

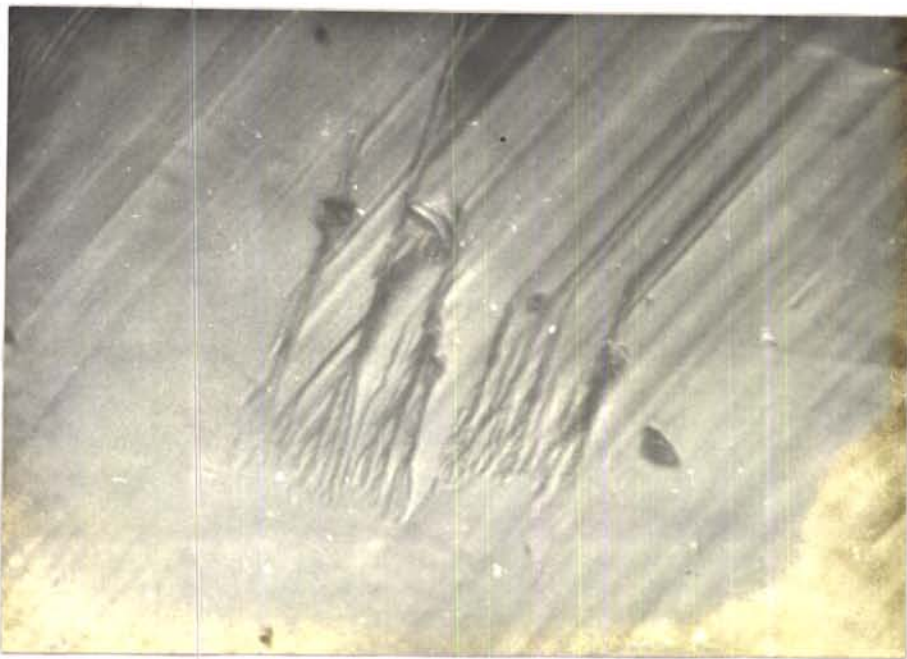


Fig.8.5 Rivers converging to impurity centers. (x160)



Fig.8.6 An etched cleavage surface containing river patterns. (x200)

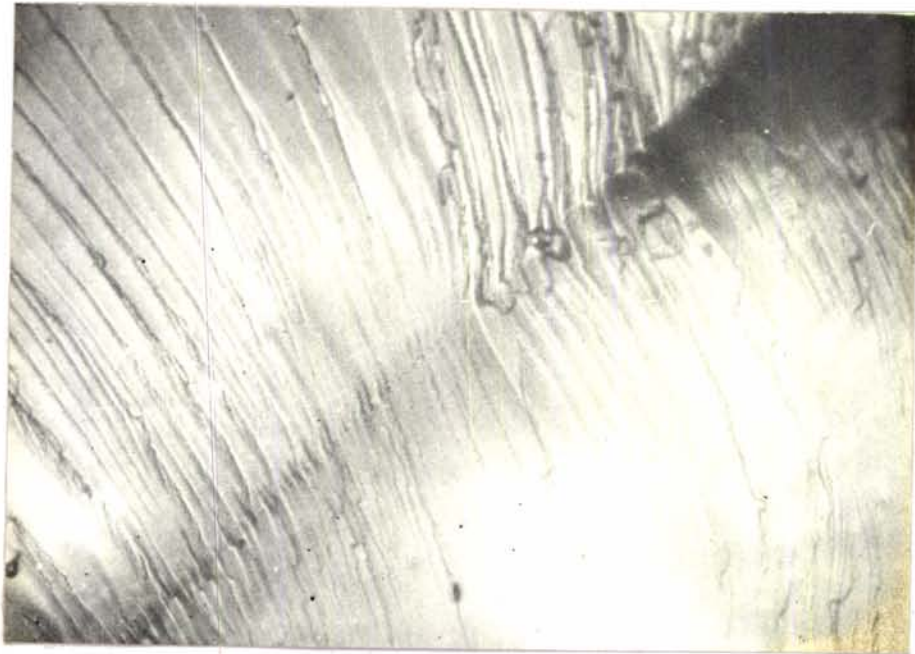


Fig.8.7 A grain boundary observed on a cleavage. (x120)

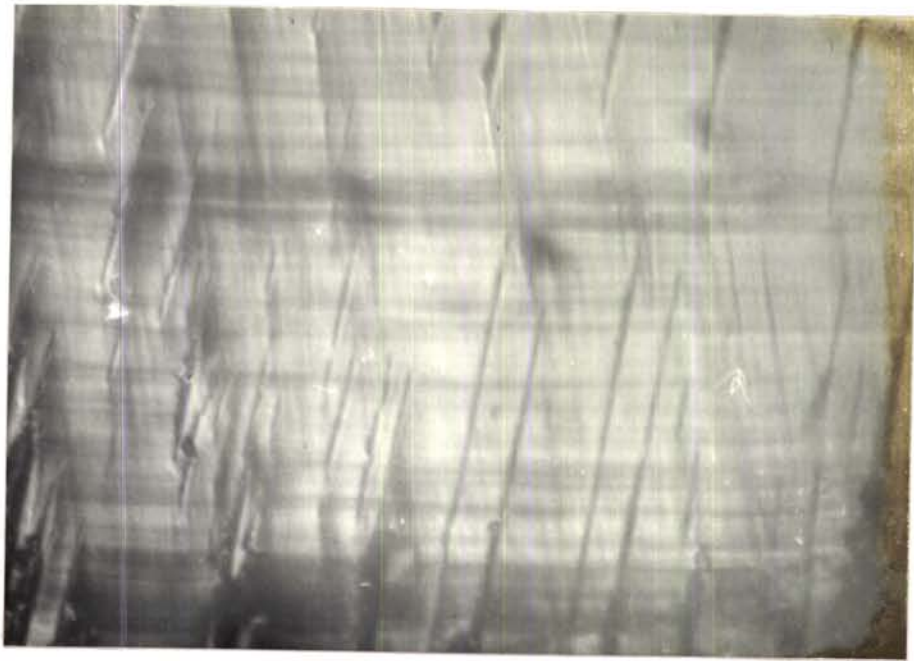


Fig.8.8 Micrograph showing radial Wallner lines as light dark bands perpendicular to the cleavage direction.
(x300)

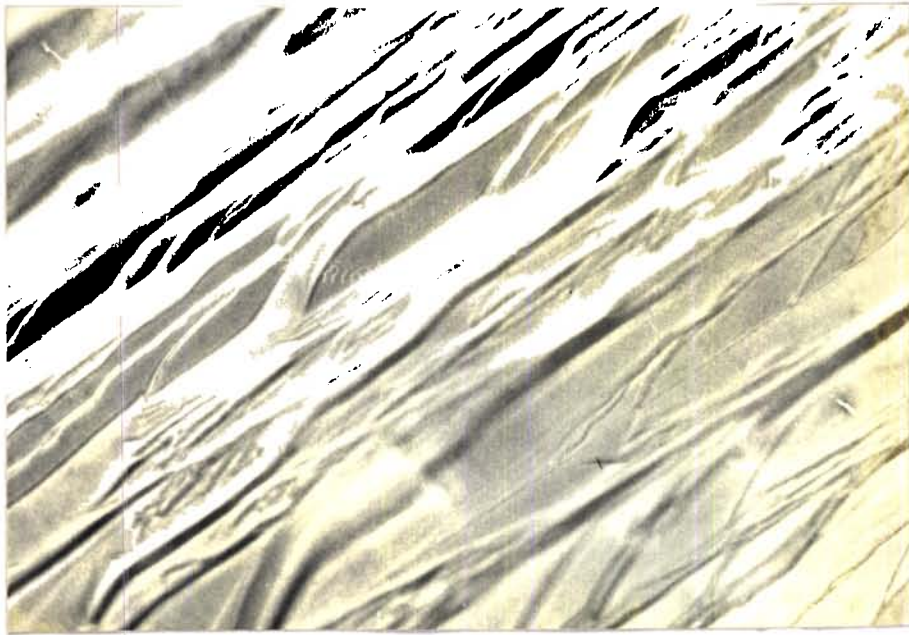


Fig.8.9 A cleavage surface showing the lamellar structure. (x600)

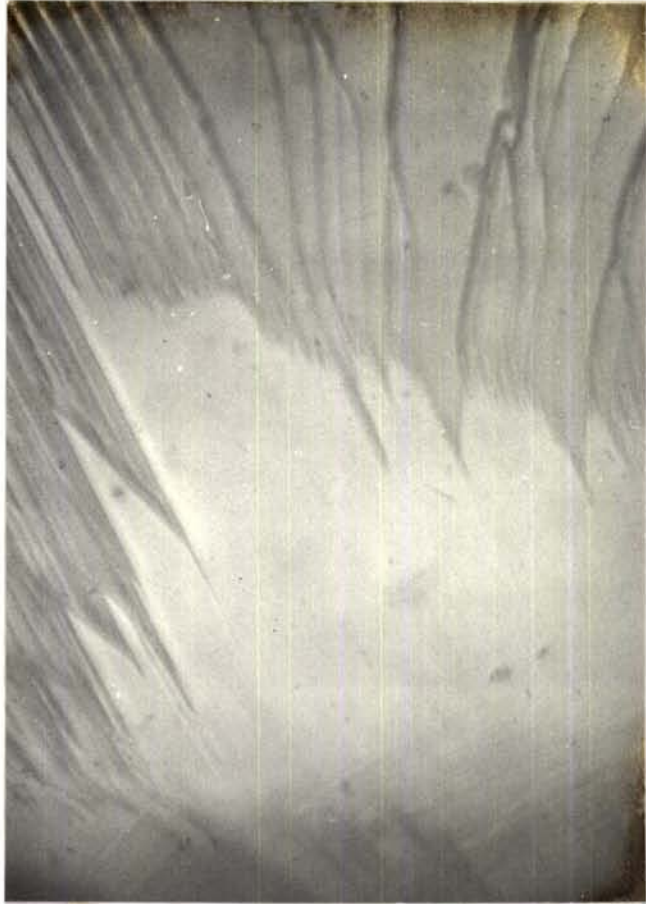


Fig.8.10 A stepped tilt boundary observed on the cleavage surface. (x100)



Fig.8.11 Rectilinear markings showing instances of rectilinear cleavage. (x600)

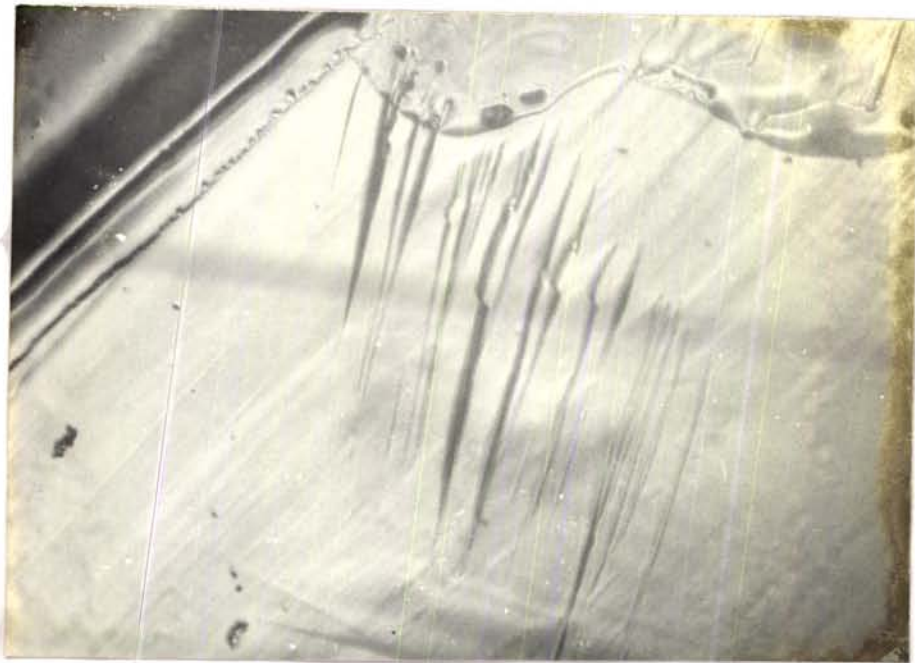


Fig.8.12 Steps having opposite sign which disappear on merging. (x200)



Fig.8.13 A layer structure on a cleavage face. (x200)

variation in growth conditions. Fig. 8.14 shows a zone where different grains with cleavage lines oriented in different directions meet.

8.6. CONCLUSIONS

Fractographic technique is useful to study the history of DAHC crystals. Cleavage faces of these crystals show hackle structures, river patterns, grain boundaries, Wallner lines, lamellar structures and a number of other interesting features related to the growth of DAHC crystals.

REFERENCES

1. C.A.ZAPFFE and C.O.WORDEN, Acta Cryst. 2(1949)377.
2. M.S.JOSHI and A.V.ANTONY, Ind. J. Phys. 55A(1981)96.
3. J.K.MATHAI, Ph.D Thesis, (Sardar Patel University, 1970).
4. F.C.FISHER, Acta Met. 2(1954)9.
5. J.J.GILMAN, Acta Met. 3(1955)277.
6. J.R.LOW, " Fracture ", (Wiley, N.Y., 1959).
7. J.FRIEDEL, " Dislocations ", (Addison-Wesley, London,1964).
8. J.FRIEDEL, " Fracture ", (Wiley, N.Y., 1959).
9. C.A.ZAPFFE and C.O.WORDEN, Acta Cryst. 2(1949)383.



Fig.8.14 A zone where different grains with cleavage lines oriented in different directions meet. (x200)

CHAPTER NINE
DIELECTRIC PROPERTIES OF DAHC CRYSTALS

9.1. INTRODUCTION

Dielectric studies have provided valuable information regarding structure, molecular motion, relaxation processes, dipole moment, phase transitions etc. in organic materials /1-4/. In this chapter, polarization of dielectrics, dependence of permittivity on frequency and temperature, dielectric losses, dependence of loss tangent on frequency and temperature, measurement of dielectric constant and loss and the dielectric properties of DAHC are discussed.

9.2. POLARIZATION OF DIELECTRICS

The most important property of an organic dielectric crystal is its capacity to be polarized under the action of an external electric field. The phenomenon of polarization can be considered as the change in the arrangement of the electrically charged particles of a dielectric in space. Due to this change in the arrangement, the dielectric acquires an electric moment. The state of a dielectric which is acted upon by an electric field can be described by two vector quantities; intensity of an electric field and polarization.

Permittivity of a dielectric, ϵ , is the basic parameter describing its properties from the view point of the process of its polariza-

tion. It is a macroscopic parameter of a dielectric which reflects the properties of a given substance in a sufficiently large volume but not the properties of the separate atoms and molecules in the substance.

9.2.1. POLAR DIELECTRICS

All dielectrics are subdivided into 1) polar dielectrics and 2) nonpolar dielectrics. In the case of a polar dielectric if all the positive and negative charges of a molecule are replaced by one positive and one negative charge, the centers of this summary charges does not coincide, whereas in the case of a nonpolar dielectric they coincide. For a polar dielectric, even in the absence of an external electric field, the molecule is an electric dipole with electric moment different from zero, sometimes referred to as a permanent or rigid dipole. The molecule is polar as the material consisting of such molecules. The magnitude of the electric moment of a molecule is $\mu = ql$, where q is the summary positive electric charge of a molecule and l is the arm of the dipole. Irrespective of the results obtained in the study of the electrical properties of a dielectric, its polarity can be judged from the chemical structure of its molecule. And, conversely, an experimental definition of the dipole moment μ leads us to very important conclusions regarding the structure of the molecules of matter. Thus, obviously, symmetrically arranged molecules (having a center of symmetry) are nonpolar since in this case the centers

of gravity of both positive and negative charges of a molecule coincide with the centre of the symmetry of the molecule and therefore with each other. In this case the sign of the charge of separate atoms and ions from which the molecule is built may be disregarded. Asymmetric molecules on the other hand are always polar.

9.2.2. PHYSICAL ESSENCE OF POLARIZATION

Polarization is a type of ordering in space of the charged particles with their displacement in a dielectric under the influence of an external electric field. This causes the formation of an electric moment in the entire volume of the dielectric and in each separate polarizing particle which may be an atom, ion, or a molecule. There are several types of polarization, each of which can be explained by its intrinsic physical mechanism. The three basic types of polarization from among these are: electronic, ionic and dipole polarization /5/.

Electronic polarization is due to the displacement of electrons with respect to the molecules of the atom. It occurs in all atoms or ions and can be observed in all dielectrics irrespective of whether or not other types of polarization are displayed in the dielectric. One specific feature of electronic polarization is the fact that when an external electric field is superposed, this type of polarization occurs during a very brief interval of time.

Ionic polarization is the mutual displacement of ions forming heteropolar or ionic molecule. For ionic polarization to set in, only a short time is required. But this is longer than for electronic polarization.

Both ionic and electronic polarization may be regarded as the varieties of polarization caused by deformation which is a displacement of charges with respect to each other in the direction of the electric field. Apart from the very high velocity with which the state of polarization sets in, the process of deformational polarization is practically unaffected by the temperature of the dielectric and is not connected with an irreversible dissipation of energy. Therefore, deformational polarization does not entail any dielectric losses.

Polar dielectric exhibit a tendency towards dipole or orientational polarization /6/. The essence of this kind of polarization lies in the rotation (orientation) of the molecules of a polar dielectric having a constant dipole moment in the direction of the electric field. In the strict sense it must be understood as the introduction of a certain orderliness in the position of polar molecules which are in uninterrupted chaotic thermal motion, and not as a direct rotation of polar molecules under the action of an electric field. For this reason dipole polarization is connected by its nature with the thermal motion of molecules, and the temperature must exert an appre-

ciable effect on the phenomenon of dipole polarization. In some cases rotation of not the whole molecules but of their separate unit occurs.

After a dielectric is energized, the process of establishing a dipole polarization or annihilation of this state requires a relatively long time as compared with that of practically almost inertialess phenomena of deformational polarization. The time needed differs in each case. For example, more time is required if the dimensions of the molecules are large and the absolute viscosity or co-efficient of internal friction of matter is high. This time may be of the same order as that of the half period of alternating voltages employed in radio engineering or even longer. Therefore, orientational polarization belongs to slow or relaxation types of polarization.

Unlike deformational polarization, dipole polarization and other types of relaxation polarization such as ionic relaxation and thermal relaxation polarization dissipate electric energy which transforms into heat in a dielectric, i.e. this energy leads to what is called dielectric loss which will be discussed shortly. In substances with a dipole polarization, as in substances in which polarization is caused by ionic displacement, permittivity is larger than the square of light refractive index.

9.3. DEPENDENCE OF PERMITTIVITY ON FREQUENCY AND TEMPERATURE

9.3.1. DEPENDENCE OF PERMITTIVITY ON FREQUENCY

As already mentioned the time of electronic and ionic polarization is small compared with the time of the voltage sign change, i.e. half the period of the alternating voltage. Therefore, the polarization of dielectrics, distinguished only by a deformational mechanism of polarization, completely settles itself during a very short period of time compared with the voltage sign change and as a consequence, practically essential dependence of ϵ on frequency cannot be expected in such dielectrics. The permittivity of nonpolar dielectrics are found not to depend on frequency.

But in the case of dipole polarization, when the frequency of the alternating voltage increases, the value of ϵ of a polar dielectric at first remains invariable but beginning with a certain critical frequency f_c , when polarization fails to settle itself completely during one half period, ϵ begins to drop approaching the value typical of a nonpolar dielectric at very high frequencies. As a general rule, when the frequency of the applied voltage increases, ϵ remains practically unaffected or drops but never increases.

9.3.2. DEPENDENCE OF PERMITTIVITY ON TEMPERATURE

Temperature does not seem to affect the process of electronic

polarization in dielectrics which are nonpolar, and thus the electronic polarizability of molecules does not depend on temperature. Due to thermal expansion of matter, the ratio of the number of molecules to the effective length of the dielectric diminishes when temperature is increased and ϵ decreases in this case for nonpolar dielectrics. In the case of polar dielectrics, the molecules cannot orient themselves in the low temperature region in most cases. When the temperature rises the orientation of dipoles is facilitated resulting in an increase in permittivity. As the temperature increases the chaotic thermal oscillations of molecules are intensified and the degree of orderliness of their orientation is diminished. This causes ϵ to pass through a maximum when the temperature is increased. In the case of polar dielectrics having a distinct melting point, a jumplike change in ϵ is observed during melting. Characteristic sets of curves are obtained if the dependences of the permittivity of strongly polarized dielectrics are plotted against frequency and temperature.

9.4. DIELECTRIC LOSSES

The dielectric acted upon by an electric field dissipates a certain quantity of electric energy. This phenomenon is named loss of power, which means an average electric power dissipated in matter during a certain interval of time. The loss of power in a specimen of a material is generally directly proportional to the square of the electric voltage applied to the specimen.

9.4.1. DIELECTRIC LOSS ANGLE

In an ideal dielectric used as a capacitor, the current through the capacitor would be ahead of the voltage exactly by 90 degrees. The total current through the capacitor in this case can be resolved into the active component and the reactive component. Thus, the phase angle describes a capacitor from the view point of losses in a dielectric. With a high quality dielectric the phase angle is very close to 90 degrees. Thus,

$$\delta + \phi = 90 \quad (9.1)$$

where the angle δ is called the dielectric loss angle. If I_a and I_r denote the active and reactive components of the current, then

$$\tan \delta = \tan (90 - \phi) = I_a / I_r = P_a / P_r \quad (9.2)$$

where P_a is the active power (power loss) and P_r the reactive power.

The dielectric loss angle is an important parameter for the dielectric material. If all other conditions are equal, the dielectric loss grows with this angle. $\tan \delta$ is often described as the loss tangent.

The permittivity can be considered as a complex quantity as

$$\epsilon = \epsilon_1 - i\epsilon_2 \quad (9.3)$$

where ϵ_1 is called the true permittivity and ϵ_2 takes into account the losses. It can be shown that

$$\epsilon_2 / \epsilon_1 = \tan \delta \quad (9.4)$$

Obviously $\epsilon_2 = \epsilon_1 \tan \delta$, which is called the loss index.

9.4.2. PHYSICAL ESSENCE OF DIELECTRIC LOSSES

The graph of current i flowing through a dielectric versus time t , from the moment of energizing the dielectric by a direct voltage is given in Fig. 9.1. The current i can be broken into two components: current i_0 with a constant magnitude and absorption current i_{abs} . The steady state conduction current obeys Ohm's law and is given by

$$i_0 = U/R_{in} \quad (9.5)$$

where U is the voltage and R_{in} is the resistance of the dielectric.

The absorption current is

$$i_{abs} = US \exp -t/\tau \quad (9.6)$$

where S is the conductance corresponding to absorption current and τ is the relaxation time. In polar dielectrics, absorption current is caused by the orientation of dipole molecules. Dipole molecules rotate under the action of an external electric field overcoming the forces of internal friction of matter, which is attended by the expenditure of a part of electric energy and its conversion into heat. Besides rotations of parts of dipole molecules and other kinds of molecular transfer from one position to another are possible. The orientation of dipole molecules is one of the clearest physical causes for the appearance of absorption current.

Absorption current can exist with any changes of voltage across the dielectric, particularly for sinusoidal voltages. The power loss under alternating voltage may be larger than under direct voltage

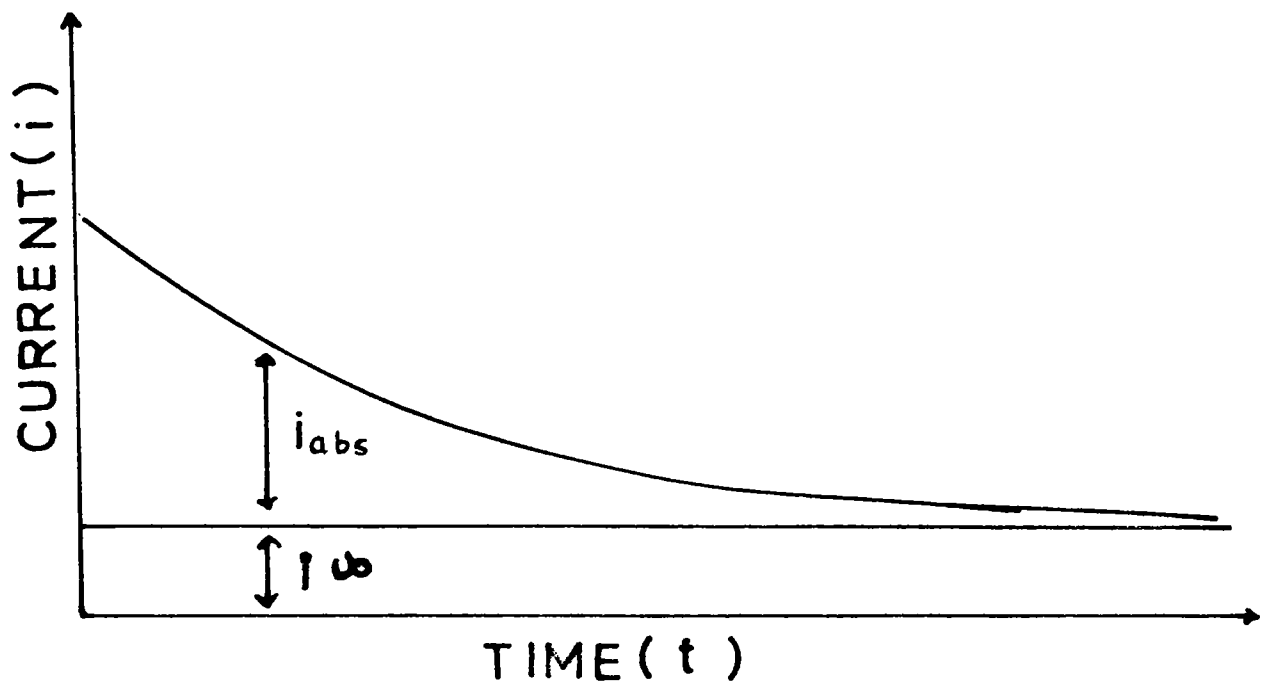


Fig.9.1 Theoretical plot of current i flowing through a dielectric versus time t from the moment of energizing the dielectric by a direct voltage.

of the same magnitude. When the dielectric operates under a sinusoidal voltage, the absorption current should also be sinusoidal alternating current with two components; the active component and the reactive component. Thus, three sinusoidal currents flow through the dielectric, namely, a) capacitive current (I_{cap}) or displacement current shifted 90 degrees ahead of the voltage vector, b) absorption current with active (I'_{abs}) and reactive (I''_{abs}) components and c) residual conduction current (I_{res}). The presence of absorption current increases both the active conductance and the capacitance. The components of the total current are equal to active,

$$I_a = I'_{abs} + I_{res} \quad (9.7)$$

and reactive,

$$I_r = I''_{abs} + I_{cap} \quad (9.8)$$

the loss tangent,

$$\tan \delta = I_a / I_r = \omega^2 \tau^2 (G_{in} + S) + G_{in} / \omega I S + C_g (\omega^2 \tau^2 + 1) I \quad (9.9)$$

where ω is the angular frequency of the sinusoidal voltage across the dielectric, τ is the relaxation time, G_{in} is the conductance for the residual current, S is the conductance corresponding to the absorption current and C_g is the geometrical capacitance.

9.5. DEPENDENCE OF LOSS TANGENT ON FREQUENCY AND TEMPERATURE

9.5.1. DEPENDENCE OF LOSS TANGENT ON FREQUENCY

From the equation 9.9 for loss tangent, a graph of loss tangent

with frequency is presented in Fig. 9.2. We obtain the following relations,

$$\lim_{\omega \rightarrow 0} \tan \delta = \omega \quad (9.10)$$

$$\lim_{\omega \rightarrow \infty} \tan \delta = 0 \quad (9.11)$$

The maximum of the curve is obtained by equating the first derivative to zero. If ω' is the corresponding frequency, for a particular case when the residual current is very small, that is the losses are mainly of relaxation nature, so that $I_{res} \ll I'_{abs}$ and $G_{in} \ll S \approx 0$ we get a simplified expression for ω' and $\tan \delta_{max}$ as

$$\omega' = (1/\tau^2 + S/C_g \tau)^{1/2} \quad (9.12)$$

$$\tan \delta_{max} = S\tau/2C_g (1+S\tau/C_g)^{1/2} \quad (9.13)$$

From a physical stand-point, in the case of purely dipole mechanism of losses, the frequency ω' corresponds to a ratio between the period of an external electric field and the time τ of the relaxation of dipoles for observing the greatest loss of energy to overcome the resistance of the viscous medium by the dipoles. Assuming $S \ll C_g \tau$, this ratio $\omega' \tau = 1$, gives the condition of the maximum of dielectric losses in a polar dielectric at a given temperature.

In a case where the losses are only due to electrical conduction, the dependence of $\tan \delta$ on frequency is given by

$$\tan \delta = 1.8 \times 10^{10} / f \epsilon \rho \quad (9.14)$$

where f is the frequency, ϵ is the permittivity and ρ is the volume resistivity(ohm. m).

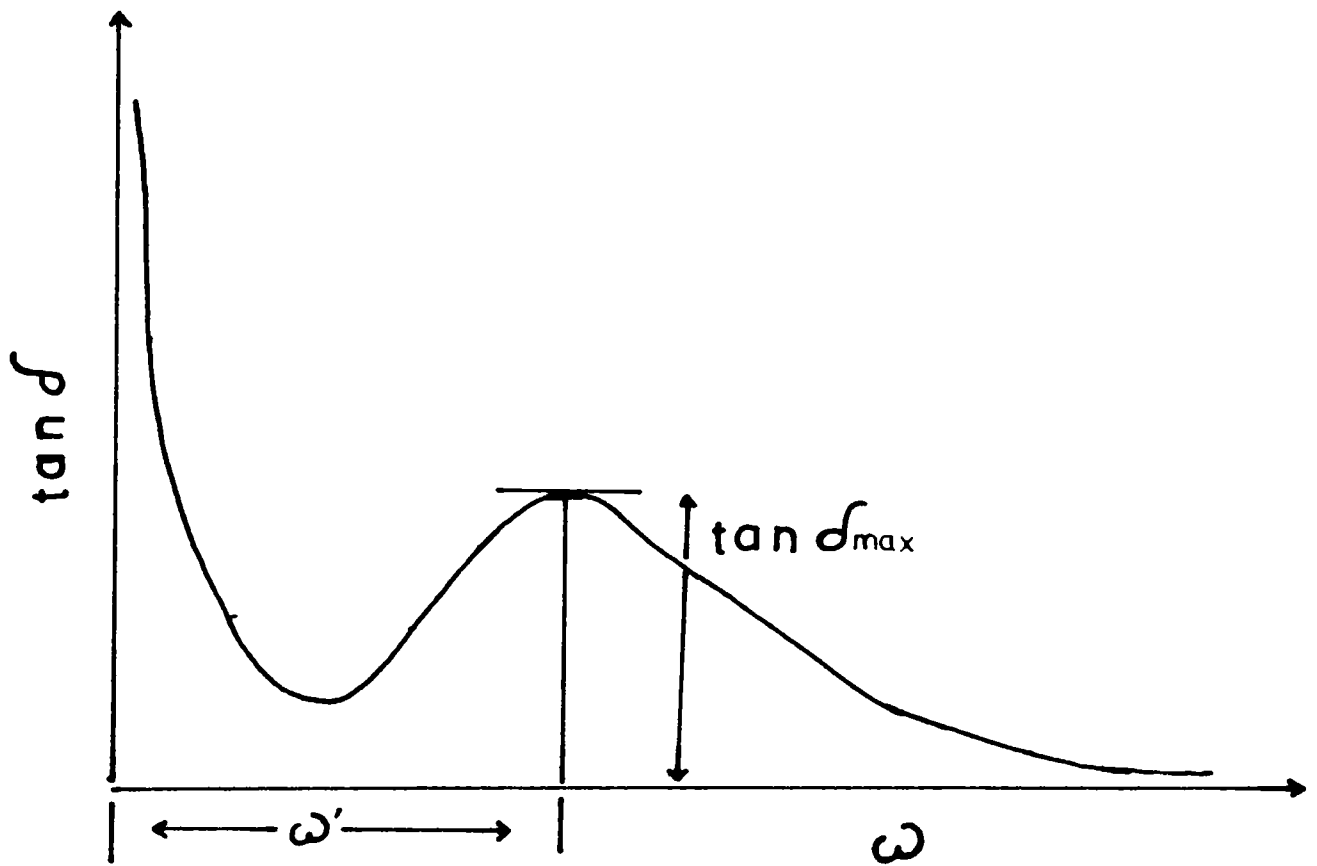


Fig.9.2 Graph showing the theoretical dependence of loss tangent of a dielectric on frequency.

From the practical point of view, when the dependence of $\tan \delta$ of an electrical insulating material on frequency is considered it is possible to observe different nature of dependence in the range of frequency change - an increase or decrease at a higher frequency or transition through one or several maxima.

9.5.2. DEPENDENCE OF LOSS TANGENT ON TEMPERATURE

As a general rule $\tan \delta$ appreciably increases when temperature rises. The dielectric loss due to dipole mechanism reach their maximum at certain definite temperature T_k . The rise in temperature and the resulting drop in viscosity exert a double effect on the amount of losses due to the friction of the rotating dipoles: on the one hand, the degree of dipole orientation increases thus increasing $\tan \delta$ and on the other hand, there is a reduction in the energy required to overcome the resistance of the viscous medium when the dipole rotates through a unit angle, diminishing the magnitude of $\tan \delta$. Polar substances apart from dipole losses exhibit losses due to electrical conduction which grow with increase in temperature.

The typical dependence for $\tan \delta$ of polar substances are observed with a simultaneous change both in temperature and frequency. As the temperature rises the maximum of $\tan \delta$ on the curves shift towards higher frequencies. Similarly, as a general rule, when the frequency of an alternating voltage increases the temperature corresponding

to the maximum of $\tan \delta$ shift towards higher temperatures. At very low temperatures, $\tan \delta$ of various dielectrics is, as a rule, extremely small.

9.6. EXPERIMENTAL

The experimental technique for the measurement of dielectric permittivity, ϵ , and the loss tangent, $\tan \delta$, of DAHC are described in chapter four. The technique is based on the measurement of the capacitance C_0 of an empty condenser and the capacitance C and the resistance R of the condenser filled with the dielectric material. The basic principle involved in the measurement of capacitance using the universal bridge described earlier is that of Wheatstone's bridge (Fig. 9.3). The balancing condition is

$$Z_1/Z_2 = Z_s/Z_x \quad (9.15)$$

where Z_1 and Z_2 are fixed standard impedences, Z_s is a variable impedance and Z_x is the unknown impedance. The balance condition can be obtained by adjusting Z_s or the ratio Z_2/Z_1 or both. Generally Z_2 and Z_1 are fixed. Expressing $Z_x = 1/\omega C_x$, and $Z_s = 1/\omega C_s$ where ω is the frequency of the applied voltage, equation 9.15 can be written as

$$C_x = Z_1 \cdot C_s / Z_2 \quad (9.16)$$

Hence, the unknown capacitance C_x can be measured against a standard capacitance C_s . Denoting C_x by C , the dielectric permittivity is

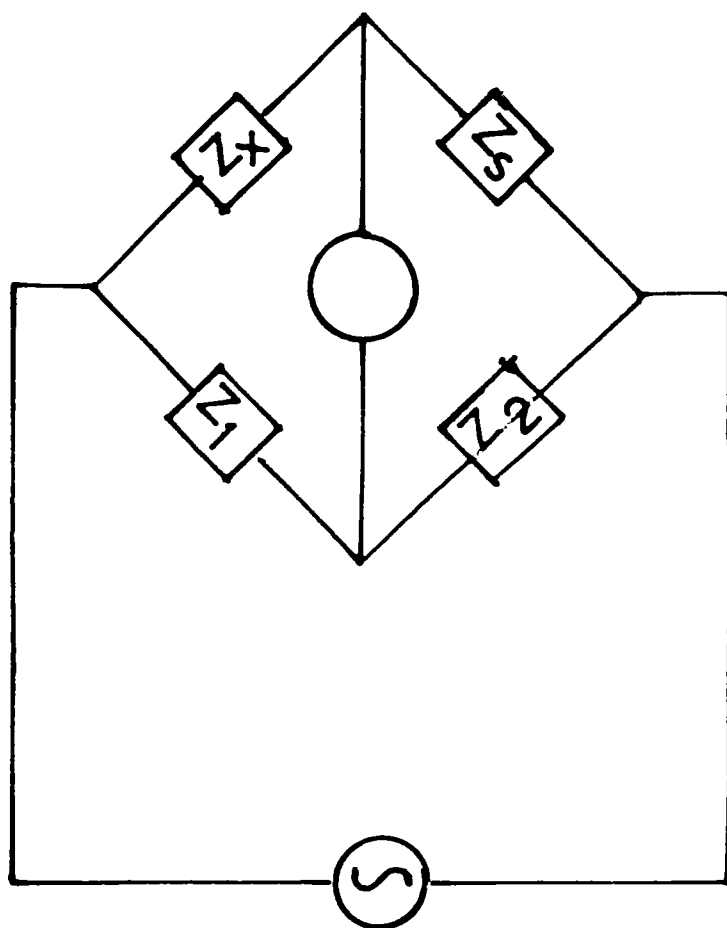


Fig.9.3 Schematic diagram showing the principle of a Wheatstone's bridge.

$$\epsilon = C/C_0 \quad (9.17)$$

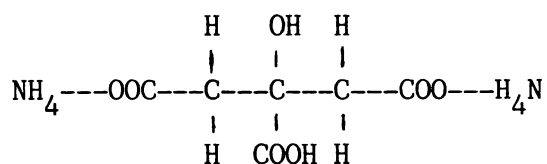
where $C_0 = 0.08854 A/t$ pF, A is the area of the condenser in cm^2 and t is the thickness in cm. The dielectric loss is obtained from the widths of the resonance curves. If f is the resonance frequency, the loss tangent is obtained from the relation,

$$\tan \delta = 1/2\pi fCR \quad (9.18)$$

The quantities C and R are measured by adjusting the oscillator to a predetermined frequency and tuning the measuring circuit to resonance. The variation of ϵ and $\tan \delta$ within the temperature range of 133°K to 373°K was studied in a frequency range of 20 Hz to 20,000 Hz.

9.7. RESULTS AND DISCUSSION

The chemical structure of DAHC molecule is



The structure clearly shows that the molecule is polar containing asymmetric polar groups like OH. The molecule contain two ammonium groups and three carboxylic groups. Being a polar molecule all the three types of polarizations are supposed to be present in DAHC crystal.

Fig.9.4 shows a series of curves showing the variation of ϵ with

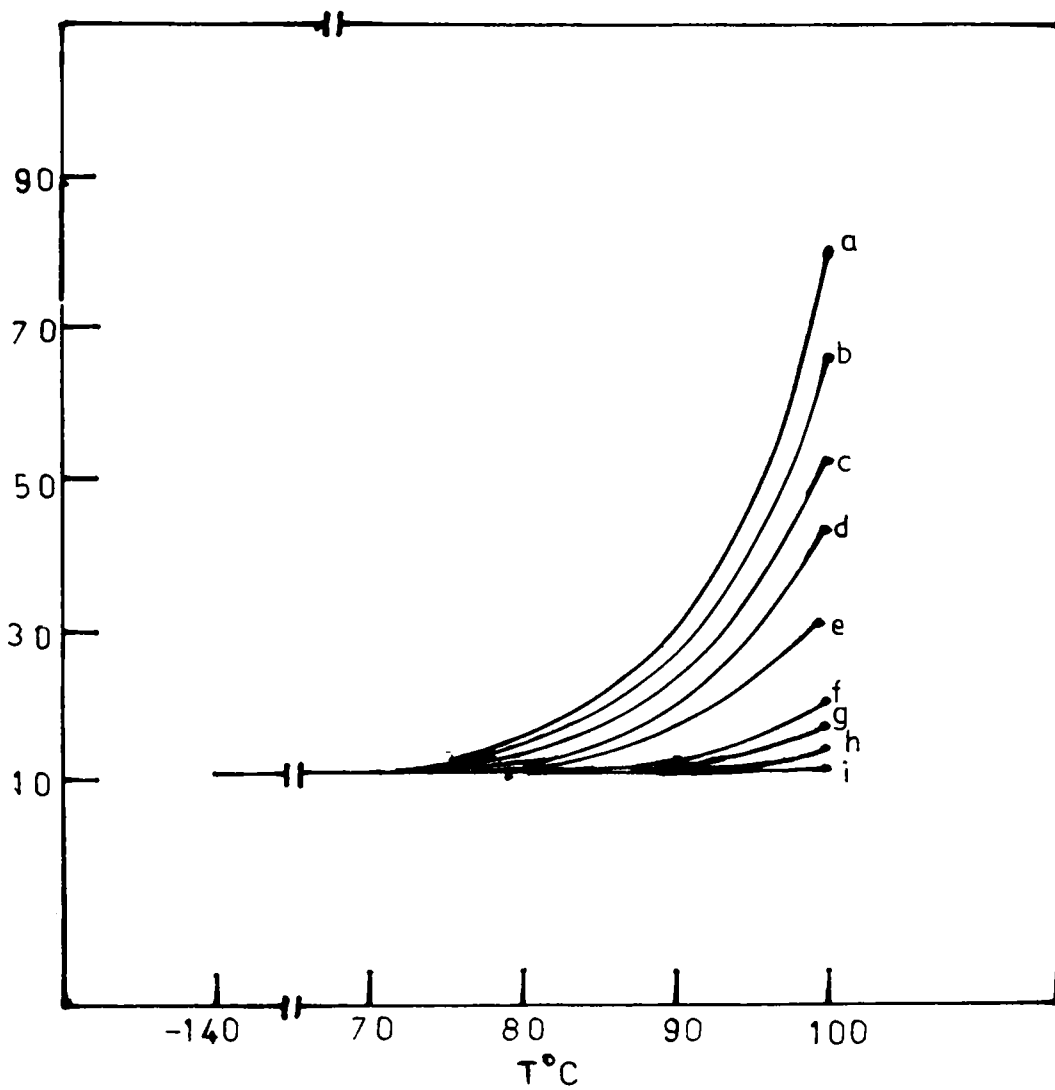


Fig.9.4 Variation of dielectric permittivity with temperature for different frequencies along the $[001]$ direction of DAHC crystals.

a) 0.2, b)0.4, c) 0.6, d) 0.8, e) 1, f) 5, g) 10, h) 15 and

i) 20 kcs/s.

temperature for different frequencies measured along the $[001]$ direction. The dielectric constant slightly increases upto a particular temperature and thereafter, as the temperature increases there is a sharp increase in the value of the dielectric constant. The sharp increase initiates at different temperatures depending on the frequencies; the initiation temperature being higher at higher frequencies. For low temperature ϵ is found to have a value around 10 in the c-direction for all the frequencies considered.

The orientation of the polar molecules is considerably influenced by lattice force in the case of solids /7/. Investigations of structure by means of nuclear magnetism /8, 9/ reveals hindered molecular motion in solids. Due to such hindrances, for large molecules such as DAHC orientation of dipoles is difficult at low temperatures. Therefore the sharp increase in dielectric constant for DAHC may partly be due to the loosening of the molecular lattice as the melting point is approached. Such behaviour, where very slight increase in dielectric constant with temperature at low temperatures and more pronounced rise below the melting point are typical of many organic materials /10/. For example, this type of sharp increase in dielectric constant is found in nitrobenzene and isopropyl bromide.

In the case of DAHC a transition of ammonium ion from ordered to disordered orientation may be another cause for the sharp increase in dielectric constant. Such transitions are found in ammonium halides

/11/. These transitions do not however exclude rotation of ammonium ion in the disordered orientation. Hornig /12/ has suggested that free rotation can be considered as a particular case of disordered orientation. For molecules having shapes which prevent rotation of the whole molecule in the lattice, orientational polarization is often attributed to the movement of molecular segments. Dependence of ϵ on frequency strongly suggest some kind of molecular orientation.

Compounds containing hydroxyl groups capable of hydrogen bonding are reported to show strong frequency dependence of dielectric constant and high conductivity /13/. This behaviour is attributed to proton transfer facilitated by rotation of the chains about an axis. Hydroxyl group is present in DAHC. Therefore the sharp increase in dielectric constant with temperature may partly be attributed to proton transfer.

The variation of dielectric loss with temperature along c-axis is presented in Fig.9.5. The curves are similar to those observed in the case of variation of dielectric constant with temperature. $\tan\delta$ shows appreciable increase with temperature. This increase in $\tan\delta$ is brought about by an increase both in conduction of residual current and the conduction of absorption current. As the frequency is increased the region of sharp increase of the curves shift towards higher temperatures. This and the observation of dielectric loss retracing its path on cooling suggest energy dissipation in which a relaxational process is involved. Very high value of $\tan\delta$ for DAHC for

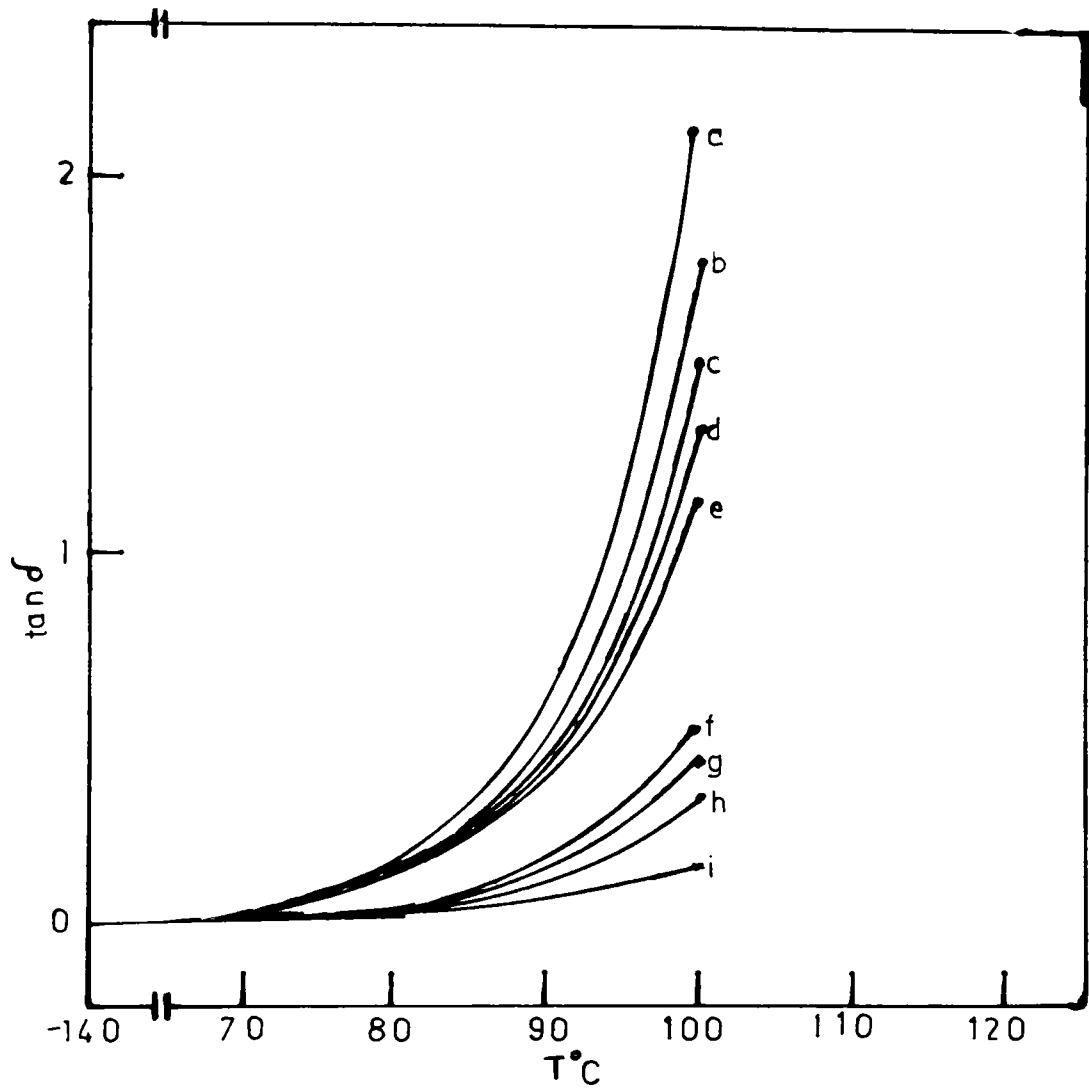


Fig.9.5 Variation of dielectric loss with temperature for different frequencies along $[001]$ direction of DAHC crystals.

- a) 0.2, b) 0.4, c) 0.6, d) 0.8, e) 1, f) 5, g) 10, h) 15 and
i) 20 kcs/s.

a particular value of frequency and temperature also points to the relaxation nature of the dielectric loss.

The dielectric constants of DAHC along a and b axes at low temperatures are found to be nearly equal to 15 and 20 respectively for all the frequencies used. The variation of dielectric constant and loss tangent along these axes are found to be similar to that along the c-axis.

9.8. CONCLUSIONS

The dielectric constant for DAHC along the three mutually perpendicular axes a, b and c at low temperatures is found to be nearly equal to 15, 20 and 10 respectively in the frequency range 20 Hz to 20,000 Hz. The dielectric loss at low temperatures is nearly zero along these three directions. The dielectric constant and loss is found to increase slightly with temperature upto a particular point and thereafter increase sharply. As the frequency is increased the region of sharp increase is shifted towards higher temperatures.

REFERENCES

1. N.KOIZUMI et al., *Ferroelectrics* 57(1984)99.
2. M.KHATRY and J.M.GHANDHI, *J. Mol. Liq.* 30(1985)63.
3. M.R.DELA FUENTE et al., *Ferroelectrics* 54(1984)417.
4. H.J.ROTHER et al., *Ferroelectrics* 54(1984)447.
5. C.KITTEL, " Introduction to solid state physics ",
(Wiley, N.Y., 1976)
6. C.P.SMYTH and W.S.WALLS, *J. Chem. Phys.* 3(1935)557.
7. C.P.SMYTH, *Chem. Revs.* 19(1936)329.
8. H.S.GUTOWSKY and G.E.PAKE, *J. Chem. Phys.* 18(1950)162.
9. E.R.ANDREW, *J. Chem. Phys.* 18(1950)607.
10. C.P.SMYTH, *Trans. Faraday Soc.* 42 A(1946)175.
11. E.L.WAGNER and D.F.HORNING, *J. Chem. Phys.* 17(1949)105.
12. D.F.HORNIG, *J. Chem. Phys.* 17(1949)1346.
13. R.W.CROWE and C.P.SMYTH, *J. Am. Chem. Soc.* 72(1950)4427.

CHAPTER TEN

SPECTRAL AND THERMAL STUDIES

10.1. INTRODUCTION

Infra-red (IR) spectroscopy is being employed to an ever increasing extent for the recognition and quantitative analysis of structural units in compounds. The spectra can also be used to obtain fundamental data on the mechanics of molecules. These studies are extremely useful to the analyst, in that the particular motions associated with the various characteristic frequencies are determined, so that it is possible to assess to some extent the likelihood of frequency shifts occurring with changes in local environment of the group. Techniques used for qualitative and quantitative analysis are quite refined. The vast majority of the spectra of interest result from absorption experiments. Classical electrodynamics shows that interaction between waves and molecules in the form of emission or absorption is only possible if the interaction is connected with an alteration in the electrical dipole moment of the interacting molecules. The same result is obtained by the application of quantum theory. Only those rotations and vibrations which cause an alteration in the electric dipole moment are excited by radiation, i.e. can be measured by absorption methods.

The IR absorption spectrum of organic compounds shows a number of sharp absorption bands which can be correlated with asymmetric

vibrations of atoms and groups of atoms. Bands in the shorter wavelength region ($4000-1000\text{ cm}^{-1}$) are thought to result mainly from stretching and bending vibrations of individual bonds and are therefore considered characteristic of the diatomic structural units of functional groups. Bands in the longer wavelength region ($1400-600\text{ cm}^{-1}$) appear to be caused by more complex vibrations of polyatomic units and of the molecules as a whole. Although there is some overlapping, the shorter wavelength bands are used mainly in the detection of particular functional groups, while the longer wavelength bands are used to gain information about environments of functional groups and to identify compounds by comparison.

The absorption of light by organic materials in the ultraviolet and visible region of the electromagnetic waves involves the excitation of electrons in σ , π and n-orbitals from the ground state to higher energy states. These higher energy states are referred to molecular orbitals represented by σ^* and π^* respectively corresponding to the ground states σ and π . Since n electrons do not form bonds, there are no antibonding orbitals associated with them.

The electronic transitions that occur in the ultraviolet and visible regions are of the following types, namely, $\sigma \rightarrow \sigma^*$, $n \rightarrow \sigma^*$, $n \rightarrow \pi^*$ and $\pi \rightarrow \pi^*$. The energy required for the $\sigma \rightarrow \sigma^*$ transition is very high; consequently, compounds in which all valence electrons are involved in single bond formation, such as saturated hydrocarbons,

do not show absorption in the ultraviolet region. Compounds containing nonbonding electrons on oxygen, nitrogen, sulphur or halogen atoms are capable of showing absorptions owing to $n - \sigma^*$ transitions.

Thermal analysis continues to be one of the fastest growing instrumental techniques for the study of a material and differential scanning calorimetry (DSC) is one of the advanced technique in the field of thermal analysis. Thermal analysis using DSC has been successfully employed to study the equilibrium between the different phases in complexes, the thermodynamic properties, crystallization energies, microstructural evolution in alloys, phase transitions, effect of temperature rise on structural change, heat capacity, enthalpy, etc. of organic materials. Combined with IR spectroscopy and dielectric measurements, DSC has been used for the study of certain organic materials /1, 2/. Basically, the DSC technique allows the determination of the time derivative of the heat content per unit mass of the sample, $\dot{H}(t) = dH/dt$, as a function of time t for a given heating rate, $\dot{T} = dT/dt$, and a given temperature, $T(t)$.

The IR and UV spectra of DAHC and the DSC traces of DAHC and CA crystals are presented and discussed in this chapter.

10.2. EXPERIMENTAL

The IR and UV spectra of DAHC were taken by the spectrometers described in chapter four. The IR spectrum of DAHC was recorded in the region $4000 - 200 \text{ cm}^{-1}$ in nujol mull and KBr pellet at room temperature. The UV spectrum of DAHC was obtained in the wavelength range of 195 to 500 nm from aqueous solution.

The DSC traces of DAHC and CA crystals were obtained using the calorimeter described in chapter four. Sample specimens of DAHC were sealed in Al sample pans and heated at the rate of $20^{\circ}\text{K}/\text{min}$ in dry nitrogen atmosphere. The DSC traces of CA crystal were also obtained in a similar way.

10.3. RESULTS AND DISCUSSION

The IR spectrum of DAHC in nujol mull is presented in Figs. 10.1a and 10.1b. The absorption peaks are observed at 3400, 3200, 3060, 2920, 2860, 1690, 1600, 1460, 1370, 1330, 1230 and 1090 cm^{-1} . The peaks at 2920, 1460 and 1370 cm^{-1} are due to absorption of IR by nujol. The peak at 3400 cm^{-1} can be assigned to OH stretching vibrations and that at 3200 cm^{-1} to intermolecular hydrogen bonds. The intensity of the absorption peak due to hydrogen bonds is usually considerably greater than that of free OH vibration which is found to be true in the case of DAHC. The broad shape of such bands is usually attributed

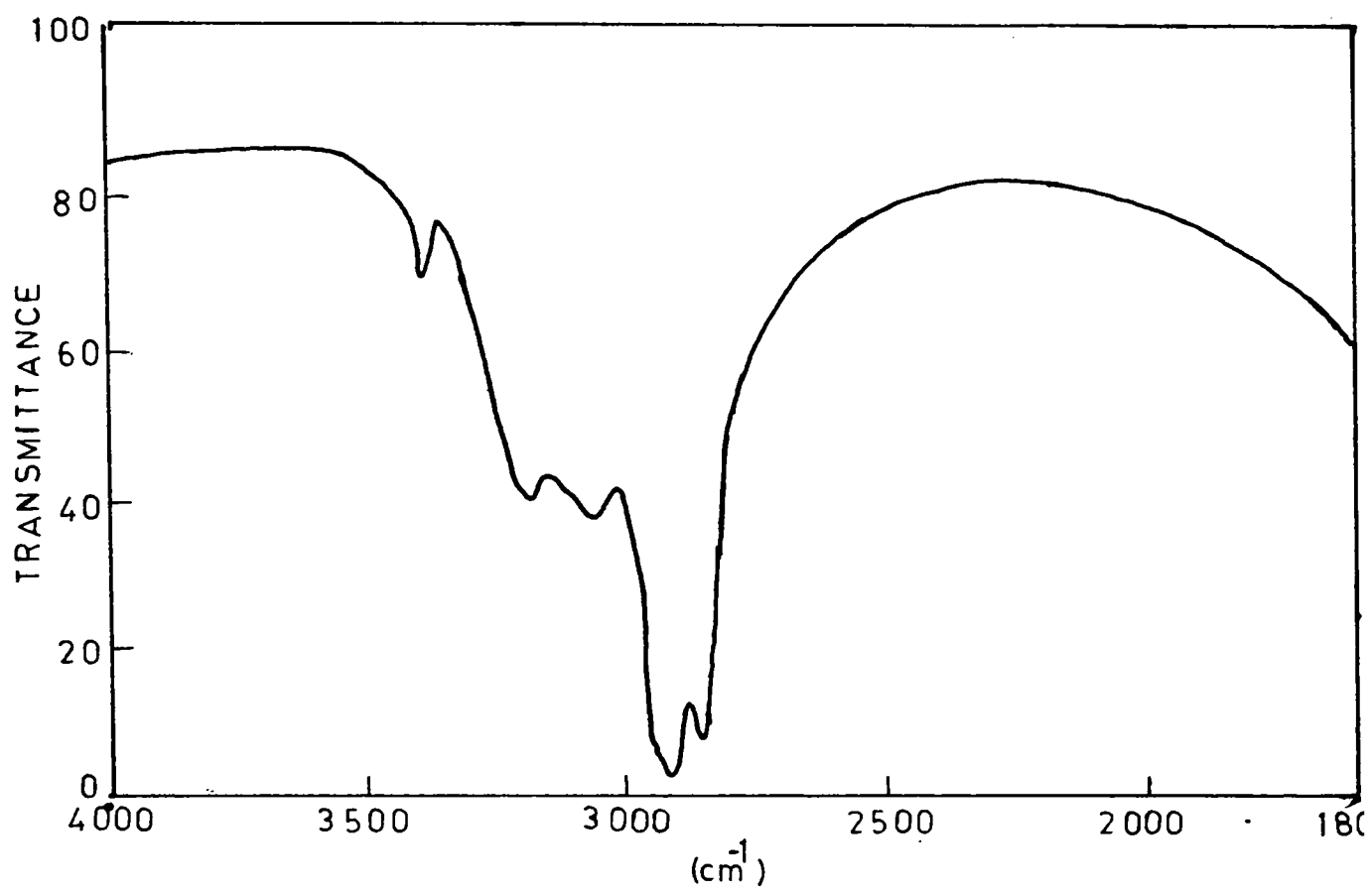


Fig.10.1(a) IR spectrum of DAHC in nujol in the region 4000-1800 cm⁻¹.

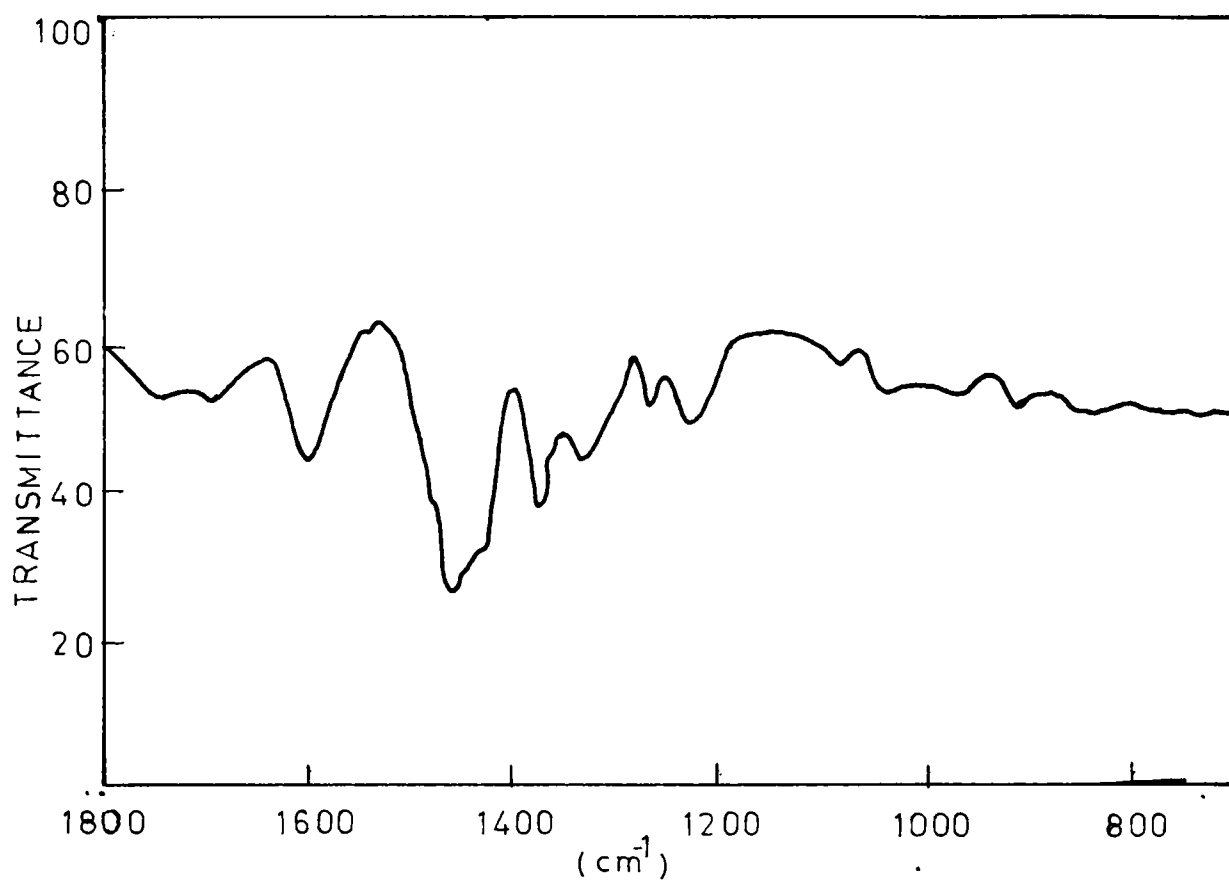


Fig.10.1(b) IR spectrum of DAHC in nujol in the region 1800-200 cm⁻¹.

to the fact that alcoholic groups associate into various polymeric forms in which molecules are involved in hydrogen bonding to different extents, so that the broad band observed is a number of composite bands /3/.

The peak at 3060 cm^{-1} may be assigned to the ammonium group present since absorption bands are reported to be observed in ammonium salts of acids around 3060 cm^{-1} /4/. On comparison with the IR spectrum of citric acid shown in Fig.10.2, it is clear that this peak is absent in citric acid.

The CH_2 group is found to give rise to two characteristic bands at 2926 and 2853 cm^{-1} corresponding to the in phase and out of phase vibrations of hydrogen atoms /5, 6/. The absorption of 2860 cm^{-1} by DAHC can thus be due to the CH_2 vibrations. The other peak has probably merged with the nujol peak appearing at this place. The peak observed at 1690 cm^{-1} for DAHC spectrum may be due to the $\text{C}=\text{O}$ stretching in the acid group that exist in DAHC. Peaks around 1700 cm^{-1} have been observed in many carboxylic acids by Flett /7/. Also, in a number of salts of organic acids examined by Duval and his co-workers /8/, characteristic absorption peaks were observed between 1610 and 1550 cm^{-1} and between 1400 and 1300 cm^{-1} which are due to ionised carboxylic group. In the spectrum of DAHC 1600 and 1330 cm^{-1} peaks are found which lie in this region. In many acids, a regular series of evenly spaced absorption in the region 1350 to 1180 cm^{-1} is reported. DAHC

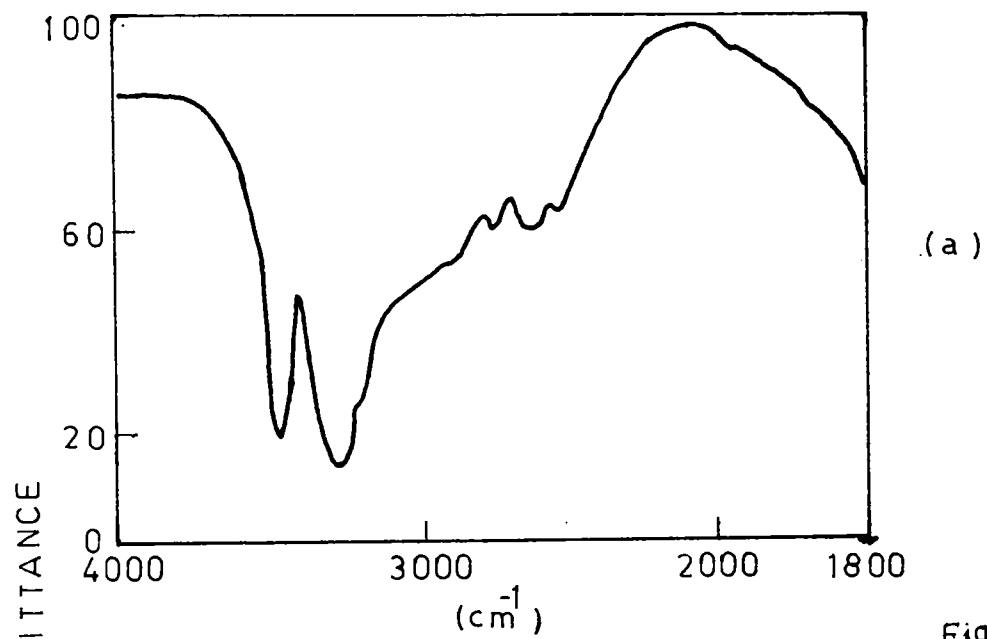


Fig. 10.2

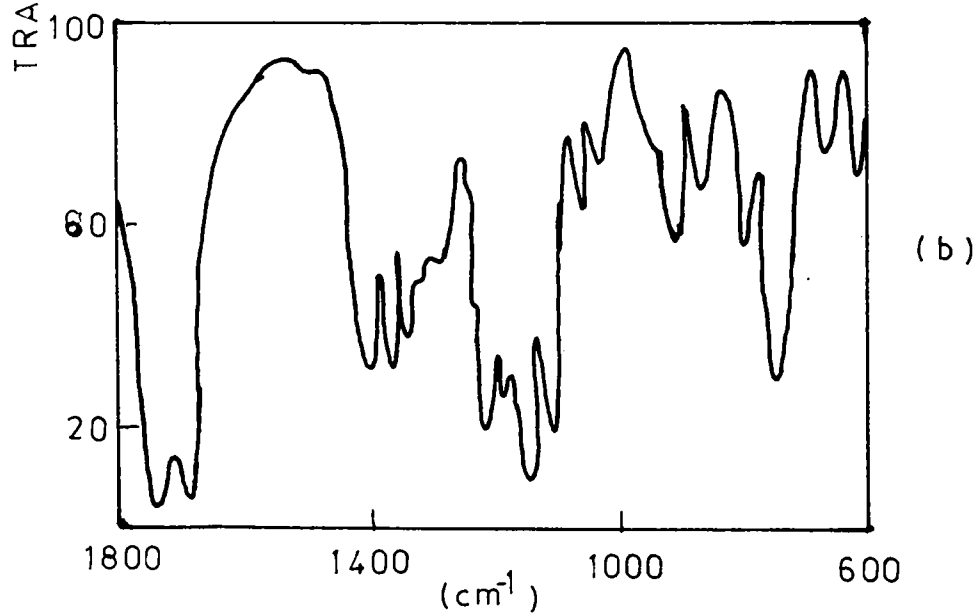


Fig.10.2 (a), (b) IR spectrum of citric acid in the region 4000-1800 cm^{-1} and 1800-600 cm^{-1} respectively in KBr pellet.

shows three evenly spaced peaks between 1270 to 1090 cm^{-1} with a spacing of 40 cm^{-1} . Jones and co-workers /9/ have shown that the number and appearance of these bands can afford information as to the length of the carbon chain involved.

Figs. 10.3a and 10.3b show the characteristic spectrum of DAHC obtained using KBr pellet. The pellet spectrum is capable of revealing those peaks which may be eclipsed by the characteristic peaks of nujol. For example, peaks at 1480, 1430 and 1380 cm^{-1} were not distinct in the nujol mull spectrum. These peaks can be attributed to the CH_2 deformation frequencies due to the CH_2 groups in DAHC.

The UV spectrum of DAHC is presented in Fig.10.4. The spectrum shows only one absorption peak at 210 nm. Absorption of ultraviolet frequencies is chiefly caused by electronic excitation; the spectrum provides only limited information about the structure of the molecule. The magnitude of the molar extinction coefficient for a particular absorption is directly proportional to the probability of the electronic transition; the more probable a given transition the larger the extinction coefficient. The molar extinction coefficient of DAHC can be obtained from the relation $\epsilon = A/cl$, where A is the absorbance given by $A = \log I_0/I$, I_0 is the intensity of the incident light and I is the intensity of the transmitted light, c is the molar concentration and l is the path length in cms. The value of ϵ is found to be 8600. The absorption at 210 nm of DAHC is thought to be due to the carboxyl

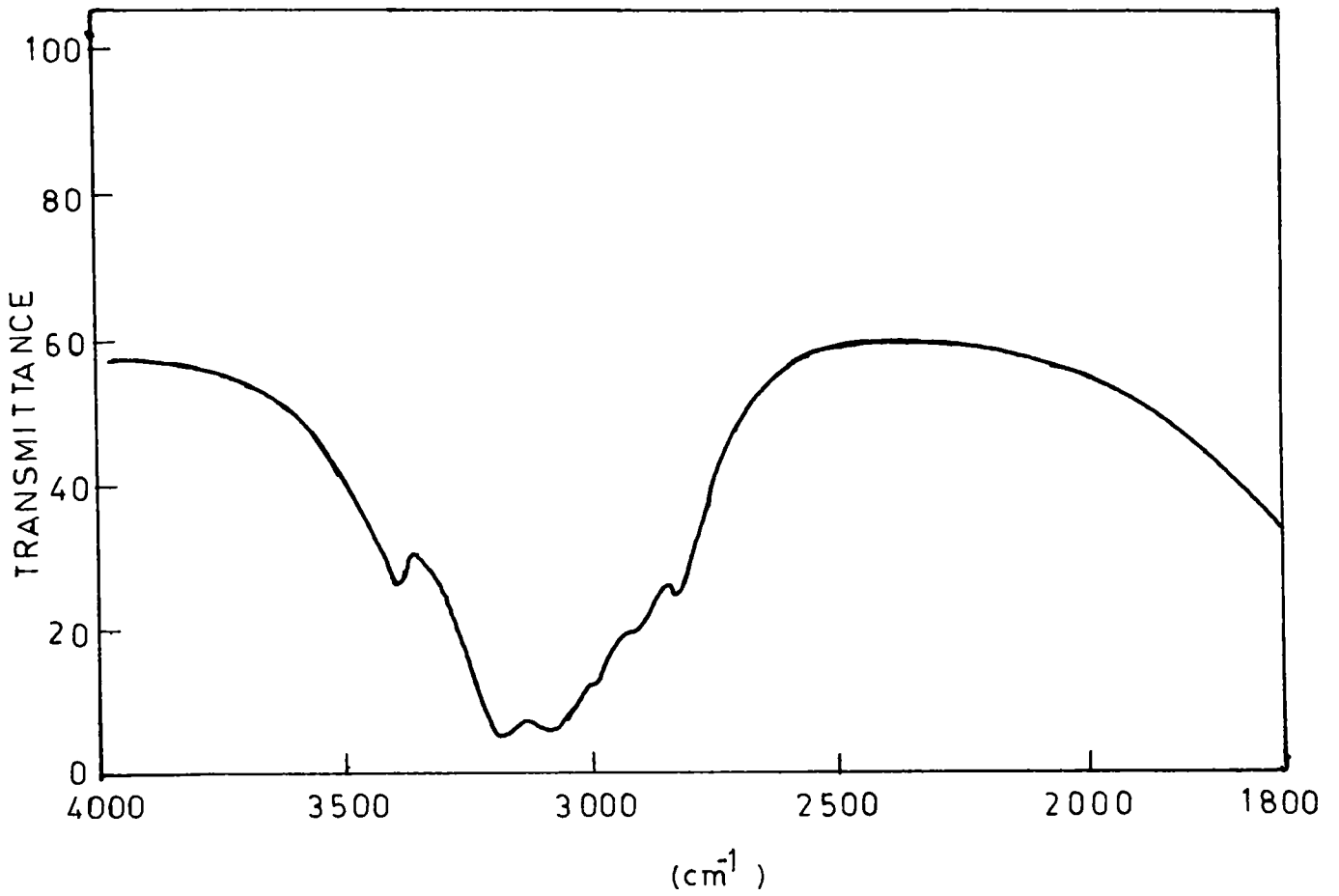


Fig.10.3(a) IR spectrum of DAHC in the region 4000-1800 cm^{-1} in KBr pellet.

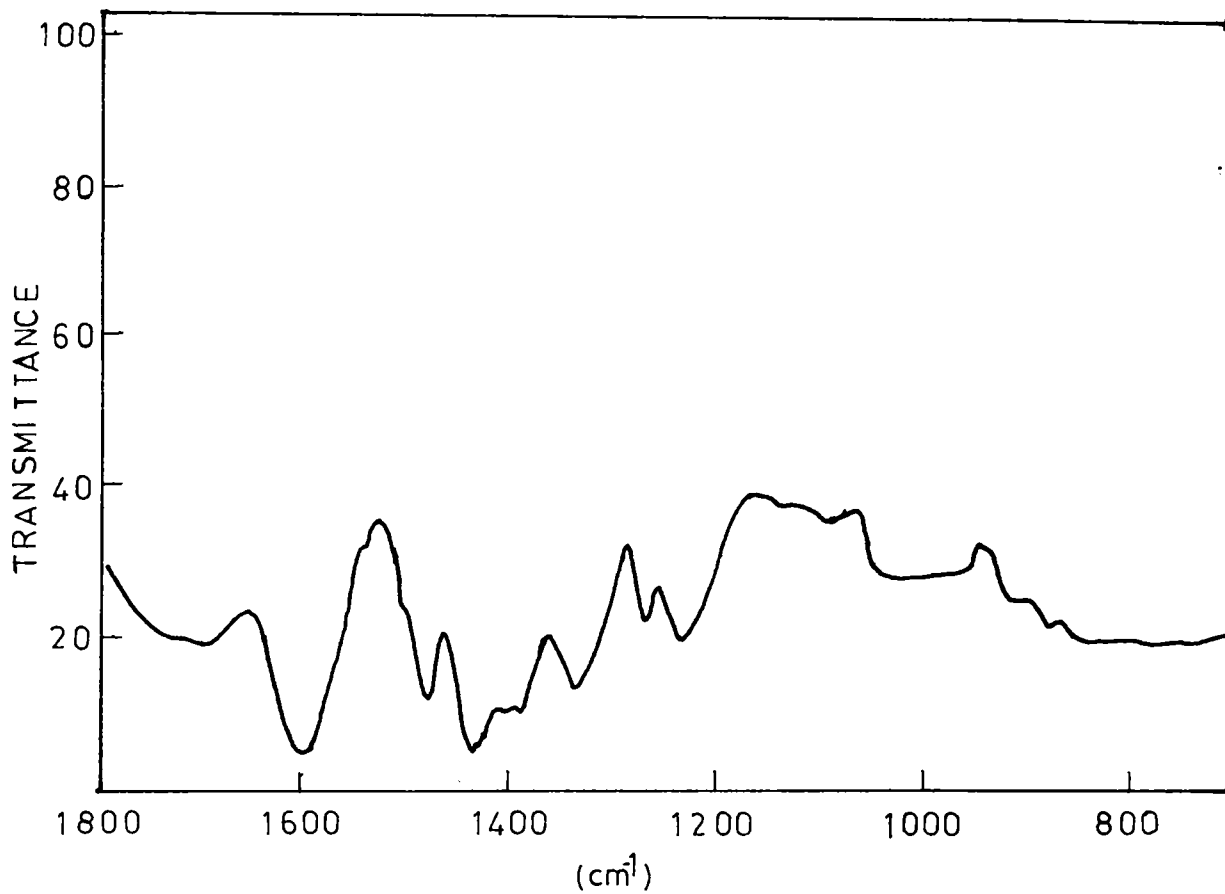


Fig.10.3(b) IR spectrum of DAHC in the region $1800-200\text{ cm}^{-1}$ in KBr pellet.

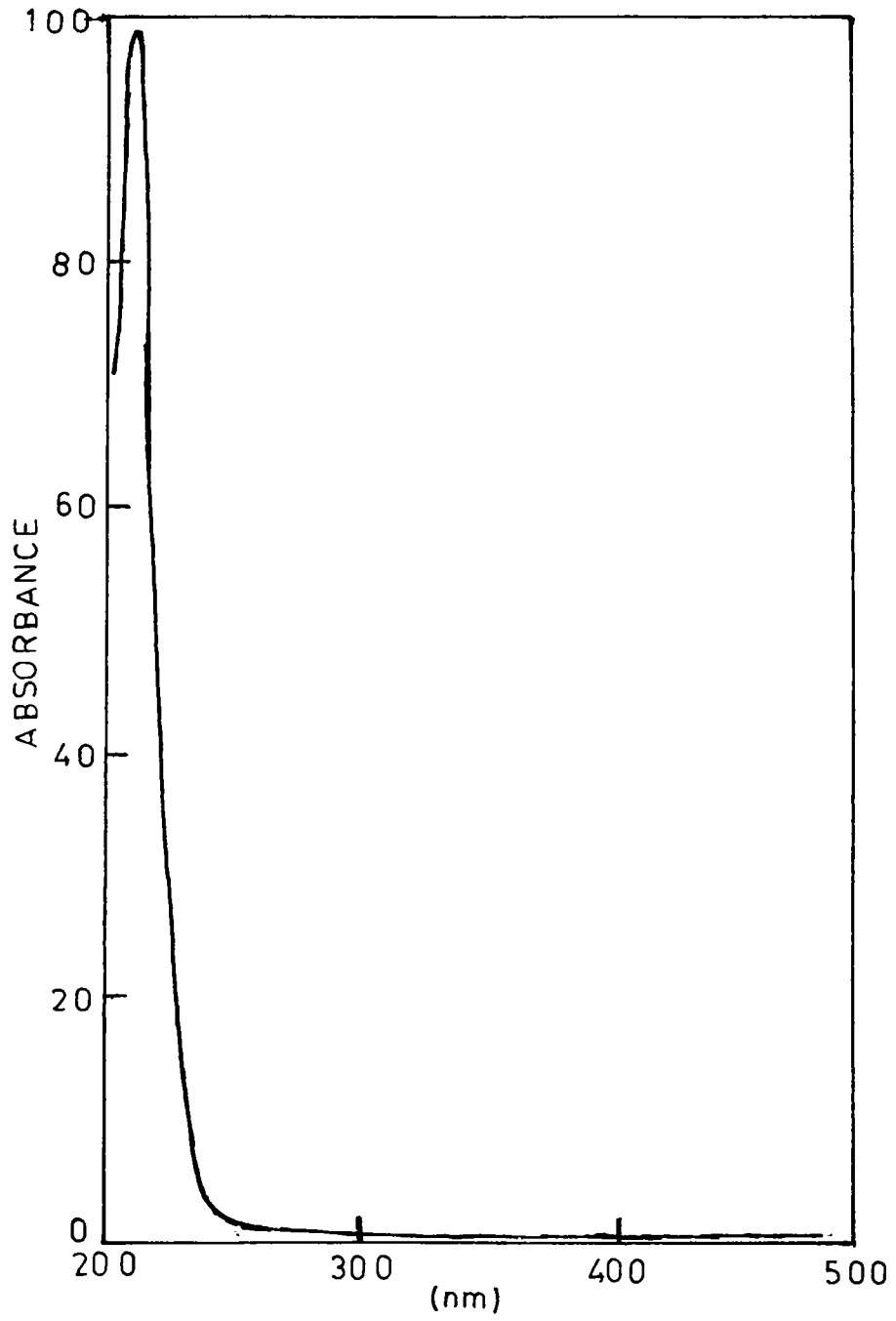


Fig.10.4 UV spectrum of DAHC in the wavelength range 195-500 nm.

groups present in the material. Aliphatic carboxylic acids are reported to be absorbing in the region 200 - 210 nm /10/ and DAHC contains three carboxylic groups.

Fig.10.5 gives the DSC trace for DAHC crystal sample. It consists of a fairly constant endothermic signal upto nearly 430^oK followed by a large endothermic increase. This increase is due to pre-melting effects. The DSC trace shows characteristics similar to that obtained in the case of variation of dielectric constant with temperature and loss tangent with temperature.

DSC trace of CA crystal is presented in Fig.10.6. Prominent peaks are observed at 349, 363, 418 and 427^oK. The peak at 349^oK is due to the loss of water of hydration and that at 427^oK is due to melting of CA crystals. Other peaks are probably due to structural transformations.

10.4. CONCLUSIONS

Various absorption peaks observed in the IR spectrum of DAHC are assigned to the functional groups present in DAHC. The molar extinction coefficient of DAHC obtained from UV spectrum is 8600 and the only absorption peak observed at 210 nm is attributed to the presence of carboxyl group. The DSC trace of DAHC crystal shows a large endothermic increase near the melting temperature due to pre-melting effects. The prominent DSC peaks of CA are correspond to dehydration and melting of the crystal.

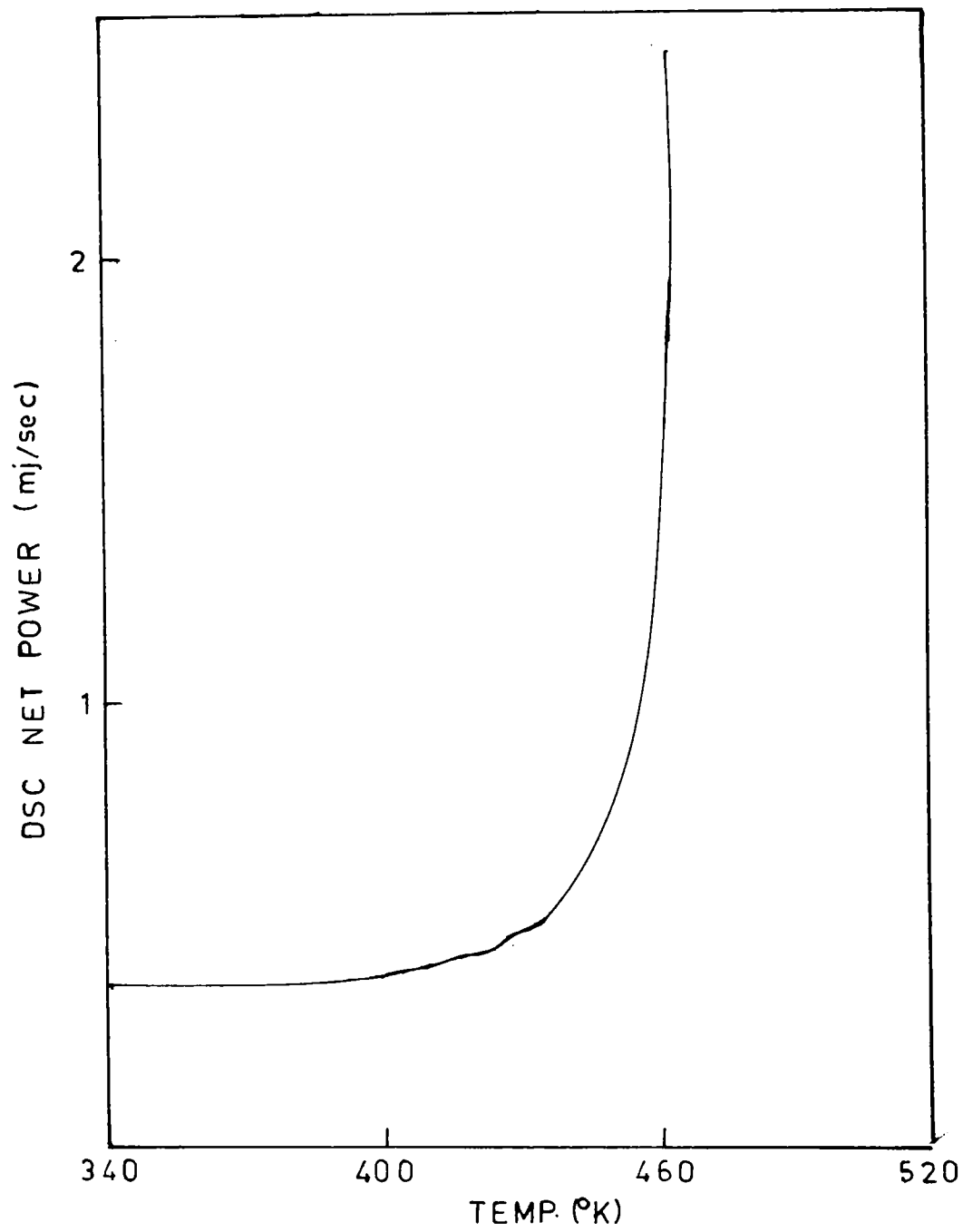


Fig.10.5 DSC trace of DAHC crystal.

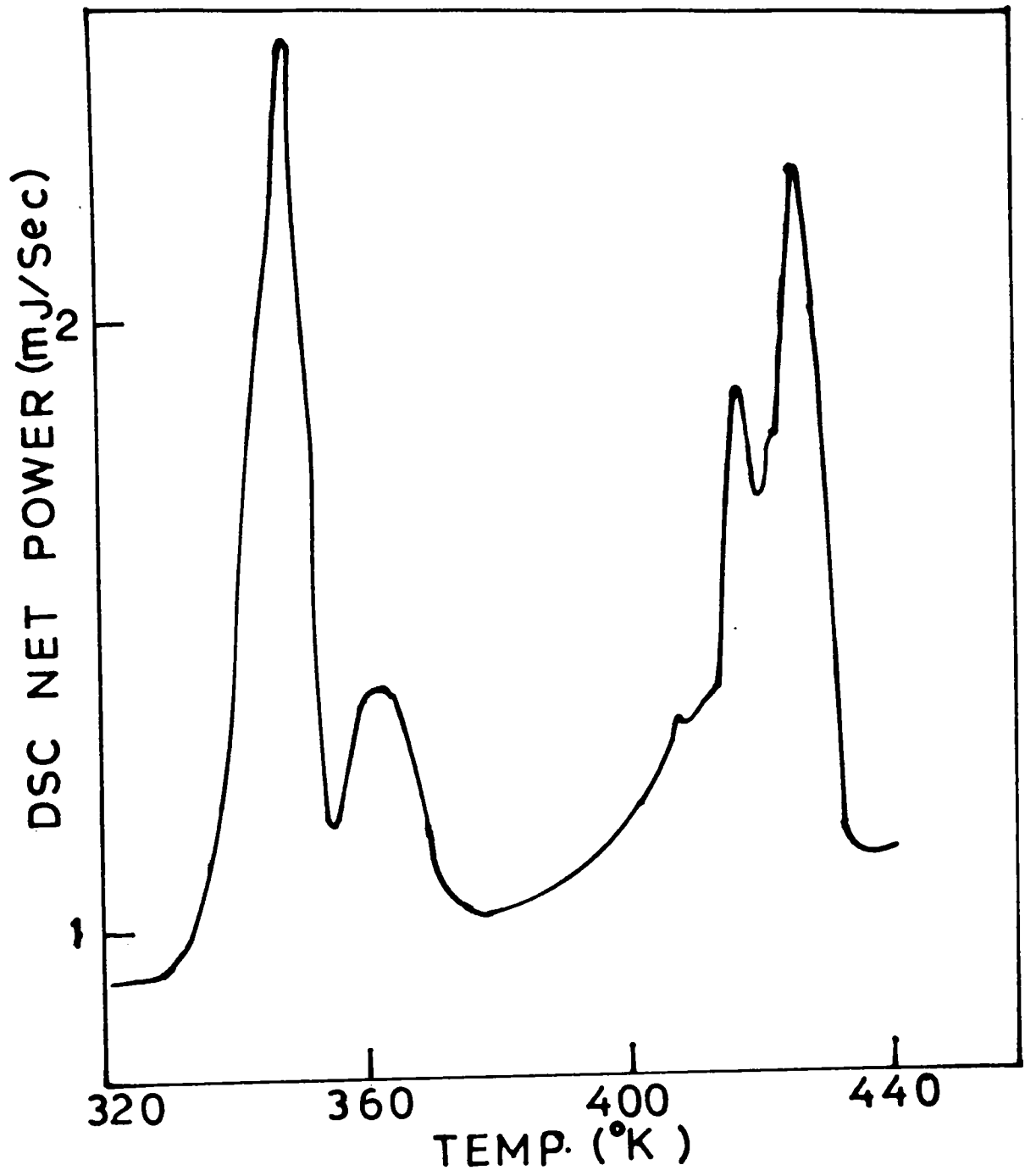


Fig.10.6 DSC trace of CA crystals.

REFERENCES

1. E.Y.MALINCHKA et al., Fiz. Met. & Metalloved 56(1983)746.
2. D.SENATRA et al., J. Phys. 45(1984)1159.
3. KUHN, J. Amer. Chem. Soc. 74(1952)2492.
4. MILLER and WILKINS, Analyt. Chem. 24(1952)1253
5. FOX and MARTIN, Proc. Roy. Soc. A167(1938)257.
6. FOX and MARTIN, Proc. Roy. Soc. A175(1940)208.
7. FLETT, J. Chem. Soc. (1951)962.
8. DUVAL et al., Ann. Physique 17(1942)5.
9. JONES et al., J. Amer. Chem. Soc. 74(1952)2575.
10. BURAWOY, J. Chem. Soc. (1939)1177.

ACKNOWLEDGEMENTS

I would like to acknowledge my indebtedness to Dr Joy George, Professor of Industrial Physics, Cochin University of Science and Technology, for his excellent guidance all through this work.

Grateful acknowledgement is made to Prof. K. Sathianandan and to Prof. K.G. Krishna Pillai, Head of the Department of Physics, for providing the laboratory and library facilities.

Thanks are due to all faculty members especially Mr. P.K. Sarangadharan, office staff of the Department of Physics, staff of the University Services and Instrumentation Centre for the help rendered during this research work.

I acknowledge with gratitude Prof. P.S. Narayanan, Dr. H.L. Bhat and the staff and fellow research scholars of the department of Physics, I.I.Sc, Bangalore, for providing necessary assistance to do short term research work at I.I.Sc.

The co-operation and friendly attitude of my fellow research scholars and associates, especially, Mr. A.V. Alex, Dr. K.S. Joseph, Mr. T.I. Palson, Mr. B. Pradeep, Dr. C.K. Valsala Kumari, Mr. P. Gopakumar and Miss A.G. Omanas are gratefully acknowledged.

I express my gratitude to the U.G.C for awarding me teacher fellowship and to the manager and the principal of S.H.College, Thevara, for sanctioning leave.

Words are insufficient to express my gratitude to many others who have given me very valuable support for this research work.